

Master thesis and internship[BR]- Master's thesis : Simulation of martian surface conditions with the MarsWRF GCM to assess the deliquescence potential of particular regions on Mars[BR]- Integration internship

Auteur : Link, Lola

Promoteur(s) : 8568; 8567

Faculté : Faculté des Sciences appliquées

Diplôme : Master en ingénieur civil en aérospatiale, à finalité spécialisée en "aerospace engineering"

Année académique : 2020-2021

URI/URL : <http://hdl.handle.net/2268.2/13173>

Avertissement à l'attention des usagers :

Tous les documents placés en accès ouvert sur le site le site MatheO sont protégés par le droit d'auteur. Conformément aux principes énoncés par la "Budapest Open Access Initiative"(BOAI, 2002), l'utilisateur du site peut lire, télécharger, copier, transmettre, imprimer, chercher ou faire un lien vers le texte intégral de ces documents, les disséquer pour les indexer, s'en servir de données pour un logiciel, ou s'en servir à toute autre fin légale (ou prévue par la réglementation relative au droit d'auteur). Toute utilisation du document à des fins commerciales est strictement interdite.

Par ailleurs, l'utilisateur s'engage à respecter les droits moraux de l'auteur, principalement le droit à l'intégrité de l'oeuvre et le droit de paternité et ce dans toute utilisation que l'utilisateur entreprend. Ainsi, à titre d'exemple, lorsqu'il reproduira un document par extrait ou dans son intégralité, l'utilisateur citera de manière complète les sources telles que mentionnées ci-dessus. Toute utilisation non explicitement autorisée ci-avant (telle que par exemple, la modification du document ou son résumé) nécessite l'autorisation préalable et expresse des auteurs ou de leurs ayants droit.



**Simulation of martian surface conditions
with the MarsWRF GCM to assess the
deliquescence potential of particular regions
on Mars**

Promoters

Dehant Véronique

Karatekin Ozgur

Author

Link Lola

Graduation Studies conducted for obtaining the Master's degree in

Aerospace Engineering by Lola Link

Academic year 2020 – 2021

Acknowledgements

First of all, I would like to thank the professors Véronique Dehant and Ozgur Karatekin, my promoters, for their kindness and their wise advices.

Thanks also to Elodie Gloesener and Cem Berk Senel for their presence and their constructive remarks.

Special thanks to Orkun Temel for his availability, his explanations without which this work would not have been possible, and his proofreading.

To conclude, I thank my friends and family for their encouragement, as well as my parents who have always believed in me, especially in my moments of doubt. Finally, thank you Brieux for your patience and unwavering support during the realisation of this work.

Lola Link

Abstract

The planet Mars, so close and yet so different from Earth, has since the first observations of the sky aroused great interest. Our neighbour has been observed and explored for 50 years and yet many mysteries remain to be solved. This work attempts to answer one of them by establishing the Martian regions whose surface conditions are favourable to the deliquescence of salt. This process allows the formation of salt water (a brine) in which life can, under certain conditions, develop.

A global scale modelling (MarsWRF Global Circulation Model) is performed to acquire the surface conditions. First, diurnal and seasonal variations for the entire planet are analysed. This shows that the areas with the conditions are mainly in the Northern Hemisphere in summer, between 50°N and 50°S in spring and autumn and mainly around the equator in winter.

Then, some interesting locations were investigated in more detail. On the one hand, landing sites and on the other, sites where the absorption spectrum revealed the presence of salts. What emerges primarily from this study is that calcium perchlorate is the most likely salt to deliquesce under Martian conditions. For sites located at high latitudes, they can host brines in the first half of the year. Mid-latitude sites in the north allow salt deliquescence throughout the year but the maximum number of hours for which conditions are satisfied is about ten hours around the winter solstice. The same is true for sites near the equator but a hollow period is visible during the autumn and the maximum number of consecutive hours encountering the conditions is lower. In the Southern Hemisphere, only Hale Crater showed surface conditions favourable for the deliquescence of calcium perchlorate.

To conclude, many locations have favourable surface conditions for a determined interval of consecutive hours, but this study does not establish whether during this time brines form and remain stable.

Contents

| | | |
|----------|---|-----------|
| 1 | Introduction | 5 |
| 1.1 | Climate and atmosphere | 5 |
| 1.2 | Liquid water on early Mars | 6 |
| 1.3 | Definitions | 7 |
| 1.4 | Structure of this work | 8 |
| 2 | State of art | 9 |
| 2.1 | Recurring slope lineae | 9 |
| 2.2 | Salts on Mars | 9 |
| 2.3 | Evaporation rate | 11 |
| 2.4 | Wind and dust storms | 13 |
| 2.5 | Thermal models | 13 |
| 2.6 | Thermal inertia | 14 |
| 2.7 | Water and brines stability | 15 |
| 2.7.1 | Stability of brines regardless of formation process and composition . | 15 |
| 2.7.2 | Stability of brines produced through deliquescence of perchlorates . | 15 |
| 2.7.3 | Stability of brines formed in the subsurface | 19 |
| 3 | Global Circulation Model | 20 |
| 3.1 | Description | 20 |
| 3.2 | Validation | 20 |
| 4 | Mars | 22 |
| 4.1 | Methodology | 22 |
| 4.2 | Results | 22 |
| 4.2.1 | Spring equinox | 22 |
| 4.2.2 | Summer solstice | 24 |
| 4.2.3 | Autumn equinox | 26 |
| 4.2.4 | Winter solstice | 28 |
| 4.3 | Discussion | 30 |
| 5 | Landing sites | 32 |
| 5.1 | Methodology | 32 |
| 5.2 | Results | 32 |
| 5.2.1 | Vastitas Borealis | 33 |
| 5.2.2 | Utopia Planitia | 35 |
| 5.2.3 | Chryse Planitia | 36 |
| 5.2.4 | Jezero Crater | 38 |
| 5.2.5 | Oxia Planum | 40 |

| | | |
|----------|-----------------------------------|-----------|
| 5.2.6 | Elysium Planitia | 42 |
| 5.2.7 | Gale Crater | 44 |
| 5.3 | Discussion | 46 |
| 6 | RSL sites | 55 |
| 6.1 | Methodology | 55 |
| 6.2 | Results | 55 |
| 6.2.1 | Terra Meridiani | 55 |
| 6.2.2 | Margaritifer Terra | 57 |
| 6.2.3 | Valles Marineris | 58 |
| 6.2.4 | Horowitz Crater | 59 |
| 6.2.5 | Hale Crater | 61 |
| 6.2.6 | Palikir Crater | 62 |
| 6.3 | Discussion | 64 |
| 7 | Conclusion and future work | 66 |
| 7.1 | Conclusion | 66 |
| 7.2 | Future work | 67 |
| | References | 68 |
| | Annexes | 72 |

1 Introduction

Mars is the fourth planet in the solar system from the Sun, about ten times less massive than the Earth and accompanied by two moons (Phobos and Deimos). It is a telluric planet, i.e. mostly composed of rocks and metal, as opposed to gaseous planets. Owing to its composition and position relative to the Sun, it is one of the candidates for the presence of liquid water on its surface, let alone the existence of life as we know it. It is this possible discovery that drives scientists to explore Mars from all angles.

Since the mid-1960s, numerous missions have been developed to first fly over the planet (Mariner 4 in 1965), and then to conquer it with a first touchdown in 1971 by The Soviet Mars 3. Missions then followed, notably the National Aeronautics and Space Administration's (NASA) Marth Pathfinder, Spirit and Opportunity. Recently, India and the Arab Emirates have sent spacecraft into orbit around Mars, while China has successfully deployed a rover on the Red Planet. The European Space Agency (ESA) had planned an exploration mission for 2016, which was eventually postponed to 2022. Nowadays, there are five active objects on Mars.

The main objective of this work is to establish a kind of database listing the places and times where single component brines can be formed. This is done by post processing with `Matlab` the parameters simulated by a Global Circulation Model and by taking the locations and times of temperature and relative humidity conditions suitable for the deliquescence of salts.

1.1 Climate and atmosphere

The planet Mars is considered to be a cold, hyper-arid desert. Its topography and the seasonal condensation of CO_2 at the poles cause large variations in pressure at its surface (up to 30%) [11]. In addition, the planet experiences a strong diurnal variation in the surface temperature. This is due to its thin atmosphere, the suspended dust which absorbs solar radiation and the low thermal inertia of the surface [47]. Seasonal differences are also strongly marked due to the high eccentricity of Mars (0.0934) [28].

Today's climate is controlled by these changes in temperature and pressure which result in a complex wind circulation. It impacts the distribution of dust and local dust storms are common. Two kinds of waves shape the wind pattern. First, the planetary waves present at mid-latitudes that break the symmetry of the west-east winds. Secondly, the buoyancy waves generated by the flow of the winds over the topography. The latter travel vertically, in contrast to planetary waves which propagate horizontally [45]. Con-

cerning the climate itself, Hargitai established in 2010 global climate zones displayed in Fig. 1. They are mostly based upon temperature, albedo and topographic data from the Thermal Emission Spectrometer (TES) since there is no rainfall or vegetation to suggest a climate classification on Mars. There are 8 climate zones: Glacial, Polar, Transitional, Tropical, Low albedo tropical, Subpolar Lowland (Basins), Tropical Lowland (Chasmata) and Subtropical Highland (Mountains). Note that a distinction is made between the north and south transitional zones. He explains that the Southern Hemisphere climate is more extreme (stronger winds, more dust storms) and colder in the (southern) winter because Mars is further from the Sun at that time. Therefore, south transitional zone is extreme while north transitional zone is mild. In addition, surfaces covered by dark sand have lower albedo and higher thermal inertia.

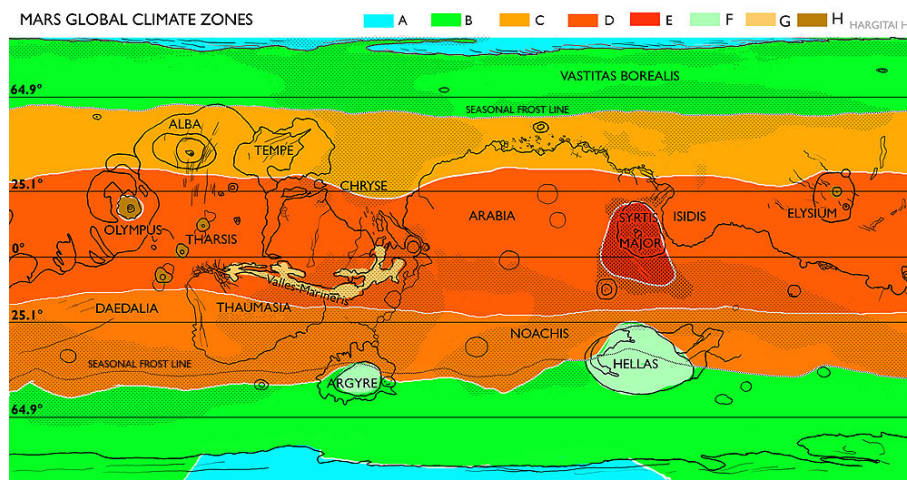


Figure 1: Mars Global Climate Zones. A = Glacial, B = Polar, C = Transitional (north: mild, south: extreme), D = Tropical, E = Low albedo tropical, F = Subpolar Lowland (Basins), G = Tropical Lowland (Chasmata) and H = Subtropical Highland (Mountains). Retrieved from [24].

Finally, the two hemispheres are different from each other in terms of their topography. On the one hand, the Northern Hemisphere has a lower elevation and is smoother, on the other hand, the Southern Hemisphere is very hilly. This phenomenon is known as the hemispheric dichotomy. The inner structure of Mars is similar to that of the Earth: the crust rests on the mantle, which itself surrounds the core of Mars. Although fairly quiet today, historically Mars has been the scene of many phenomena: volcanism, impacts, erosion, water flows, cratering, weathering, etc. But gradually, water and geologic activities stopped and liquid water has been redistributed in the atmosphere and as subsurface ice in Early Hesperian [27]. The polar ice caps have their own weather systems [12] [28].

1.2 Liquid water on early Mars

The search for liquid water today is not meaningless as many scientists agree that there is plenty of evidence of liquid water on ancient Mars. Numerous shapes carved into the rocks

during the Noachian are very similar to those found on Earth caused by water erosion and giving rise to lakes, rivers, canyons, seas or oceans [12]. In this paper, they specify, however, that the conditions necessary for fluvial activity were only rarely encountered. It is also worth mentioning the presence of deposits (sulphates, chlorides, etc.) in eroded areas, which typically form in contact with liquid water [35] and are the remains of aqueous processes [27].

1.3 Definitions

On Mars, no calendar is defined. Thus, to find one's bearings in the Martian year, it is customary to use the *solar longitude* L_s . Taking the Northern Hemisphere as a reference, a solar longitude of 0° corresponds to the spring equinox, a solar longitude of 90° to the summer solstice, a solar longitude of 180° represents the autumn equinox and a solar longitude of 270° corresponds to the winter solstice. It is shown in Fig. 2. Moreover, concerning the hours, it is useful to define the Airy Mean Time (AMT) and the Local Solar Time (LST). The first is the martian counterpart of the Greenwich Mean Time on Earth whereas the second gives the local time at a given longitude [5].

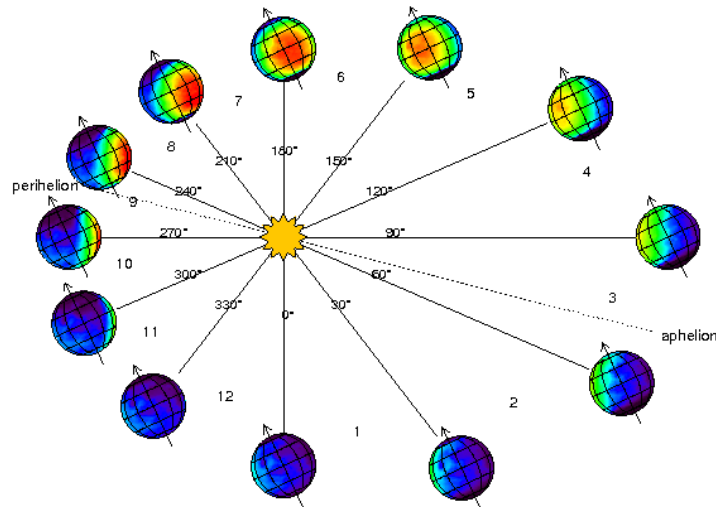


Figure 2: Diagram of the revolution of Mars around the Sun representing the solar longitude. Retrieved from [16].

A *brine* is a salty aqueous solution and the *stability* is a situation in which something is not likely to move or change. Hence, when referring to *brine stability*, it means the ability of a brine to remain in its liquid state for a certain period of time determined by the observer. The *metastability* can also be defined as the situation in which a system exists at an energy level above that of a more stable state and requires the addition of a small amount of energy to induce a transition to the more stable state.

Pure water in its liquid state can only exist under certain temperature and pressure conditions. On Earth, at a pressure of 1 atm, water is in a liquid state between 273.15 K and 373 K. On Mars, the atmospheric pressure is 0.006 atm. However, this pressure difference does not imply that the melting temperature of water varies on Mars because the molar volume of water in its liquid state and that of water in its solid state are close. The effect of pressure on this almost identical volume is therefore small. On the other hand, even if the surface temperature on Mars is favourable to the presence of liquid water, the low pressure induces its almost instantaneous evaporation. Thereupon, to study liquid water on Mars, it is necessary to understand the concept of eutectic temperature. Indeed, the presence of salts has the advantage to lower the melting point of water. Hence, the *eutectic temperature* is the fixed temperature at which a brine changes from a solid to a liquid state and consequently it is the lowest temperature at which liquid water can be found. Note that this temperature varies with the salt forming the brine. Additionally, the assumption that temperature and relative humidity vary inversely can be made.

Another useful notion is the *water activity* which is a measure of salinity ($a_w = 1$ is pure water) [50]. It is given by, when brines are stable against evaporation,

$$a_w = \frac{e_b}{p_{\text{sat},l}} \quad (1)$$

with e_b the water vapour pressure just above the brine and $p_{\text{sat},l}$ the saturation vapour pressure above pure liquid water [41]. This quantity is equal to the equilibrium relative humidity ($a_w = RH_{\text{eq}}$) [49].

1.4 Structure of this work

The structure of this work is as follows: The first chapter will review, in a non-exhaustive way, the previous studies done on the subject and will define important notions necessary for the understanding of the rest of the work. The MarsWRF model will be described and validated in Chapter 3. Chapter 4 will study the temperature and relative humidity seasonal variations on Mars' surface. The analysis of the temperature and relative humidity of the landing sites will be done in chapter 5 while chapter 6 will establish these same parameters but for some particular sites of Mars which are not landing sites. Finally, the 6th and last chapter will conclude this work by also presenting some perspectives for improvement.

2 State of art

The purpose of this section is to overview previous studies in relation to the availability of salts and brines on Mars as well as their stability.

2.1 Recurring slope lineae

Brines could be one of the causes of the formation of Recurring Slope Lineae (RSL). RSL are dark narrow streaks forming in certain area of the surface of Mars. They were discovered by Ojha et al. (2015) using images taken by the High Resolution Imaging Science Experiment (HiRISE) instrument of the Mars Reconnaissance Orbiter (MRO) probe, which show flows on the Martian surface and in particular on the slopes of the Newton Crater as shown in Fig. 3. These flows generally appear and develop on slopes facing the equator during warm seasons, when the temperature reaches about 250 K to 300 K [17][34]. Moreover, confirmed RSL are mostly located in the Southern Hemisphere. Although the temperature in areas with RSL is favourable for the presence of brine, according to Dundas et al. (2017) RSL are only the result of granular flows [30]. Nonetheless, by analysing the spectral data from HiRISE, they were able to determine the nature of the salts present on the several studied site.

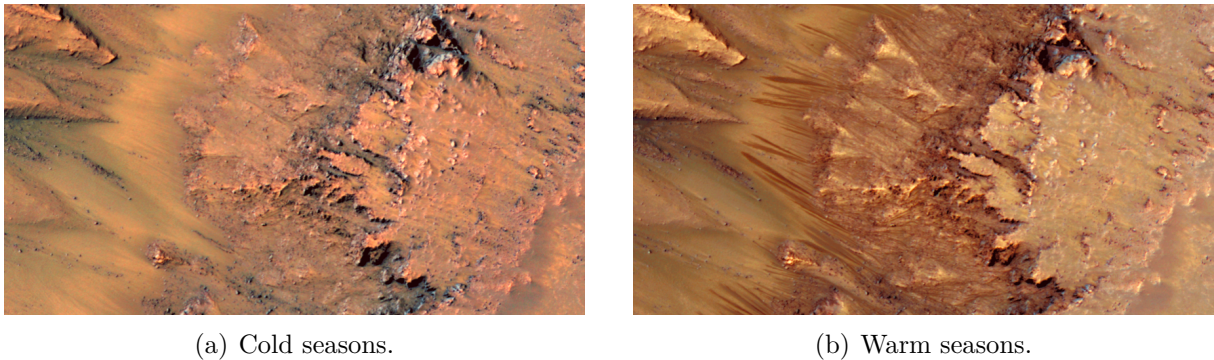


Figure 3: Comparison of the slopes of the Newton Crater during the cold and warm seasons when recurring slope lineae develop. Photographs taken by the Mars Reconnaissance Orbiter probe, retrieved from [8].

2.2 Salts on Mars

As mentioned above, Ojha et al. (2015) reported the presence of salts in the RSL they analysed [34]. Using the Compact Reconnaissance Imaging Spectrometer for Mars (CRISM) on board the MRO spacecraft, they obtained absorption spectra from various sites on Mars, which then allowed them to establish the nature of the salts present in these locations. The absorption spectrum from RSL on the slopes of Palikir Crater is consistent with that of various hydrated salts. From this spectral analysis, they conclude

that a mixture of Martian soil and magnesium perchlorate ($\text{Mg}(\text{ClO}_4)_2$), magnesium chlorate ($\text{Mg}(\text{ClO}_3)_2$) and magnesium chloride (MgCl_2) is found in this crater. RSL were also observed on the slopes of the Horowitz Crater peaks. The absorption spectrum of two of these peaks corresponds to that of a mixture of Martian soil and sodium perchlorate (NaClO_4). Finally, among the most active RSL in the Southern Hemisphere are those on the central peak of Hale Crater. The observations made are similar to those of Palikir Crater: the spectrum is consistent with that of a mixture between Martian soil and $\text{Mg}(\text{ClO}_4)_2$. Therefore it is seen that although according to Rivera et al. (2020) $\text{Mg}(\text{ClO}_4)_2$ is only present in high latitudes ($> 50^\circ\text{N}$), it is also found in the Southern Hemisphere: at Hale Crater and Palikir Crater. According to Glavin et al. (2013), the presence of calcium perchlorate ($\text{Ca}(\text{ClO}_4)_2$) has been confirmed in Gale Crater by the Sample Analysis at Mars (SAM) instrument on board MSL [20]. In addition, it can be noted that following the detection of nitric oxide release by the SAM instrument, nitrates are potentially present in Gale Crater [29]. Gough et al. (2019) suggest that MgCl_2 and calcium chloride (CaCl_2) are present in this crater [22]. The presence of $\text{Ca}(\text{ClO}_4)_2$ has been identified in situ at the Viking probe landing sites (Chryse Planitia and Utopia Planitia)[42]. Glavin's and Rivera's papers are in agreement with Rivera et al. (2020) who concluded that this salt is mainly found in the Northern Hemisphere [41]. At Vastitas Borealis, the potential perchlorates present are $\text{Mg}(\text{ClO}_4)_2$ and NaClO_4 [13]. These findings are corroborated in the study by Chevrier et al. (2012) in which they state that $\text{Mg}(\text{ClO}_4)_2$ was identified in the Phoenix landing site. Furthermore, they report that magnesium sulfate (MgSO_4) is widely present on Mars while chlorides (NaCl) are more likely to be detected in the Southern Hemisphere RSL [14]. Using data from the OMEGA spectrometer on the ESA Mars Express probe, Gendrin et al. (2005) established the presence of MgSO_4 at Terra Meridiani (a region of Meridiani Planum), at several sites in Valles Marineris and at Margaritifer Terra [19]. To summarise (see Fig. 4), according to the analyses in the reports cited, seven salts are most common on the surface of Mars (non-exhaustive list): $\text{Ca}(\text{ClO}_4)_2$, NaClO_4 , $\text{Mg}(\text{ClO}_4)_2$, MgCl_2 , NaCl , CaCl_2 and MgSO_4 . Note that salts can lower the melting temperature of a brine up to 80 K [34] and that $\text{Ca}(\text{ClO}_4)_2$ brine has the lowest eutectic temperature of all relevant-brines on Mars (198 K).

Another key element to investigate is the water activity in salts solutions since it is one of the conditions to get deliquescence phenomenon. Concerning perchlorates, Toner & Catling (2016) report that water activities in $\text{Na}(\text{ClO}_4)_2$ solution increase with decreasing temperature when considering all concentrations [49]. Precisely for concentrated solutions they increase by 0.25 from 298 to 175 K. On the contrary, water activities in $\text{Ca}(\text{ClO}_4)_2$ and $\text{Mg}(\text{ClO}_4)_2$ decrease with decreasing temperature when the temperature is greater than 200 K and increase for temperatures below 210 K. Toner et al. (2014) and Möhlmann

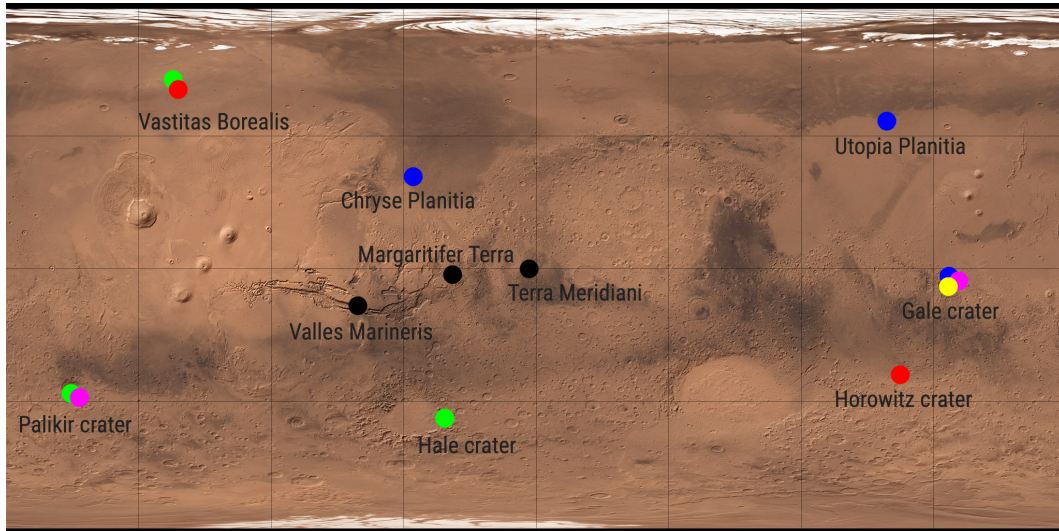


Figure 4: Map of Mars with salts pointed out. Green: $\text{Mg}(\text{ClO}_4)_2$, pink: MgCl_2 , red: NaClO_4 , blue: $\text{Ca}(\text{ClO}_4)_2$, yellow: CaCl_2 , black: MgSO_4 .

et al. (2011) also worked respectively on $\text{Ca}(\text{ClO}_4)_2$ and $\text{Mg}(\text{ClO}_4)_2$ properties. Note that Pestova et al. (2005) had previously studied $\text{Ca}(\text{ClO}_4)_2$ and $\text{Mg}(\text{ClO}_4)_2$ mixtures to reduce the lack of data concerning the water activities in several perchlorate solutions over a wide temperature range [37]. In their study, Altheide et al. (2009) use the water activity in MgCl_2 and MgSO_4 solutions at eutectic temperature [10]. Finally, Davila et al. (2010) studied chlorides (NaCl and CaCl_2) and established the evolution of their deliquescence in the course of a martian year. Tab. 1 exhibits the eutectic temperature and the water activity at the eutectic of relevant salts available on today Mars' surface. Note that for both temperature and relative humidity, perchlorates have wholesale the lowest values, followed by the chlorides and then come the NaCl and the MgSO_4 .

| Salt | T_e (K) | References | a_w (-) | References |
|-----------------------------|-----------|-----------------------|-----------|-----------------------|
| $\text{Ca}(\text{ClO}_4)_2$ | 198 | Gough et al. 2019 | 0.51 | Toner 2014 |
| $\text{Mg}(\text{ClO}_4)_2$ | 206 | Chevrier et al., 2012 | 0.53 | Möhlmann et al., 2011 |
| CaCl_2 | 223 | Chevrier et al., 2012 | 0.62 | Davila et al., 2010 |
| NaClO_4 | 236 | Chevrier et al., 2009 | 0.48 | Toner 2016 |
| MgCl_2 | 240 | Chevrier et al., 2012 | 0.78 | Altheide et al., 2009 |
| NaCl | 252 | Chevrier et al., 2012 | 0.82 | Davila et al., 2010 |
| MgSO_4 | 269 | Chevrier et al., 2012 | 0.95 | Altheide et al., 2009 |

Table 1: Eutectic temperature (T_e) and water activity at the eutectic (a_w) of present-day Mars' surface relevant salts.

2.3 Evaporation rate

In order to determine the stability of brines on Mars, it is essential to study the evaporation rate of these solutions. It will allow to define a *residence time* which represents the time

duration of a brine in the liquid state. According to Rivera-Valentín et al. (2020), a brine is stable against evaporation when the difference between the atmospheric water vapour pressure e and e_b is minimum (i.e. when $e_b \simeq e$) [41]. The water activity corresponding to this condition is then

$$a_w = \frac{e}{p_{\text{sat},l}} \quad (2)$$

and coincides with the ambient relative humidity with respect to liquid (RH_{liq} , abbreviated to RH for ease of writing) [41].

Two mechanisms are responsible for the evaporation of a brine: the difference between the vapour concentrations of the brine and the atmosphere and the convection near the surface due to the wind circulation. Indeed, if the wind velocity rises, more evaporated water vapour are carried into the atmosphere which increases the evaporation rate. The parameterisation of this quantity thus needs to include the two phenomena. Ingersoll (1970) were the first to study the evaporation rate of liquid water on Mars and thanks to heat flux data they came up with a formulation of the Fick's equation for the mass flux of water vapour above an evaporating frost which includes the effect of buoyancy in the atmosphere [26]. Chevrier et al. (2020) use a parameterisation of the evaporation rate developed in Ingersoll (1970) where they do not consider the assumptions made in Ingersoll [15][26]. In their paper, Temel et al. (2021) ran a Global Circulation Model (GCM) and used its outputs in a formulation of the evaporation rate based on Monin-Obukhov similarity theory [47]. Their method takes into account near surface winds and atmospheric stability. Note that their study doesn't consider the brines formation through deliquescence. The results showed good agreement both with the experimental data from M. H. Hecht (2002) and the theoretical data obtained by Chevrier et al. (2020). These several studies clearly show the impact of wind velocity on the evaporation rate. Altheide et al. (2009) investigated the evaporation rate of MgSO_4 and MgCl_2 brines on Mars [10]. According to them, the evaporation rate depends proportionally on the brines temperature and the brines water activity and inversely proportionally on the brines concentration. Thus, the higher the temperature and water activity, the faster the water will evaporate, whereas if the solution concentration is high, the evaporation rate will be lower. This means that pure solutions evaporate faster than concentrated or saturated solutions. Ultimately, they say that the evaporation rate on Mars is related to that on Earth by a multiplicative factor as follows

$$\left(\frac{g_{\text{Mars}}}{g_{\text{Earth}}} \right)^{1/3} = 0.726. \quad (3)$$

2.4 Wind and dust storms

As the playground of the Mars Science Laboratory (MSL) rover, the Gale Crater is a data-rich and therefore much studied site. The conclusions drawn from its study will make it possible to extrapolate its weather conditions to other sites. As seen above, the wind circulation is complex and thus complicated to defined. Moreover, the evaporation rate is greatly impacted by the wind speed. Newman et al. (2017) have investigated the wind circulation in the late fall around the Bagnold Dunes, located in the Gale Crater [33]. In particular, they studied the slopes of the dunes and concluded that during the day, the winds are upward while they are downward at night. The wind rotation between these periods is clockwise. Concerning the wind speed, they did not find any correlation between sols. They compared their results with that of the MarsWRF model and it showed good agreement. This study is interesting in that it provides a better understanding of the near-surface wind circulation in Gale Crater and thus a better global scale modelling of Mars which includes the evaporation rate.

Martian winds are also very much affected by dust storms. Indeed, it is the dust cycle that drives the wind circulation. On the one hand, there are annual storms of reasonable intensity and on the other hand, from time to time, there is a much larger storm of higher intensity. According to M. Smith, these massive events occur about every three years (Martian year), can be the size of a continent, last for weeks and usually occur in the summer in the Southern Hemisphere [32]. They are the evolution of a moderate storm and cover the entire planet. When this happens, the storm eventually kills itself as it is powered by the radiative heat of the Sun reaching the ground and heating the surface air, which rises, carrying dust with it. Note that dust storms have nothing to do with storms on Earth. The winds in these storms do not exceed 100 km/h. Dust storms cause surface temperatures to increase at night and decrease during the day. As a result, the mean temperature decreases (approx. 20 K) and increases at higher altitudes [44]. Moreover, during a storm, the atmosphere optical depth substantially increases since the storm creates an opaque layer that transmits much less sunlight to the ground.

2.5 Thermal models

As mentioned by Temel et al. (2021), thermal models are used to model the temperature and pressure on Mars because remote sensing observations only give point temperatures during the day but do not provide the evolution of surface temperatures, which is necessary to determine whether liquid water is possible on Mars at a global scale [48]. Indeed, locations at the same latitudes and with the same elevation and seasonal radiative forcing may experience different temperatures and pressures. This is due to discrepancies in surface properties (albedo, topography,...). Haberle et al. (2001) were the first to ex-

exploit a GCM in order to determine where and for how long liquid water could exist on today-Mars by analysing the temperature and the pressure [23]. They conclude that five regions, representing 29% of Mars' surface, meet the conditions to have pure liquid water: Amazonis, Arabia and Elysium plains as well as Hellas and Argyre basins. Regarding brines solutions, the suitable regions are more numerous. They even say that most of the planet could welcome highly concentrated salty water. But the formation of salty liquid water depends on the availability of ice, heat and evaporation rate.

2.6 Thermal inertia

According to Putzig et al. (2005), « *thermal inertia* is a measure of the subsurface's ability to store heat during the day and to re-radiate it during the night¹ ». Thus, when a place has a high thermal inertia, the difference between daytime and night-time temperatures will be less pronounced than in places with low thermal inertia. In Fig. 5 is mapped the global thermal inertia (resolution: $\frac{1}{20}^\circ$ per pixel), retrieved from Thermal Emission Spectrometer (TES) bolometer observations [39] during the Mars Global Surveyor (MGS) mission. They interpolated in places (between 80°N and 80°S) where no data was available. Thermal inertia is therefore an additional parameter impacting on surface temperatures.

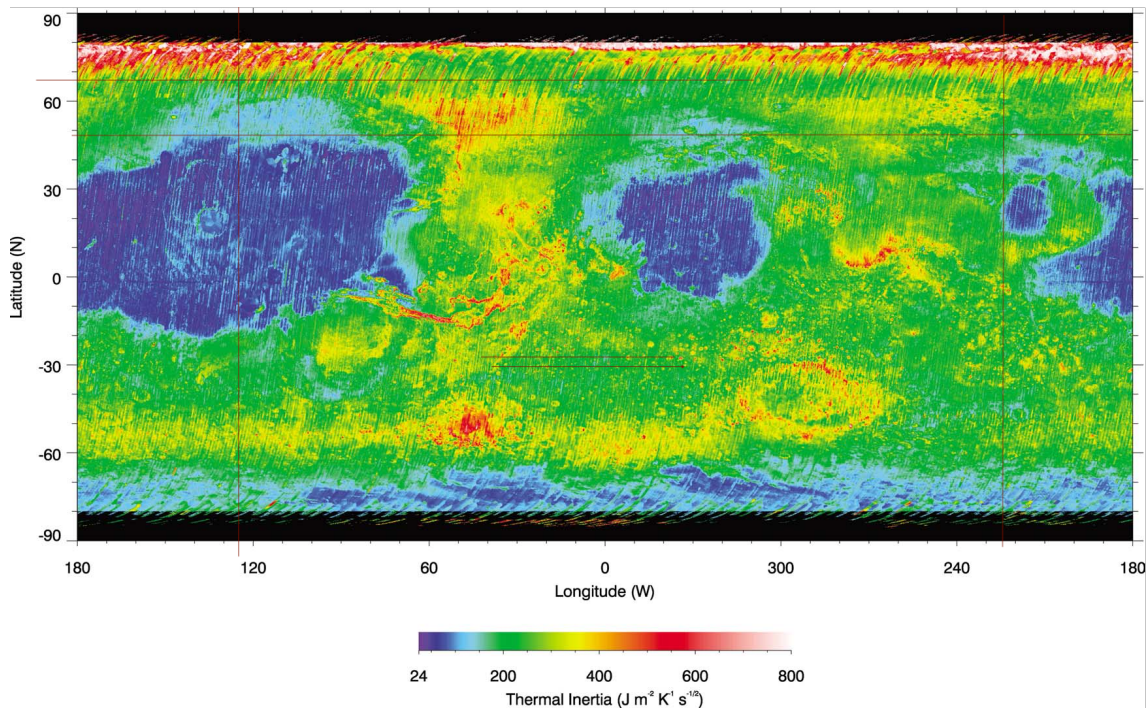


Figure 5: Thermal inertia map of Mars during the night. Data interpolated from 80°S to 80°N . Retrieved from [39].

¹Putzig et al., *Global thermal inertia and surface properties of Mars from MGS mapping mission*, Icarus (173), 2005, doi: 10.1016/j.icarus.2004.08.017

2.7 Water and brines stability

The ground and air temperatures as well as the pressure and the wind circulation are determinant parameters in the study of brine stability on the martian surface. Plenty of studies, among others McEwen et al. (2014) and Pla-García et al. (2020), have already shown that from mid-latitudes to the equator, surface temperatures can exceed the melting point of water during the day [31][38]. But at locations where this happens the pressure is not suitable and as it has already been mentioned, it results in sublimation. The study of brines is thus interesting as it lowers the melting point of water. According to Rivera-Valentín et al. (2018), for a brine to exist, its partial pressure must be above the partial pressure at the eutectic point and simultaneously the temperature should be above the eutectic temperature [42]. Since martian atmospheric conditions are not favourable to the formation of pure liquid water ($a_w = 1$) on the surface, only the stability of brines is studied in this work.

2.7.1 Stability of brines regardless of formation process and composition

In their investigation, Rivera-Valentín et al. (2020) found that for a temperature above 270 K, the water activity ensuring $e_b \simeq e$, is under the lowest a_w known for single brine component ($\text{Ca}(\text{ClO}_4)_2$ brine). Therefore, brines are not stable against evaporation above this temperature while when the temperature is comprised between the eutectic temperature of the brine and 270 K, (meta)stable brines are possible [41]. Moreover, although the relative humidity is 100% when $T < 230$ K, ice in a metastable liquid is likely. As expected, only ice exists below the eutectic temperature of the brine. In particular, they studied the eutectic temperature of a $\text{Ca}(\text{ClO}_4)_2$ brine (see Fig. 6). This figure shows that the highest water activity for the stable perchlorate brine having the lowest eutectic temperature is worth 0.66, stating that all brines with a water activity's value greater than that are unstable.

2.7.2 Stability of brines produced through deliquescence of perchlorates

One brine formation process is done through the absorption of water from the atmosphere by salts – i.e. *deliquescence* –, in particular by perchlorates. This mechanism occurs when the temperature is above the eutectic temperature and when the relative humidity with respect to liquid is equal to or greater than the deliquescence relative humidity (*DRH*) [49][36]. The last condition can be studied using the water activity knowing the relation [41]

$$\frac{DRH}{100} = a_w.$$

It is worth mentioning that *efflorescence* is the opposite phase transition occurring when the solution recrystallize, once $RH < DRH$ [41]. Nonetheless this process arises for a

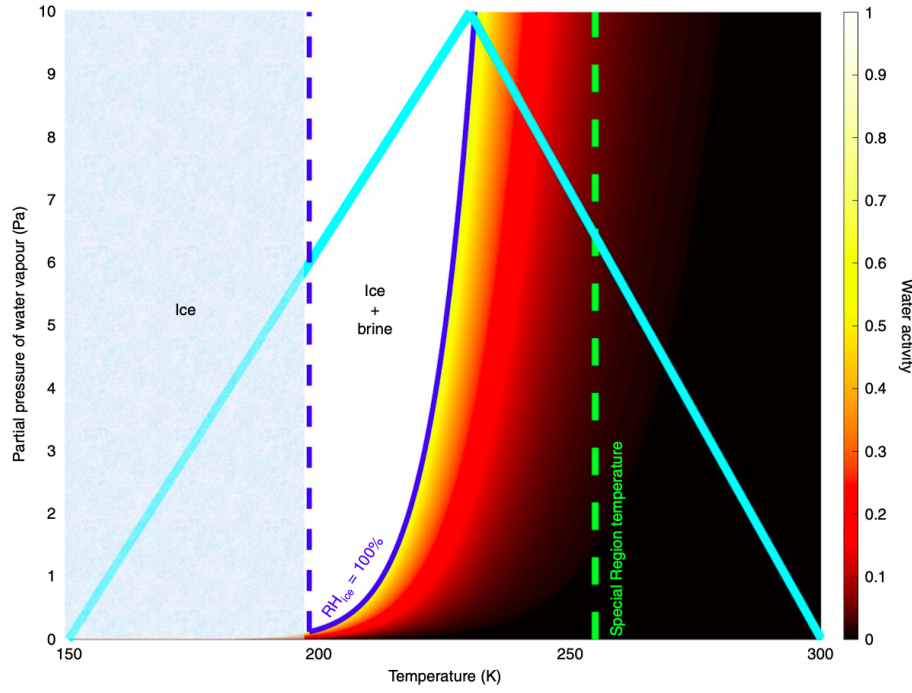


Figure 6: Stable brines water activity as a function of temperatures and water vapour pressures. The temperatures and water vapour pressures relevant to present-day Mars are contained between the cyan lines. The solid blue line corresponds to the saturation with respect to ice. The dashed blue line represents the eutectic temperature of a calcium perchlorate brine. The dashed green line marks the limit temperature at which terrestrial organisms could replicate (represented by the Special Region temperature $T = 255$ K [43]). Retrieved from [41].

lower relative humidity due to a hysteresis effect.

The second proposed mechanism is the formation of brine by melting of ice. However even if the surface temperature is higher than the eutectic temperature of the salt allowing the melting of the ice, the surface pressure must also be above the saturation vapour pressure [47]. This way, the water will be stable against boiling. In each case, two conditions must be satisfied to obtain brines on the martian surface:

- Deliquescence: $T > T_e$, $RH \geq DRH$
- Melting of ice: $T > T_e$, $p > p_{sat,vap}$

But the conditions to obtain deliquescence are easier to meet thanks to the salts which not only decrease the melting point of water, but also decrease the water activity, resulting in a linear decrease in saturation vapour pressure. This work will therefore focus only on brines formation through deliquescence.

According to Rivera-Valentin et al. (2018), no atmospheric conditions favourable to $\text{Ca}(\text{ClO}_4)_2$ deliquescence on the Martian surface have been detected [42]. They then analysed their data by considering different errors. The first one at the 1-sigma level

for surface temperature and relative humidity still does not allow the deliquescence of $\text{Ca}(\text{ClO}_4)_2$. Whereas an error at the 2-sigma level for surface temperature and relative humidity shows that two sols present favourable conditions: sol 1232 ($L_s = 99^\circ$) and sol 1311 ($L_s = 137^\circ$). A liquid can then form from $\text{Ca}(\text{ClO}_4)_2$ and survive up to one hour each sol. On the other hand, if $\text{Mg}(\text{ClO}_4)_2$ is considered with an error at the 2-sigma level only for the surface temperature, the formation of brine by deliquescence is always excluded. In their 2020 study, Rivera-Valentin et al. mapped the distribution of (meta-)stable brines on the surface of Mars (see Fig. 7) [41]. These brines are formed either by deliquescence of $\text{Ca}(\text{ClO}_4)_2$ or $\text{Mg}(\text{ClO}_4)_2$. The results are that strands formed by deliquescence of $\text{Ca}(\text{ClO}_4)_2$ are mostly formed in the Northern Hemisphere, about 6h/sol at a solar longitude of 140° in the Northern Hemisphere and 225° in the Southern Hemisphere. The brines represent 40% of the surface and are present 2% of the year. Brines formed by the deliquescence of $\text{Mg}(\text{ClO}_4)_2$ are only formed in the Northern Hemisphere ($> 50^\circ\text{N}$), about 8h/sol and at a solar longitude of 160° . They represent 5% of the surface and are present 0.2% of the year.

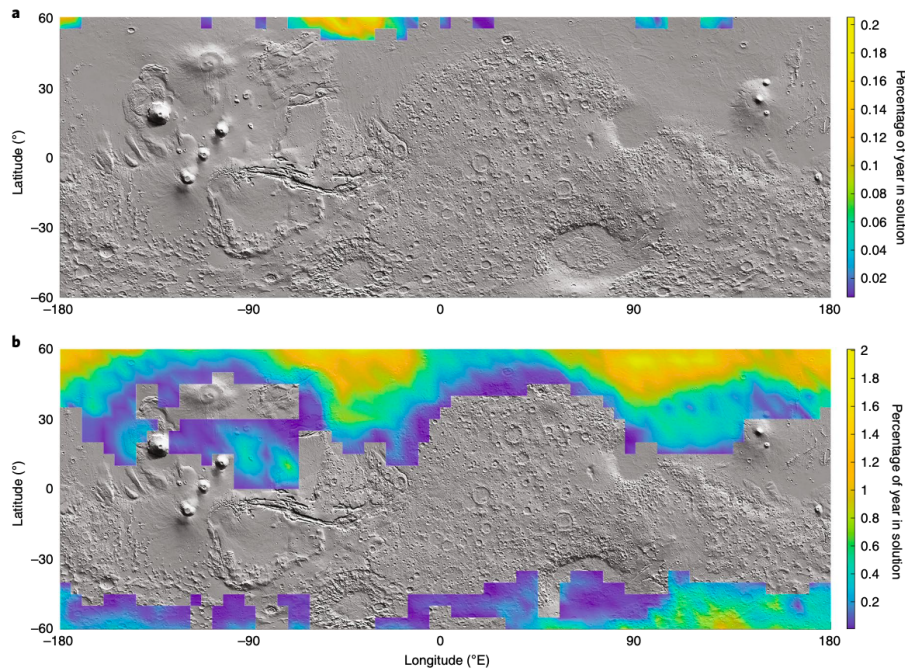


Figure 7: Distribution of (meta-)stable brines on the Martian surface. Above: $\text{Mg}(\text{ClO}_4)_2$, below: $\text{Ca}(\text{ClO}_4)_2$. Retrieved from [41].

The final step in this study was to map the maximum achievable water activity of brines formed by deliquescence of $\text{Ca}(\text{ClO}_4)_2$ and the corresponding temperature (see Fig. 8). They found that the maximum water activity was 0.8 with a temperature of 205 K while for a maximum temperature of 210 K, the water activity is 0.77.

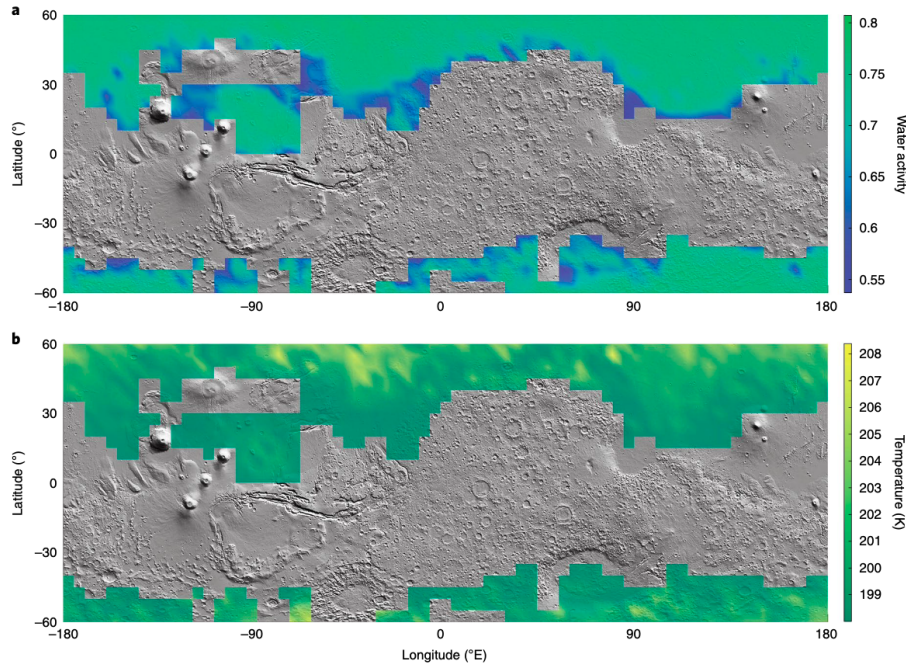


Figure 8: Maximum achievable water activity and corresponding temperature of brines formed through deliquescence of $\text{Ca}(\text{ClO}_4)_2$. Retrieved from [41].

Next, they mapped the maximum achievable temperature and the corresponding $\text{Ca}(\text{ClO}_4)_2$ brines water activity as seen in Fig. 9. In this case, they determined that for a maximum temperature of 225 K, the water activity was 0.24. These conditions are reached just before the efflorescence of calcium perchlorate.

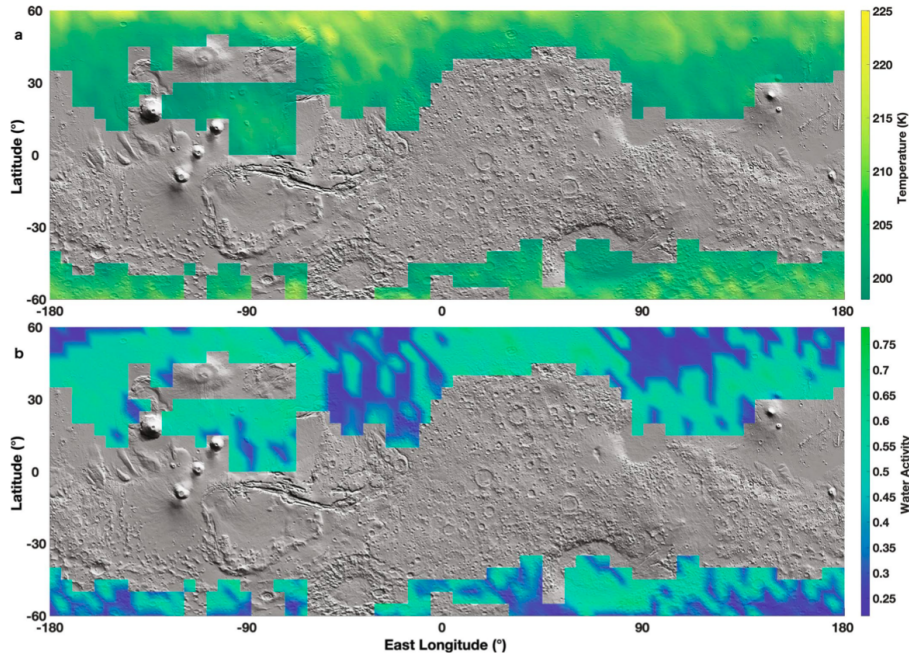


Figure 9: Maximum achievable brine temperature and corresponding water activity of brines formed through deliquescence of $\text{Ca}(\text{ClO}_4)_2$. Retrieved from [41].

2.7.3 Stability of brines formed in the subsurface

The presence and stability of brines in the subsurface have also been studied because the temperature and pressure conditions are more favourable. Notably Rivera-Valentin et al. (2018) analyzed their results from MSL as a function of the Gale Crater's thermal inertia (Γ). They noted that subsurface brine formation by deliquescence of $\text{Ca}(\text{ClO}_4)_2$ is possible only for terrains with low thermal inertia ($\Gamma \leq 180 \text{ J m}^{-2}\text{K}^{-1}\text{s}^{-1/2}$). This could occur during maximum one hour for solar longitudes between 100° and 110° . Thermal inertia and albedo combinations were also tested to deepen their results. For thermal inertia above $300 \text{ J m}^{-2}\text{K}^{-1}\text{s}^{-1/2}$, subsurface brine formation through deliquescence of $\text{Ca}(\text{ClO}_4)_2$ is unlikely. The phenomenon becomes possible depending on the albedo for thermal inertia below $300 \text{ J m}^{-2}\text{K}^{-1}\text{s}^{-1/2}$ and for thermal inertia under $185 \text{ J m}^{-2}\text{K}^{-1}\text{s}^{-1/2}$ it is possible for a large interval of albedos. These results will help to understand brine formation in equatorial terrains.

3 Global Circulation Model

This section will first describe the GCM used in this work along with approximations made in the simulations. Then its validity will be demonstrated by comparing with remote sensing data obtained via the Phoenix lander and explained in Fisher et al. (2019) [18].

3.1 Description

The numerical model used is a Global Circulation Model applied to Mars (Mars Weather Research and Forecasting MarsWRF) from the planetWRF atmospheric model [40]. It provides, among others, diurnal and seasonal evolution of the temperature and the water vapour mixing ratio, used to compute the relative humidity (T and RH are the quantities of interest in the salts deliquescence analysis). The spatial resolution of the simulation is 5° longitude x 5° latitude while the time resolution is one hour. The simulation was performed at a global scale and reproduces the martian year 29 (MY29) which runs from 9 December 2007 to 26 October 2009 (according to the Gregorian calendar) [46]. But before this simulation, a first one year simulation has been made which may be regarded as "spin-up". When plotted, the data starts at 00 : 00 at Airy Mean Time.

Some errors have been introduced in the simulation and in the post-processing. First, since the grid space both in latitude and longitude is of 5° , the outputs used to assess the deliquescence potential of the sites are not those from the exact location. Moreover, the model over-predicts the water vapour mixing ratio (detailed in the following section) and it induces errors in the relative humidity computation.

In addition to the MarsWRF model results, a dust scenario giving the dust optical depth (τ) during MY29 is retrieved from the Mars Climate Database² for which the spatial resolution is 3° longitude x 3° latitude. Temporal resolution is, in turn, of fourteen hours.

3.2 Validation

It was of first importance to verify if the MarsWRF model results matched those from Mars' observations. As said above, this was achieved by comparing the relative humidity retrieved at a region of Vastitas Borealis (Phoenix landing site) and simulated with the GCM. Remote sensing data used in Fisher et al. (2019) have been obtained by the lander for an interval of sols ranging from $L_s = 78^\circ$ to $L_s = 148^\circ$ [18]. More precisely, the parameters were recorded via a sensor named the Thermal and Electrical Conductivity Probe (TECP) mounted on a robotic arm. This allowed the acquisition of information

²Laboratoire Météorologique Dynamique, Mars Climate Database: Climatologies of the Martian Atmospheric Dust Optical Depth, http://www-mars.lmd.jussieu.fr/mars/dust_climatology/.

both in the regolith and in the air (up to a height of 2.2 m). The model simulates the water vapour mixing ratio either at the surface or at a height of 1.5 m. Henceforth, the one used in the comparison is the relative humidity computed at 1.5 m. The comparison is shown in Fig. 10. The orange dots are the results from observations detailed in Fisher et al. (2019) and the blue ones are the results simulated with the MarsWRF model. When the two data sets were compared, a temperature shift of 20 K was observed. This shift might be caused by the model over-predicting the water vapour mixing ratio. Thus, in the post-processing of the data, a recalculation of this ratio has been made by multiplying the parameter by a factor of 0.6. As a result, the relative humidity retrieved thanks to the water vapour mixing ratio and the temperature is modified leading to an improved $RH - T$ curve. This is what Fig. 10 shows, with the two sets of data being more similar, although a slight mismatch is still visible. Therefore, the version of the MarsWRF model used in this study over-predicts the water vapour content of the atmosphere. As a result, there is an uncertainty of about 40% in the results obtained. Apart from the model over-prediction, owing to the 5° resolution, an additional numerical error is induced in the plot. Indeed, the hourly temperature and water vapour mixing ratio are not exactly the ones found at Phoenix landing site. Finally, MarsWRF model simulates data at 1.5 m whereas the observations were made at 2 m.

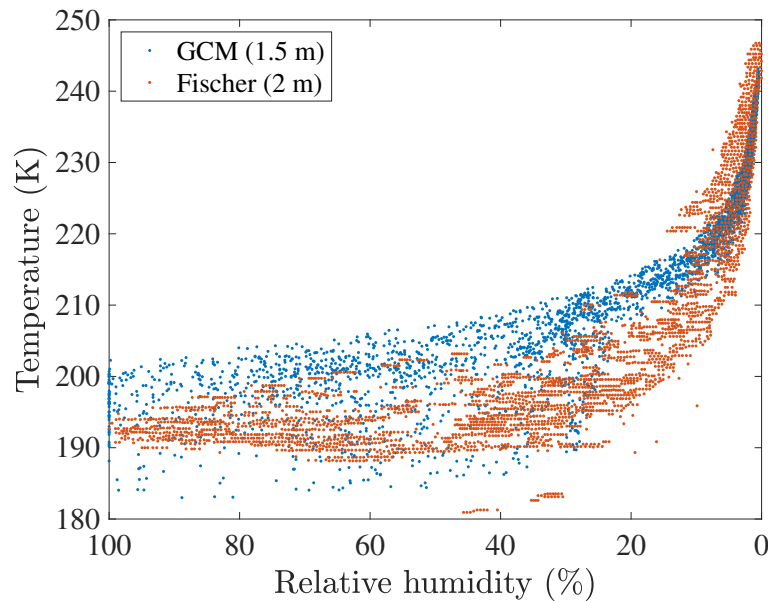


Figure 10: Relative humidity near Phoenix landing site’s surface as a function of the temperature. Orange: RH at 2 m (reproduced from [18]), blue: RH at 1.5 m (from MarsWRF model).

4 Mars

This chapter provides a discussion to understand the diurnal and seasonal temperature and relative humidity variations on the surface of Mars. This will give an overall idea of where the most favourable locations for salt deliquescence are and when the conditions are encountered.

4.1 Methodology

The idea here is to generate temperature and relative humidity plots as a function of the solar longitude representing the whole martian surface. As a result, it will be possible to determine which locations have the right characteristics for the deliquescence of salts, in a global way. Plots are created at four times of the year: the spring equinox ($L_s = 0^\circ$), the summer solstice ($L_s = 90^\circ$), the autumn equinox ($L_s = 180^\circ$) and the winter solstice ($L_s = 270^\circ$). Then, for each solar longitude, four hours spaced by six hours are analysed: 0 am, 6 am, 12 am and 6 pm. This way, a decent overall coverage of Mars is made. Note that the Airy Mean Time is considered meaning when it is 6 am, this hour is taken at 0° of longitude. The analysis is done for seven salts: $\text{Ca}(\text{ClO}_4)_2$, $\text{Mg}(\text{ClO}_4)_2$, NaClO_4 , CaCl_2 , MgCl_2 , NaCl , MgSO_4 .

4.2 Results

Outputs from GCM for the whole Mars for four solar longitudes and four hours are described hereafter.

4.2.1 Spring equinox

The northern spring equinox is defined by a solar longitude of 0° . In the Southern Hemisphere, this period corresponds to the autumn equinox. The surface temperatures and relative humidities for $L_s = 0^\circ$ at the four different times are represented in Fig. 11 and Fig. 12 respectively.

Fig. 11 shows that the temperatures in the Southern Hemisphere are roughly mirror images of those in the Northern Hemisphere. It can also be seen that the maximum temperatures ($T_{max} = 280$ K) advance throughout the day as the planet rotates. Not surprisingly, maximum temperatures occur at noon or midnight, and drop by 20 degrees when longitude 0 (or 180) is no longer in full sunlight. Additionally, maximum temperatures are located around the equator (between 50°N and 50°S) and the minimum ones encircle the poles. At places where the temperature is maximum, $\text{Ca}(\text{ClO}_4)_2$, $\text{Mg}(\text{ClO}_4)_2$, CaCl_2 , NaClO_4 , MgCl_2 , NaCl and MgSO_4 are favoured to deliquesce when $T = 280$ K but MgSO_4 is not when $T = 260$ K since the surface temperature no longer exceeds its

eutectic temperature. The further away from the center of the maximum temperature zone, the less the condition $T > T_e$ is satisfied. When the temperature reaches a value of 160 K or lower, no salt has a eutectic temperature that allows the formation of brines.

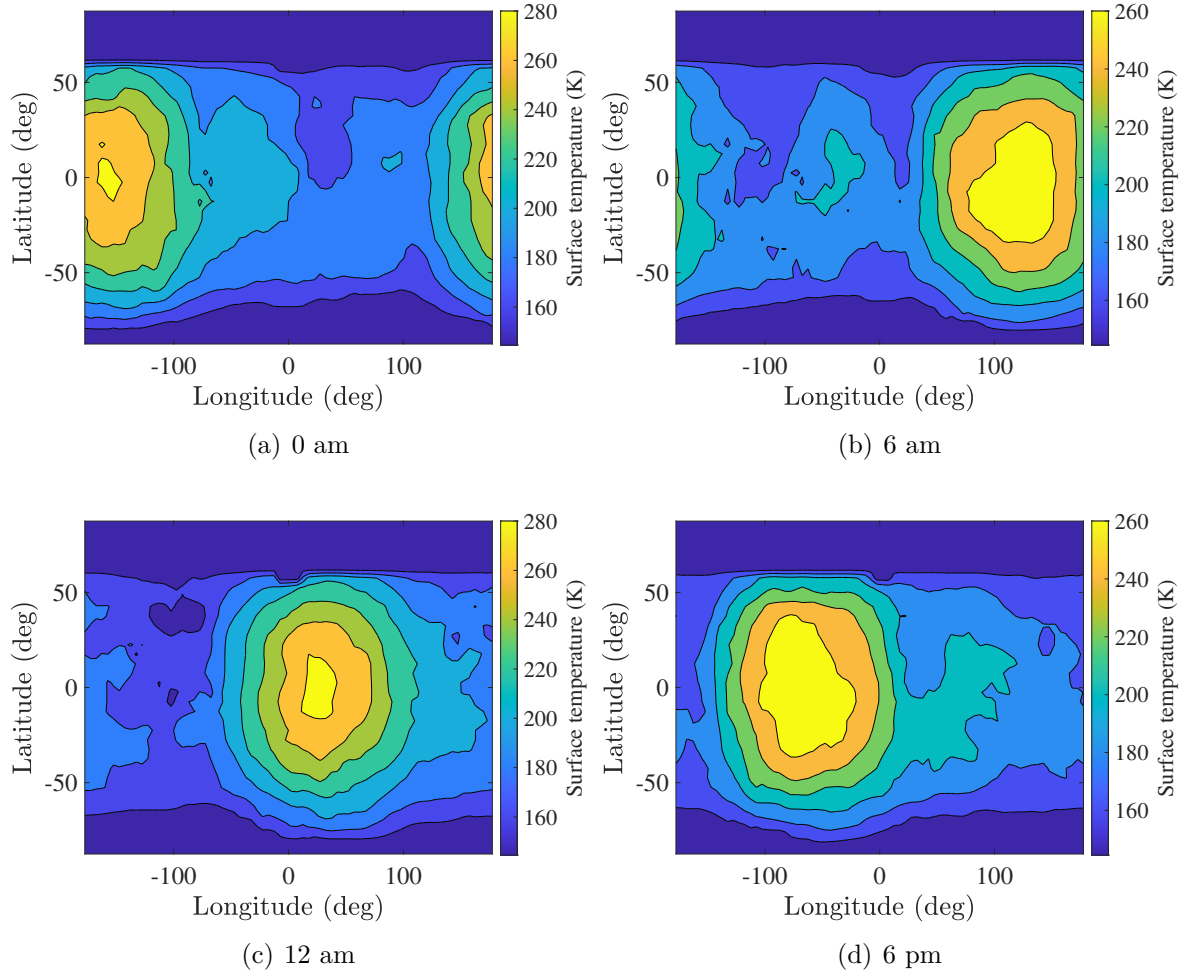


Figure 11: Temperatures on Mars at the spring equinox ($L_s = 0^\circ$) for four different AMT hours.

The relative humidities plots in Fig. 12 are similar to those of the temperature but in the opposite way: where the temperature is maximum, the relative humidity is minimum. The circle of minimum relative humidity also moves horizontally with the rotation of Mars. Apart from the main area of very low relative humidity, saturated relative humidity can be found at every latitude and the North Pole region has low values but which stagnate between 40% and 60% all day. This trend is not observed in the South Pole region. Last thing to mention about the overall shape is the small zone located around 50°W (at 0 am) which is enclosed in areas of high relative humidity and which also keeps values around 50% relative humidity throughout the day. As far as salts are concerned, at 0% relative humidity, none of them can deliquesce and conversely at 100% relative humidity, all of them are prone to the process. In areas of 40% – 60% relative humidity, NaClO_4 ,

CaClO_4 , MgClO_4 and CaCl_2 could encounter a relative surface humidity higher than their deliquescence relative humidity. For MgCl_2 , NaCl and MgSO_4 , this is more likely to occur in more humid areas.

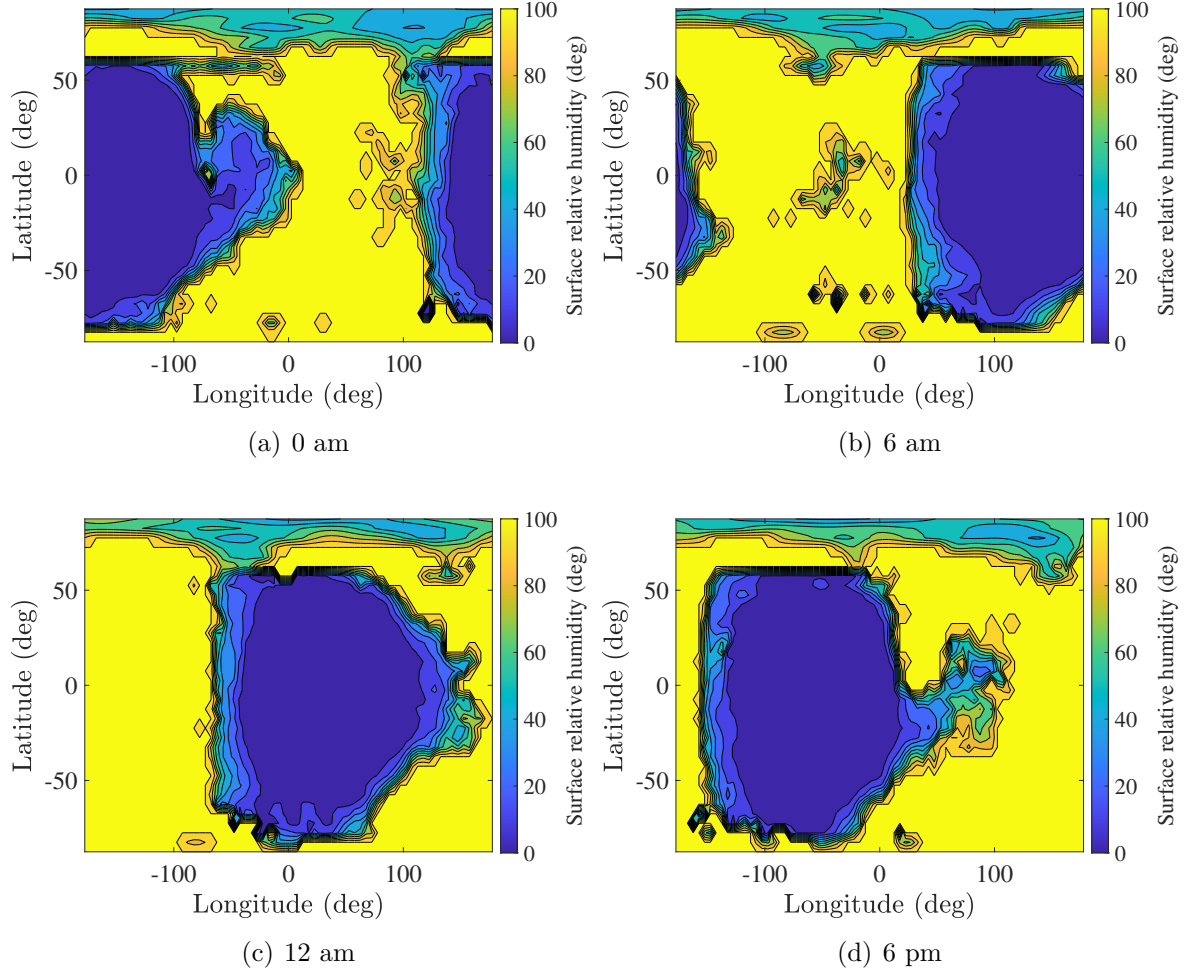


Figure 12: Relative humidity on Mars at the spring equinox ($L_s = 0^\circ$) for four different AMT hours.

4.2.2 Summer solstice

The northern summer solstice is defined by a solar longitude of 90° . In the Southern Hemisphere, this period corresponds to the winter solstice. The surface temperatures and relative humidities for $L_s = 90^\circ$ at the four different times are represented in Fig. 13 and Fig. 14 respectively.

By the summer solstice, it is clear that the high temperature zones have moved further north, leaving only temperatures below 160 K in the Southern Hemisphere (where it is winter solstice), below 50°S . As with the spring equinox, the illumination of the planet can be guessed from the different positions of the maximum temperature zone. Moreover,

it is centred around 30°N in contrast to the equator-centering during the spring equinox. In this case, maximum temperatures are around 260 K all day. Thus, salts are more likely to deliquesce in the Northern Hemisphere than in the Southern Hemisphere during the summer solstice. However, in areas of around 200 K, only $\text{Ca}(\text{ClO}_4)_2$ deliquescence remains, whose eutectic temperature is higher than the surface temperature. In region a dozen degrees warmer, another salts joins it ($\text{Mg}(\text{ClO}_4)_2$) whose eutectic temperature is 206 K.

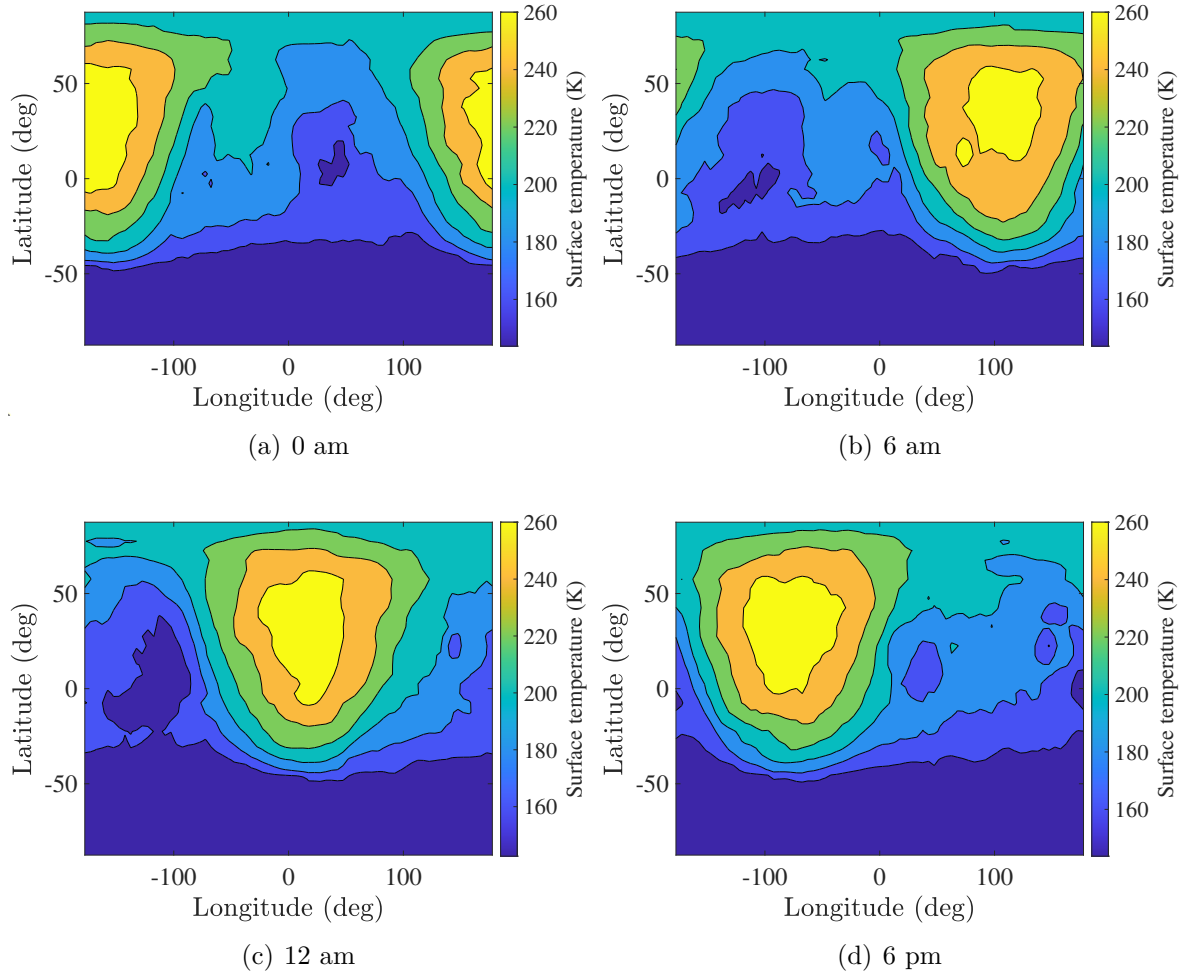


Figure 13: Temperature on Mars at the summer solstice ($L_s = 90^\circ$) for four different AMT hours.

In Fig. 14, the area of low relative humidity is larger than that observed during the spring equinox and is also shifted northwards, as are the temperatures. Here, from 50°S to the South Pole, the relative humidity is around 40% all day. The area encircling the North Pole also has more or less the same characteristics, although the relative humidity is slightly higher. In addition, the isolated area near the equator with lower relative humidities observed at the spring equinox is much less marked at the summer solstice. Again, the 0% relative humidity zone will not be able to accommodate brines while the

zone of maximum relative humidity will be favourable to the deliquescence of all salts. Between the two, the areas encircling the poles will see the formation of brines according to their surface relative humidity. This will be the case for NaClO_4 , $\text{Ca}(\text{ClO}_4)_2$, $\text{Mg}(\text{ClO}_4)_2$ and CaCl_2 . MgCl_2 , NaCl and MgSO_4 have too high a relative humidity for these places.

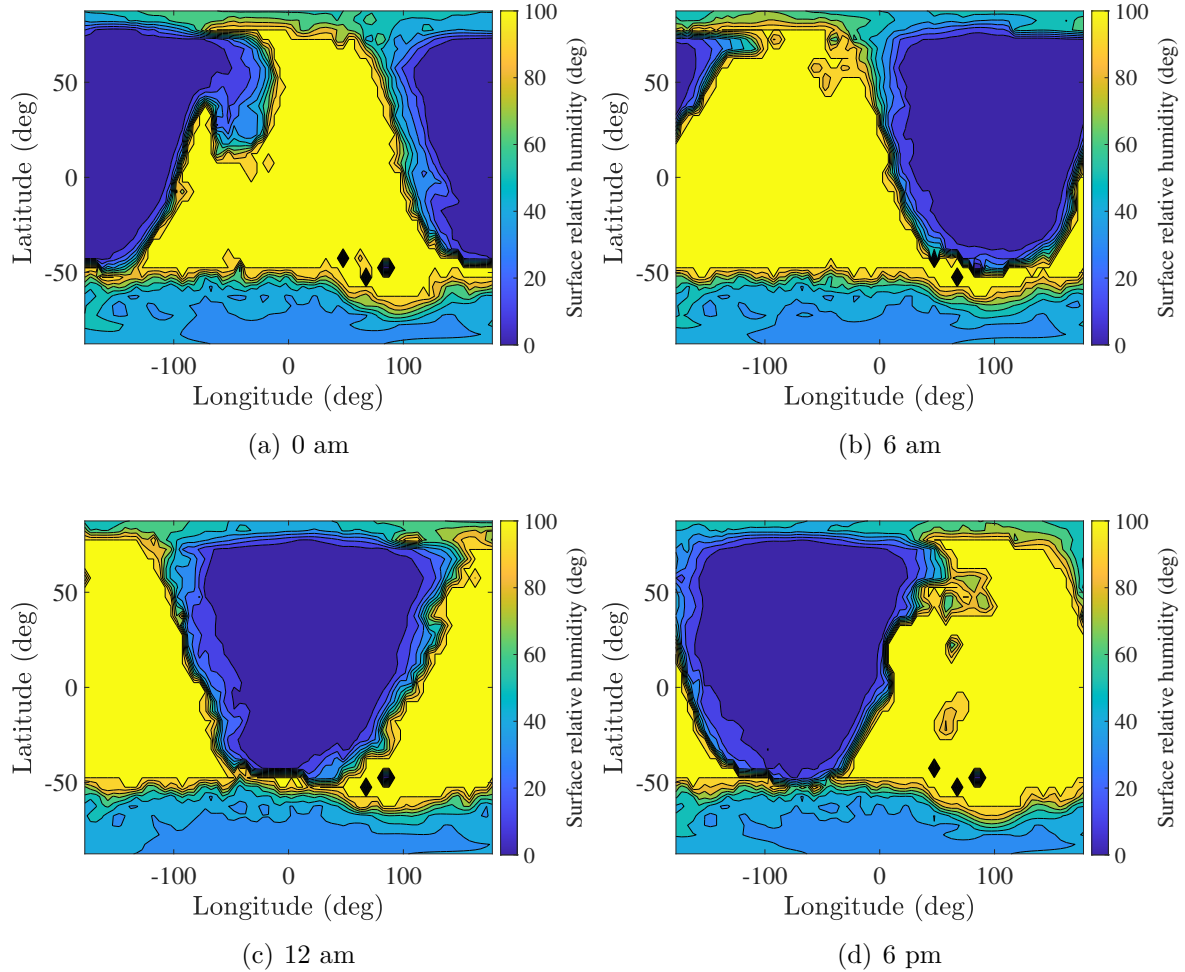


Figure 14: Relative humidity on Mars at the summer solstice ($L_s = 90^\circ$) for four different AMT hours.

4.2.3 Autumn equinox

The northern autumn equinox is defined by a solar longitude of 180° . In the Southern Hemisphere, this period corresponds to the spring equinox. The surface temperatures and relative humidities for $L_s = 180^\circ$ at the four different times are represented in Fig. 15 and Fig. 16 respectively.

When the autumn equinox comes, the situation is more balanced and returns to a form similar to that of the spring equinox. It is noticeable that, in contrast to Fig. 11, temperatures locally reach 280 K throughout the day. Another difference is that the area

from 50°S to 90°S has a constant temperature of 160 K or less. At the spring equinox this was the case but from 50°N to 90°N . The conclusions regarding the deliquescence of the salts remain similar. It is possible for all salts to deliquesce at maximum temperatures. When the temperature goes down to 260 K the deliquescence of MgSO_4 is no longer possible and it is the same for the rest of the salts the further away from the maximum temperature zone. Finally, where $T < 200$ K, the eutectic temperature of the salts is systematically above the surface temperature.

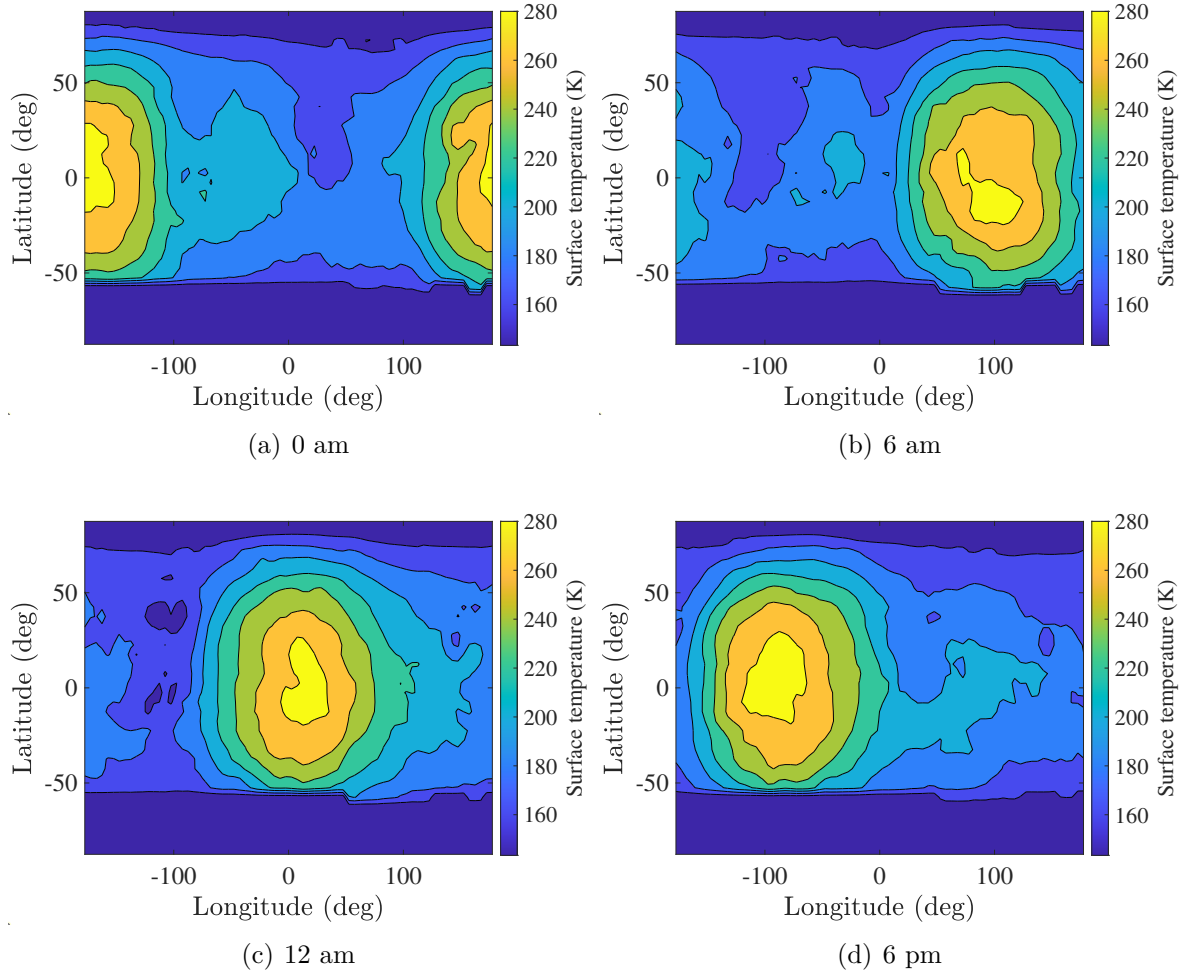


Figure 15: Temperature on Mars at the autumn equinox ($L_s = 180^\circ$) for four different AMT hours.

The relative humidities in Fig. 16 behave rather like those of the spring equinox. However, the areas of very low relative humidities are a little smaller. In addition, a small area of lower relative humidity is found around the South Pole (from 100°W to 100°E). Again, this is in contrast to the situation at the spring equinox where this area was around the North Pole. The deliquescence of NaClO_4 , $\text{Ca}(\text{ClO}_4)_2$, $\text{Mg}(\text{ClO}_4)_2$ and CaCl_2 are favoured in the zones between two extreme RH (having between 40% and 60% relative humidity), while in the saturation zone, all salts can deliquesce and in the dry

zone, no salt is concerned by the phenomenon.

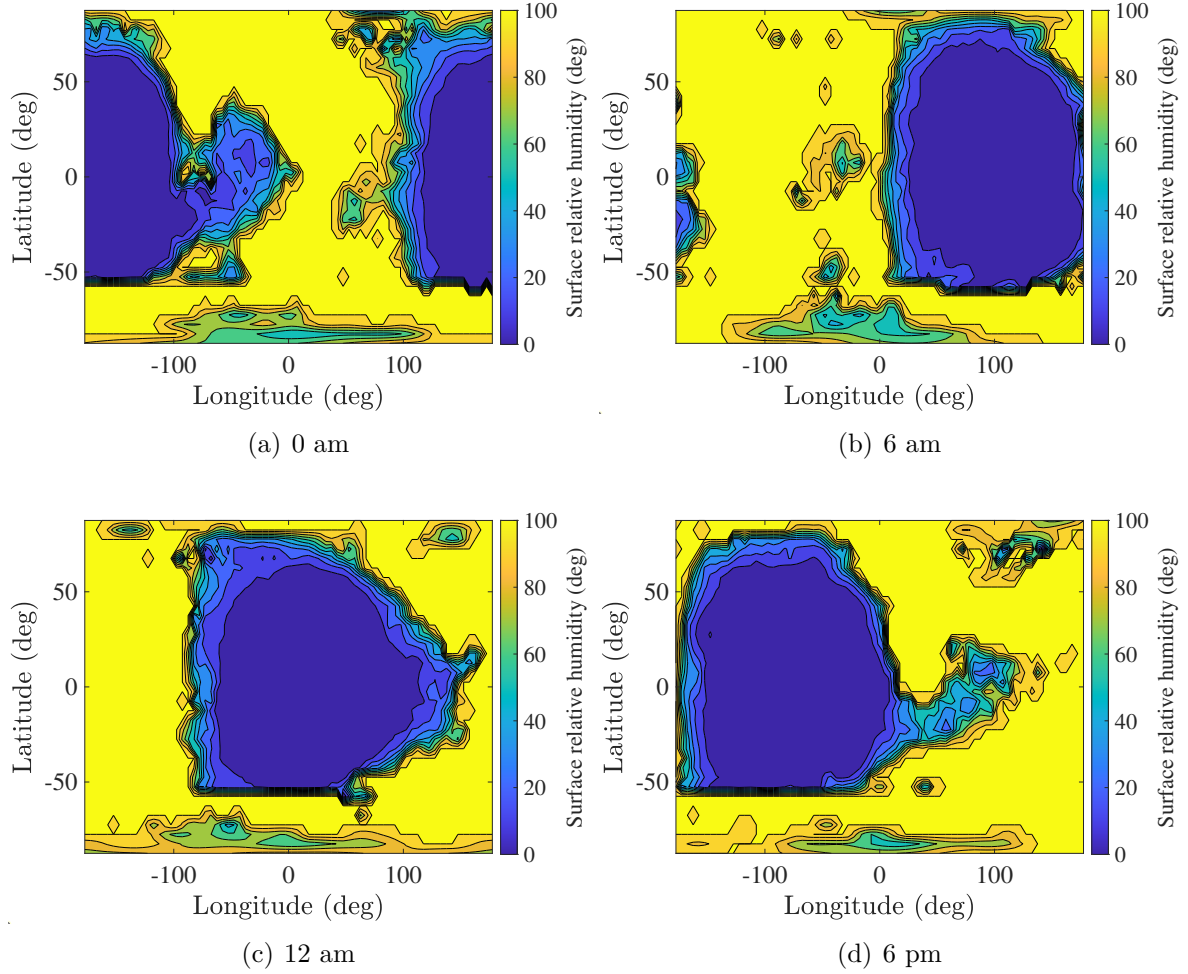


Figure 16: Relative humidity on Mars at the autumn equinox ($L_s = 180^\circ$) for four different AMT hours.

4.2.4 Winter solstice

The northern winter solstice is defined by a solar longitude of 270° . In the Southern Hemisphere, this period corresponds to the summer solstice. The surface temperatures and relative humidities for $L_s = 270^\circ$ at the four different times are represented in Fig. 17 and Fig. 18 respectively.

The temperature pattern in Fig. 17 is roughly the reverse of that observed at the summer solstice (Fig. 13). Note that minimum surface temperatures drop to 150 K in the Northern Hemisphere (above 50°N) and maximum surface temperatures are very high in the Southern Hemisphere at this time, reaching 300 K in very small areas around 40°S . Therefore, the deliquescence of salts can take place over a larger area. Indeed, it is observed that almost the whole Southern Hemisphere is concerned by a minimum

temperature of 225 K allowing the deliquescence of $\text{Ca}(\text{ClO}_4)_2$, $\text{Mg}(\text{ClO}_4)_2$ and CaCl_2 in the whole Southern Hemisphere while the deliquescence areas of NaClO_4 , MgCl_2 , NaCl and MgSO_4 are restricted. In the Northern Hemisphere, the surface temperature does not allow the process to be initiated for any salt.

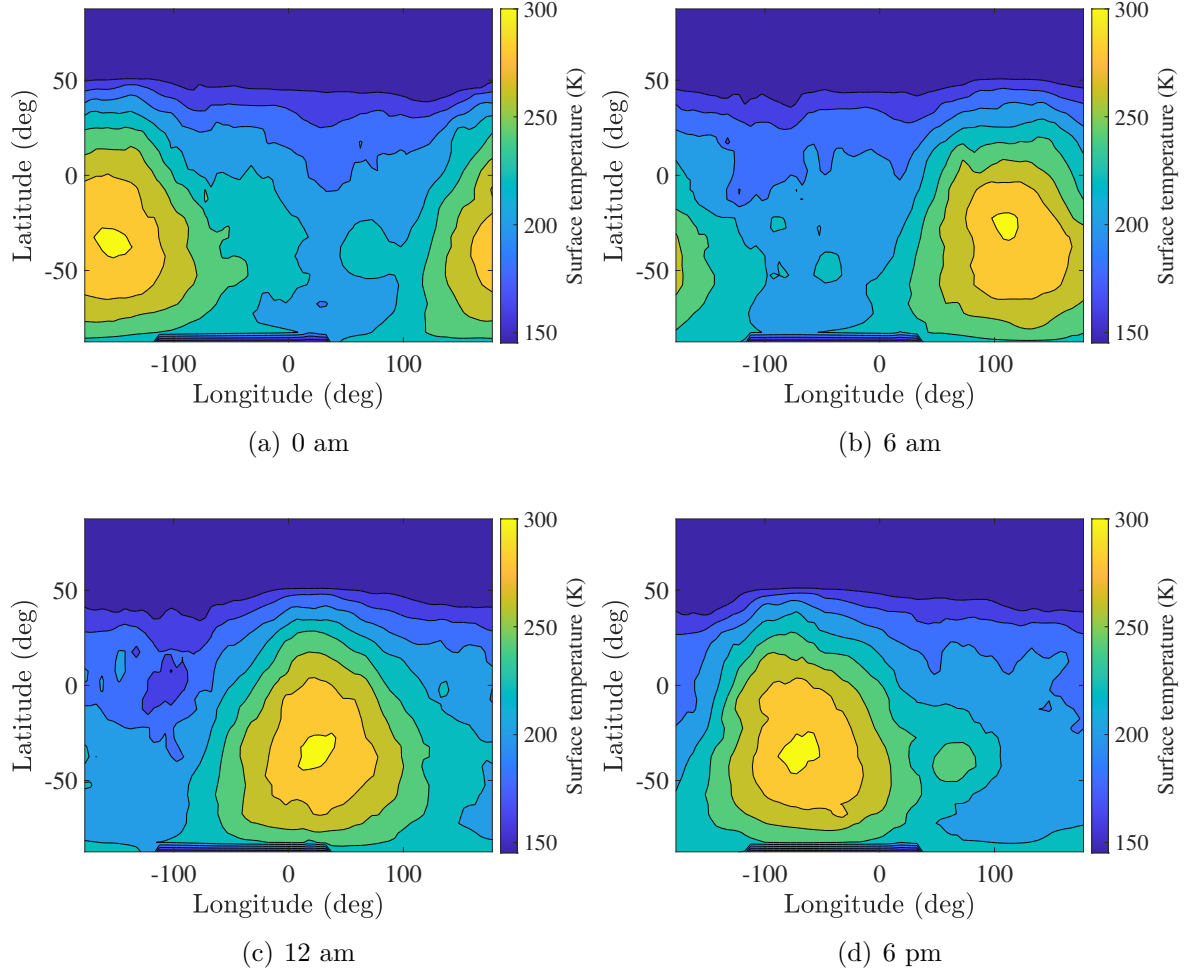


Figure 17: Temperature on Mars at the winter solstice ($L_s = 270^\circ$) for four different AMT hours.

The relative humidities seen in Fig. 18 behave in a novel way. The limited areas of maximum relative humidity are centered around 50°N and are quite complex. Moreover, they are wider in the morning (6 am) and at midday than in the evening (6 pm) and at midnight. A small region of higher relative humidity (located around 25°S) follows the two large northern regions. The north pole is surrounded by a band of medium relative humidities (between 40% and 60%). This was also the case at the summer solstice but around the south pole. The areas where all the salts can deliquesce are therefore also much smaller than in other seasons. Near the North Pole, salts with low deliquescence relative humidity (NaClO_4 , $\text{Ca}(\text{ClO}_4)_2$, $\text{Mg}(\text{ClO}_4)_2$ and CaCl_2) can deliquesce but not those with higher deliquescence relative humidity (MgCl_2 , NaCl and MgSO_4). This

conclusion applies to all areas surrounding the saturation zones.

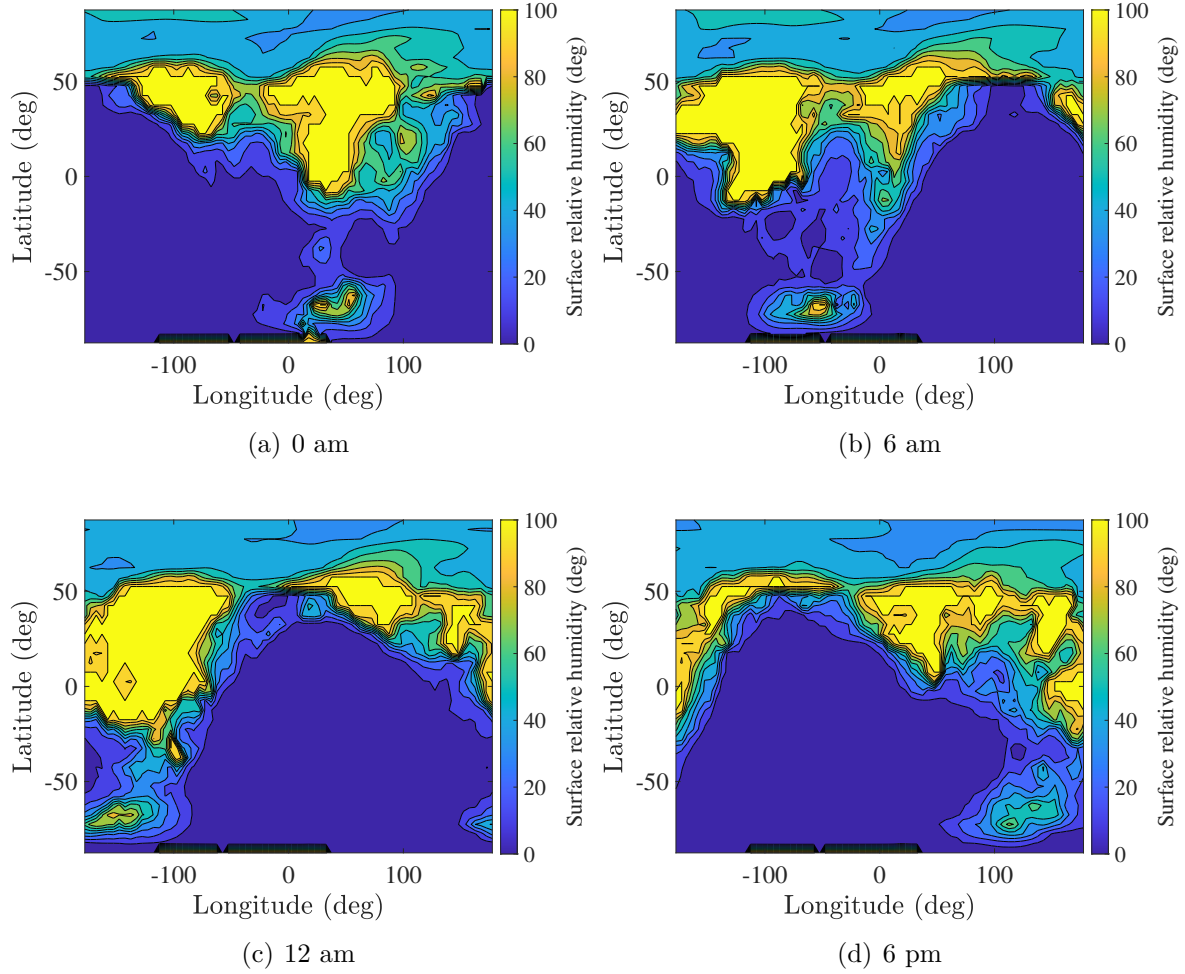


Figure 18: Relative humidity on Mars at the winter solstice ($L_s = 270^\circ$) for four different AMT hours.

4.3 Discussion

According to the global temperature graphs, the maximum temperature is higher in the southern summer and spring. This agrees with Hargitai (2010) who describes the southern hemisphere climate as more extreme and the northern hemisphere as milder. The temperatures are higher between 50°N and 50°S during the autumn and the spring equinoxes. During the northern summer solstice, the area of maximum temperatures is further north while it descends to the south in the northern winter solstice. When the planet is illuminated by the sun and the temperature is high, the relative humidity behaves in the opposite way and reaches a low value (0%). In contrast to the gradually decreasing temperatures, the relative humidities go from their minimum value to their maximum value within a few longitudes. This gradient observed for temperatures is not visible for relative humidities. Moreover, during the northern winter solstice, areas of saturated relative

humidity are smaller. With that being said, for a location to be favourable to salt deliquescence, the temperature as well as the relative humidity must be high. However, since the relative humidity is usually small when the temperature is high and vice versa, both conditions are never met at the extrema of each variable. As a result, the medium value regions, where the two conditions are met, are the most favourable for the deliquescence of salts. This shows that the conditions are encountered simultaneously between 50°N and 50°S in spring. During the summer, they are mostly met in the Northern Hemisphere and up to 50°S . In autumn, the pattern resembles that of spring, but the conditions are satisfied for a longer period of time due to the higher temperatures throughout the day. In winter, the situation is less favourable with good temperatures in the Southern Hemisphere and good relative humidity in the Northern Hemisphere. The conditions are therefore satisfactory especially for the regions around the equator.

5 Landing sites

This section will concentrate on the analysis of the landing sites. First the methodology applied to assess the data and obtain the plots is explained, followed by the description of the results themselves and finally a discussion will end the chapter by establishing the time of the year where the landing sites have the favourable conditions to the presence of brines.

5.1 Methodology

Several locations have been chosen for further analysis. First of all, landing sites because they might have been flooded in the past. By hypothesis, they could therefore have atmospheric characteristics favourable to the presence of brines. Gale Crater has sedimentary residues from ancient lake bed, the Jezero Crater would have been a river delta and Oxia Planum a lake [1][6][9]. They are represented on a map of Mars in Fig. 19. Four regions are located in the Northern Hemisphere (Elysium Planitia, Jezero Crater, Oxia Planum and Vastitas Borealis) while only one site is in the Southern Hemisphere (Gale Crater) but still close to the equator.

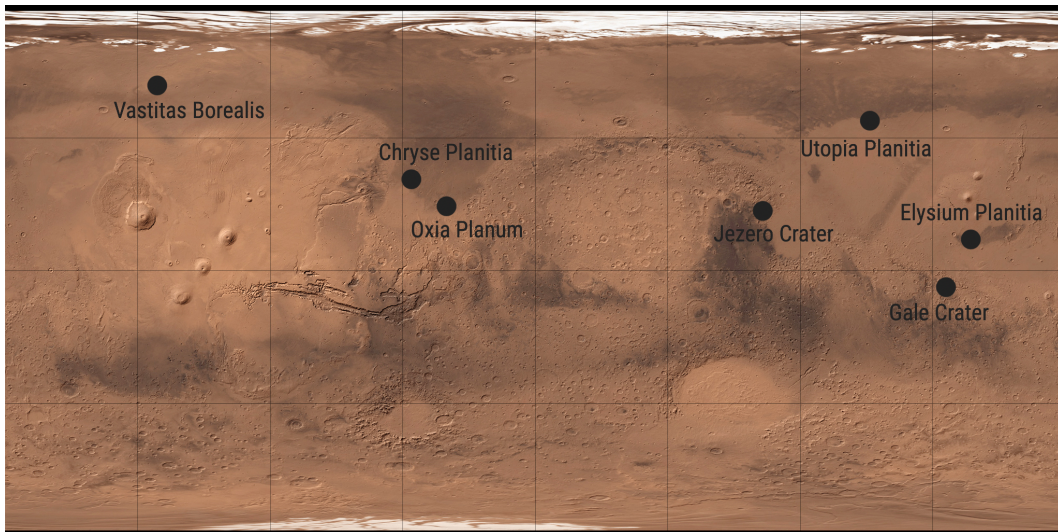


Figure 19: Map of Mars with the landing sites of interest pointed out.

5.2 Results

Here, the outputs (temperature and relative humidity) coming from the MarsWRF model are analysed in terms of salts deliquescence for the seven landing sites.

5.2.1 Vastitas Borealis

Vastitas Borealis is a large northerly lowland surrounding the polar cap. The Phoenix lander built by Lockheed Martin for NASA landed exactly at 68.2°N , 125.75°W [4]. As said in Hargitai (2010), this area regularly experiences fog due to a brighter average albedo [24]. In addition, it results in lower surface temperatures and higher relative humidities. Moreover, its northern position leads to the presence of frost during the winter (from $L_s = 270^\circ$), which disappears in summer (from $L_s = 90^\circ$) by sublimation.

The temperature and relative humidity as a function of the solar longitude at Phoenix landing site are shown in Fig. 20(a) and 20(b) respectively. Looking at both Fig. 20(a) and 20(b), the first thing that stands out is the absence of diurnal temperature variation ($T = 150\text{ K}$) from $L_s = 211^\circ$ to $L_s = 23^\circ$ and at the same time, the increase in relative humidity until the minimum values reach a plateau as well ($RH \approx 40\%$). Vastitas Borealis is near to the northern polar cap, thus it represents the moment when this region is always in the night, inducing no heat to dry out the region. Also, it can be noted that Vastitas Borealis has high temperature maximums ($T_{max} = 254\text{ K}$) due to the obliquity of Mars. It was mentioned above that during the winter the area was constantly in darkness. During spring and summer, the opposite phenomenon is observed and the soil is insulated by the Sun for longer periods of time, resulting in higher surface temperatures.

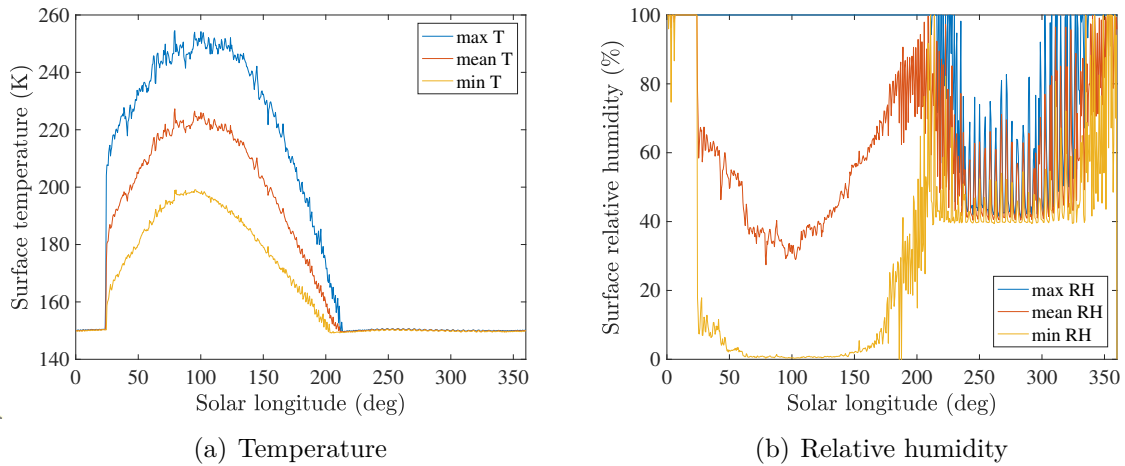


Figure 20: Temperature and relative humidity as a function of the solar longitude at Phoenix landing site. Mean, maximum and minimum values are represented.

Analysis of the data show that the surface temperature is higher than the eutectic temperature of all the salts analysed for at least one sol and for several hours per sol except the MgSO_4 whose eutectic temperature is higher than the maximum surface temperature. The temperature is above the lowest eutectic temperature ($T_{e, \text{Ca}(\text{ClO}_4)_2}$) during $L_s \in [24^\circ; 182^\circ]$. This means the temperature meets the condition during spring and summer. The same is true for $\text{Mg}(\text{ClO}_4)_2$, for which the eutectic temperature is above the

surface temperature from $L_s = 24^\circ$ to $L_s = 176^\circ$. Concerning calcium chloride, the surface temperature exceeds its eutectic temperature also for the first half of the year (from $L_s = 35^\circ$ until $L_s = 160^\circ$). For NaClO_4 , $T > 236$ K from $L_s = 54^\circ$ to $L_s = 145^\circ$ with the most hours meeting the condition in $L_s = 78^\circ$ (11 am to 8 pm). The temperature is above 239.5 K (T_{e,MgCl_2}) for $L_s \in [60^\circ; 144^\circ]$ whereas $T > 252.2$ K (T_{NaCl}) only for $L_s = 78^\circ$, 79° , 94° , 95° , 100° , 101° for about three hours.

From one day to the next, the average relative humidity remain more or less confined within the same range until $L_s = 180^\circ$ when it starts to fluctuate strongly. This happens approximately at the same time that the constant darkness and the temperature plateau. Fig. 20(b) shows that the minimum relative humidity also reach a plateau after $L_s = 200^\circ$. Moreover, it reaches a maximum value of 100% except from $L_s = 211^\circ$ where it starts to fluctuate and reach values of 40%. Therefore, the surface relative humidity is above the NaClO_4 , $\text{Ca}(\text{ClO}_4)_2$, $\text{Mg}(\text{ClO}_4)_2$, CaCl_2 , MgCl_2 , NaCl and MgSO_4 deliquescence relative humidity at least once a day, all days of the year. To begin with, $RH > DRH_{\text{NaClO}_4}$ throughout the year always during twenty-four hours. The same is true for $\text{Ca}(\text{ClO}_4)_2$ and $\text{Mg}(\text{ClO}_4)_2$ except for several point values around $L_s = 250^\circ$. But the hours differ from the range of NaClO_4 : it lasts twenty-four hours during early spring and end of winter, in between the number of hours decreases up to a minimum (from 1 am to 6 am) in $L_s = 102^\circ$. For CaCl_2 and MgCl_2 , the condition is satisfied for $L_s \in [0^\circ; 289^\circ]$ (minus punctual solar longitudes) and for $L_s \in [297^\circ; 360^\circ]$ during the same hours as mentioned before. Concerning NaCl and MgSO_4 , the situation is similar with point values not satisfying the requirement between $L_s = 215^\circ$ and $L_s = 330^\circ$.

The regional dust storms occurring around $L_s = 150^\circ$ and $L_s = 250^\circ$ are of no consequence both on temperature and relative humidity. Indeed, as shown in Fig. 21, the dust optical depth never exceeds a value of 0.25 throughout the year.

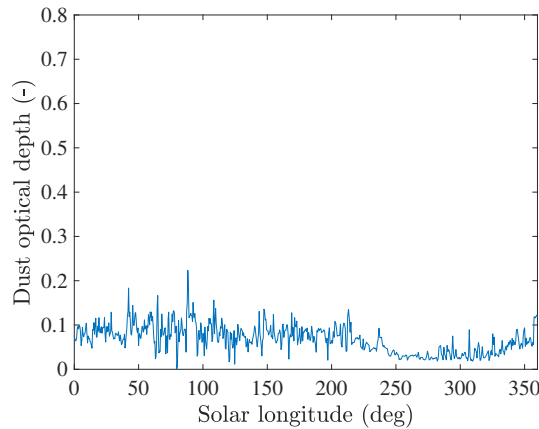


Figure 21: Dust optical depth as a function of the solar longitude at Vastitas Borealis.

5.2.2 Utopia Planitia

Utopia Planitia is also a wide plain, about two times larger than Chryse Planitia. It is the landing site of the Viking 2 probe, twin of Viking 1. More precisely, its lander touched down in the Mie Crater in early September 1976 at 47.6°N , 134.3°E [51]. Like Chryse Planitia, $\text{Ca}(\text{ClO}_4)_2$ would be present but Utopia Planitia seems to contain larger rocks.

The temperature and relative humidity as a function of the solar longitude at Utopia Planitia are represented in Fig. 22(a) and 22(b) respectively. As seen in Fig. 23, dust optical depth peaks just after $L_s = 100^\circ$ and just before $L_s = 250^\circ$. This causes jumps in the temperature plot and even higher in the relative humidity plot. The gradual increase around $L_s = 150^\circ$ did not induce any noticeable fluctuations.

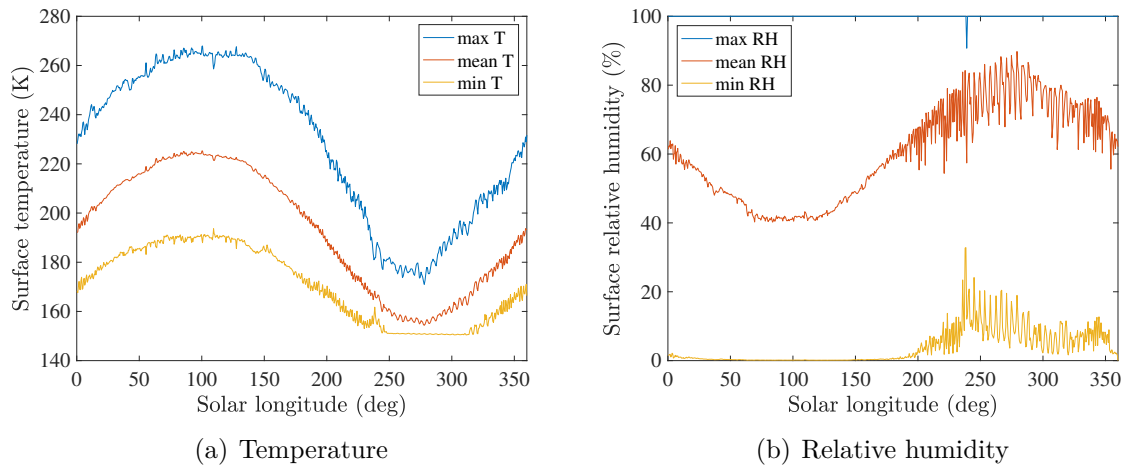


Figure 22: Temperature and relative humidity as a function of the solar longitude at Utopia Planitia. Mean, maximum and minimum values are represented.

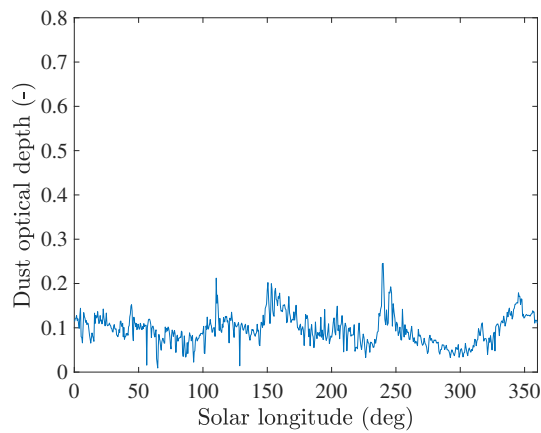


Figure 23: Dust optical depth as a function of the solar longitude at Utopia Planitia.

At Utopia Planitia, the same trend caused by the planet's obliquity (leading to high temperature at the summer solstice and a low temperature plateau during winter) as at Vastitas Borealis is observed. Nonetheless it is less pronounced (maximum temperatures continue to vary) since the plain is less in the north. Furthermore, the maximum temperature computed is higher (267.9 K) and during the temperature plateau period, the temperature is also worth 150 K. The temperature situation is more or less the same as in Vastitas Borealis but with the condition satisfied during wider intervals. $T > T_{e, Ca(ClO_4)_2}$ for $L_s \in [0^\circ; 231^\circ]$, $[317^\circ; 360^\circ]$ up to six hours per day in summer (from 7 pm to 1 am) while $T > T_{e, Mg(ClO_4)_2}$ for $L_s \in [0^\circ; 225^\circ]$ and $[325^\circ; 360^\circ]$. The surface temperature exceeds the $CaCl_2$ eutectic temperature from $L_s = 0^\circ$ to $L_s = 201^\circ$ (for a maximum of twelve hours at the summer solstice) and then from $L_s = 351^\circ$ to $L_s = 360^\circ$. For $Na(ClO_4)$, the temperature is favourable between $L_s = 4^\circ$ and $L_s = 191^\circ$. Concerning $MgCl_2$, it is the case for $L_s \in [10^\circ; 187^\circ]$. Last but not least, the surface temperature is above the $NaCl$ eutectic temperature during a smaller period of time ($L_s \in [36^\circ; 159^\circ]$) with the most hours fulfilling the requirement at $L_s = 100^\circ$ between 11 am and 5 pm.

The average relative humidity at Utopia Planitia behaves differently to that of Vastitas Borealis although large variations from day to day in the mean curve after $L_s = 200^\circ$ are also visible. The maximum value reaches 100% throughout the year except at $L_s = 239^\circ$ where it is 90.7%. Thus the surface relative humidity is above the eutectic relative humidity of all salts all year long except that of $MgSO_4$ at $L_s = 239^\circ$.

5.2.3 Chryse Planitia

Chryse Planitia (Golden Plains) is a large plain formed by the impact of an object on the planet. It was home to the NASA-built Viking 1 probe, whose lander landed on Mars in July 1976. The geographical coordinates of the landing site are $22.3^\circ N$, $49.95^\circ W$ [51]. A little further north than the Jezero Crater and Oxia Planum, the climate at Chryse Planitia is mild Transitional, at the edge of Tropical [24]. As said in Sec. 2.2, calcium perchlorate was detected there.

The temperature and relative humidity as a function of the solar longitude at Chryse Planitia are represented in Fig. 24(a) and 24(b) respectively. The optical depth shown in Fig. 25 increases largely at $L_s = 250^\circ$ ($\tau = 0.6$) suggesting that the storm occurred not far from Chryse Planitia. This second dust storm induces downwards jump in the T -plot and consequently increase in the RH -plot. The first regional (around $L_s = 150^\circ$) storm also induces temperature and relative humidity variations but less marked than those due to the second storm.

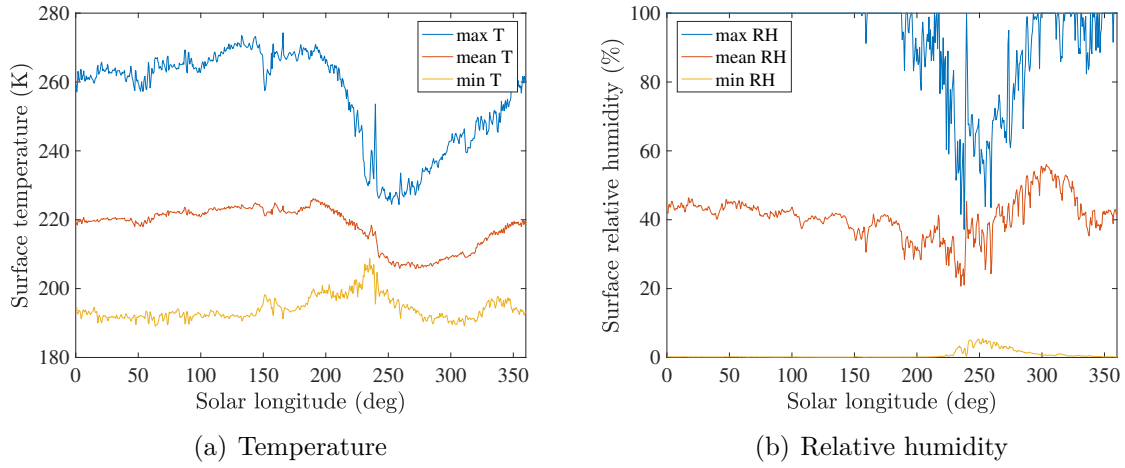


Figure 24: Temperature and relative humidity as a function of the solar longitude at Chryse Planitia. Mean, maximum and minimum values are represented.

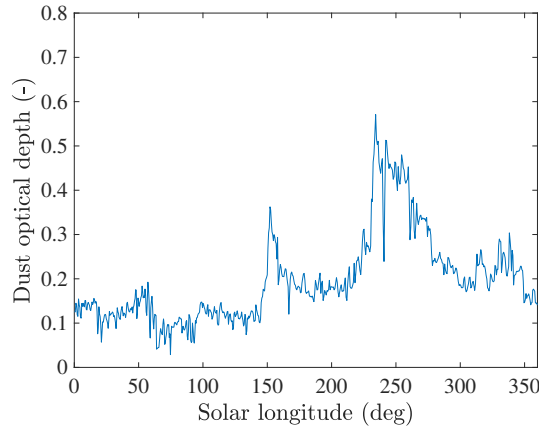


Figure 25: Dust optical depth as a function of the solar longitude at Chryse Planitia.

Chryse Planitia has less extreme seasonal temperature variations. The maximum temperature is 273.5 K at $L_s = 132^\circ$ (exactly halfway through the summer). The surface temperature allows the deliquescence of all salts at least once during the year. The surface temperature is above the eutectic temperature of the $\text{Ca}(\text{ClO}_4)_2$, $\text{Mg}(\text{ClO}_4)_2$ and CaCl_2 all year. In terms of hours, it is true for $\text{Ca}(\text{ClO}_4)_2$ during about twenty hours during spring and summer and all day between $L_s = 188^\circ$ to $L_s = 249^\circ$. It corresponds to the period when the storm arises until it dies. For $\text{Mg}(\text{ClO}_4)_2$, days with twenty-four hours valid temperatures are around $L_s = 235^\circ$. The condition is always met for more than eight hours. Next, $T > T_{e,\text{CaCl}_2}$ all year round for almost eleven hours except around $L_s = 258^\circ$ where the temperature is right only at 3 pm. This decrease in temperature is a consequence of the second storm. Considering NaClO_4 , surface temperatures are higher than its eutectic temperature from $L_s = 0^\circ$ to $L_s = 240^\circ$ and from $L_s = 286^\circ$ to $L_s = 360^\circ$. Thus it covers all seasons except a part during winter. The conclusion is almost the same for MgCl_2 with a valid period obviously shorter due to the higher eutectic temperature

of MgCl_2 ($L_s \in [0^\circ; 239^\circ]$, $[298^\circ; 360^\circ]$). Regarding NaCl , the temperature is greater than its eutectic temperature for $L_s \in [0^\circ; 221]$, $L_s = 222^\circ$ and $L_s \in [340^\circ; 360^\circ]$ meaning only during spring, summer and end of winter. Finally, for the salt with the highest eutectic temperature ($T_{e,\text{MgSO}_4} = 268.6 \text{ K}$), the interval is much narrower ($L_s \in [87^\circ; 194^\circ]$) corresponding to summertime.

The relative humidity is worth 100% until mid-year where it starts to decrease and fluctuate from one day to the next. The lowest maximum relative humidities are around 50%. Therefore all deliquescence relative humidities are below the surface relative humidity for the first part of the year. During the second half, some salts will not be able to deliquesce at punctual solar longitudes due to their high deliquescence relative humidity. It is the case for MgCl_2 , NaCl and MgSO_4 for which the condition is not met for point values during $L_s \in [220^\circ; 286^\circ]$. Whereas NaClO_4 , $\text{Ca}(\text{ClO}_4)_2$, $\text{Mg}(\text{ClO}_4)_2$ and CaCl_2 have a deliquescence relative humidity below the surface relative humidity throughout the year. Owing to the low deliquescence relative humidity value of the sodium perchlorate, the condition is always met during twenty-four hours.

5.2.4 Jezero Crater

The Jezero Crater, more specifically the Octavia E. Butler Landing, is the landing site of the US Perseverance rover built by the Jet Propulsion Laboratory. The 45 km diameter crater is located in Nili Fossae on the edge of Isidis Planitia and not far east of Syrtis Major, a high contrast terrain with a lower albedo. Its precise geographical coordinates are 18.4°N , 77.5°E [6]. This site is therefore just underneath the Tropic of Pisces but, although it is found further north, it has a tropical climate, bordering on the Low albedo tropical climate of Syrtis Major [24].

The temperature and relative humidity as a function of the solar longitude at Jezero Crater are represented in Fig. 26(a) and 26(b) respectively. The surface temperature has a high diurnal variation (80 K). The surface relative humidity curve is quite smooth during the first half of the year and then the maximum values fall downwards. Moreover, jumps in temperature associated to jumps in relative humidity are visible at $L_s = 150^\circ$ and slightly around $L_s = 250^\circ$. Fig. 27 shows an extreme increase of the dust optical depth at the first solar longitude ($\tau = 0.75$) meaning the storm was the most intense at this location. The second storm did not impact it in this way.

Owing to the high temperature maximums, five salts have a eutectic temperature below the surface temperature: $\text{Ca}(\text{ClO}_4)_2$, $\text{Mg}(\text{ClO}_4)_2$, CaCl_2 , NaClO_4 and MgCl_2 . The higher the eutectic temperature of the salt, the lower the maximum number of hours during which the condition is satisfied. The condition is met all day for $\text{Ca}(\text{ClO}_4)_2$ and $\text{Mg}(\text{ClO}_4)_2$,

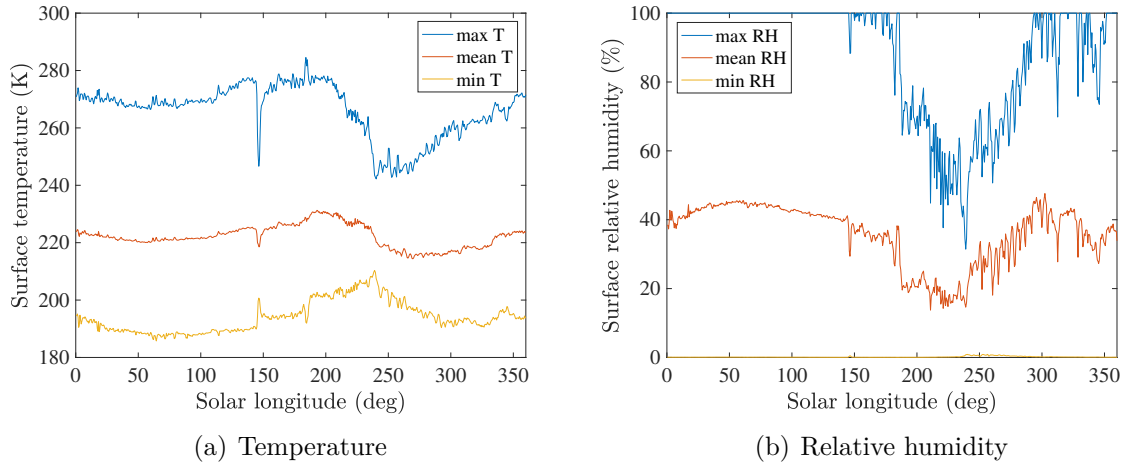


Figure 26: Temperature and relative humidity as a function of the solar longitude at Jezero Crater. Mean, maximum and minimum values are represented.

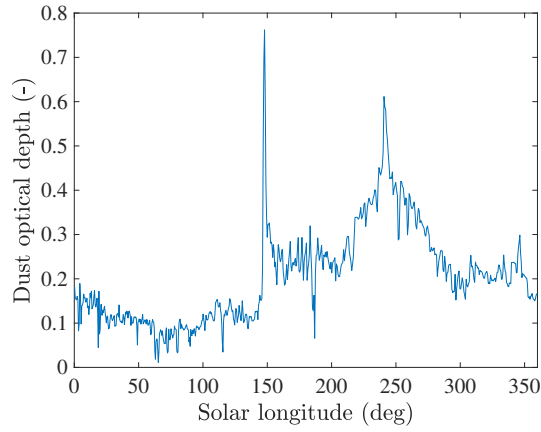


Figure 27: Dust optical depth as a function of the solar longitude at Jezero Crater.

but night hours are excluded for the three remaining salts. Concerning the other two salts, the condition is satisfied for the NaCl during 596 sols ($L_s \in [0^\circ; 236], [280; 360]$ and in $L_s = 250^\circ$) and for the MgSO_4 only for 350 sols ($L_s \in [0^\circ; 215], [349^\circ; 360^\circ]$ and in $L_s = 335^\circ$) for up to five hours. The ranges represent spring, summer, early autumn and end of winter.

In Fig. 26(b), the maximum relative humidity is equal to 100% and the minimum equal to 0% during half the year except for the one-off value jump. Then it decreases and reach low maximum value (31.5%) and then increases again to 100%. The surface relative humidity is above the deliquescence relative humidity of all salts for long periods of time. For perchlorates (NaClO_4 , $\text{Ca}(\text{ClO}_4)_2$, $\text{Mg}(\text{ClO}_4)_2$, the condition is met all year except for several sols throughout the autumn between $L_s = 219^\circ$ and $L_s = 241^\circ$). These salts are differentiated by the number of hours during which the condition is valid. Indeed, for NaClO_4 , having the lowest deliquescence relative humidity, the condition is valid every

day for twenty-four hours whereas the interval closes for $\text{Ca}(\text{ClO}_4)_2$ and $\text{Mg}(\text{ClO}_4)_2$ with only a few hours at night. Concerning calcium chloride, the requirement lasts from $L_s = 0^\circ$ to $L_s = 216^\circ$ corresponding to spring, summer and early autumn first during around nine hours then for only three to four hours. Afterwards from $L_s = 257^\circ$ to the end of the year with occasional value at $L_s = 218^\circ, 233^\circ, 245^\circ, 246^\circ, 247^\circ, 249^\circ, 250^\circ, 251^\circ$ for a number of hours that vary from day to day but reach eleven hours just after the winter solstice. For the other chloride, the valid period is from $L_s = 0^\circ$ to $L_s = 187^\circ$ with the most hours (ten hours) from mid-spring to mid-summer then from $L_s = 279^\circ$ to $L_s = 360^\circ$ with point values in $L_s = 196, 205^\circ$ and 276° . Once more, the non valid period corresponds to autumn and the number of hours in winter fluctuate strongly depending on the sol. Regarding the NaCl deliquescence relative humidity, the surface relative humidity exceeds it for 508 sols from $L_s = 0^\circ$ to $L_s = 186^\circ$ and from $L_s = 279^\circ$ to $L_s = 360^\circ$). The conclusion is the same for the salt with the highest deliquescence relative humidity (MgSO_4) but with a second period beginning at $L_s = 292^\circ$. The hours meeting the condition are relatively similar.

5.2.5 Oxia Planum

Oxia Planum has been chosen by ESA as the landing site for the ExoMars2022 mission. This basin is located on the eastern edge of Chryse Planitia at 18.2°N , 24.65°W [9]. Like Jezero Crater, Oxia Planum is close to the Tropic of Pisces, giving it a tropical climate [24]. The temperature and relative humidity as a function of the solar longitude at Oxia Planum are represented in Fig. 28(a) and 28(b) respectively.

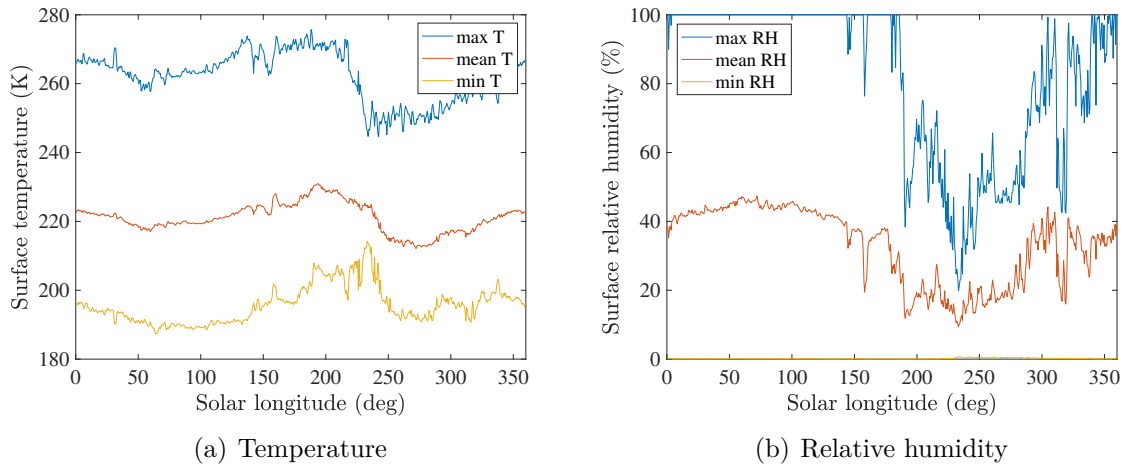


Figure 28: Temperature and relative humidity as a function of the solar longitude at Oxia Planum. Mean, maximum and minimum values are represented.

Located at the same latitude as Jezero Crater, their plots are similar. However, maximum temperatures are lower than in the crater. Compared to Chryse Planitia plots, the maximum temperatures are this time higher. Although to a lesser extent, the downward

jump in the data around $L_s = 150^\circ$ is also observed. In Fig. 29, it is seen that the dust optical depth has raised but not as much as in Jezero Crater. The second jump is more distinct since Oxia Planum is near Chryse Planitia and therefore more impacted by the second dust storm.

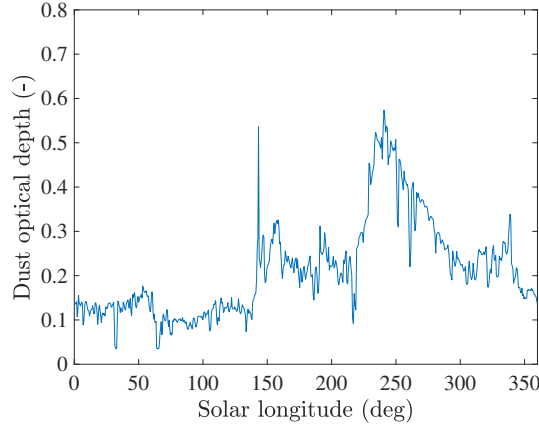


Figure 29: Dust optical depth as a function of the solar longitude at Oxia Planum.

The maximum temperature is relatively high all year with a lowest maximum value of 244 K in $L_s = 233^\circ$. Hence, the surface temperature is above the eutectic temperature of the $\text{Ca}(\text{ClO}_4)_2$, $\text{Mg}(\text{ClO}_4)_2$, CaCl_2 , NaClO_4 and MgCl_2 at least several hours per day all year. For the calcium and magnesium perchlorates, the condition is satisfied all hours of the day while only for a maximum of thirteen hours for CaCl_2 (never less than seven hours) and nine hours for NaClO_4 and MgCl_2 (never less than five hours). For salts with higher eutectic temperatures (NaCl and MgSO_4), the condition is encountered occasionally or during certain windows. T is above $T_{e,\text{NaCl}}$ between $L_s = 0^\circ$ and $L_s = 229^\circ$, punctually at $L_s = 237^\circ, 254^\circ, 259^\circ, 260^\circ$, then for $L_s \in [263^\circ; 265^\circ]$, $[284^\circ; 285^\circ]$ and $[291^\circ; 360^\circ]$ for less than seven hours a day. Finally, $T > 268.6 \text{ K}$ (T_{MgSO_4}) for $L_s = 6^\circ$ and $L_s \in [30^\circ; 32^\circ]$, $[125^\circ; 140^\circ]$, $[146^\circ; 150^\circ]$, $[158^\circ; 208^\circ]$, $[210^\circ; 211^\circ]$ and $[215^\circ; 217^\circ]$ for at most three hours.

Regarding the relative humidity, the average values oscillate between 11% and 41%. At $L_s = 143^\circ$, they start to decrease and fluctuate until the end of the year. As previously, the second half of the year does not have a maximum relative humidity value of 100%. Therefore, $RH > DRH_{\text{NaClO}_4}$ for twenty-four hours from $L_s \in [0^\circ; 208^\circ]$, $[210^\circ; 220^\circ]$, $[248^\circ; 360^\circ]$ and occasionally at $L_s = 222^\circ, 224^\circ, 242^\circ$. The surface relative humidity is above that of the $\text{Ca}(\text{ClO}_4)_2$ for $L_s \in [0^\circ; 220^\circ]$, $[248^\circ; 261^\circ]$, $[27^\circ; 360^\circ]$. Moreover there are also point values in $L_s = 222^\circ, 242^\circ$. The longest periods are in spring to early summer with $RH > DRH_{\text{Ca}(\text{ClO}_4)_2}$ for eleven hours (from 9 pm to 7 am). Then the intervals shorten until they reach only one valid hour (at 4 am, 5 am or 6 am) after the autumnal equinox. Then they increase again, but not as much as in spring. For $\text{Mg}(\text{ClO}_4)_2$, the

condition is met all year except for 7 sols between $L_s = 189^\circ$ and $L_s = 196^\circ$. The hours situation is the same as for the $\text{Ca}(\text{ClO}_4)_2$. The relative humidity is favourable to the deliquescence of CaCl_2 during $L_s \in [0^\circ; 207^\circ]$, $[286^\circ; 360^\circ]$ and occasionally for $L_s = 211^\circ$, 214° , 215° , 216° and 260° . As far as hours are concerned, it is good for ten hours (10 pm to 7 am) during spring and summer, then the range decreases. When the condition is met again, it rises up to nine hours per sol (around one third of the winter). Although similar, the ranges are smaller for MgCl_2 than for CaCl_2 ($L_s \in [0^\circ; 188^\circ]$, $[291^\circ; 360^\circ]$). The hours intervals are, in turn, equivalent. Concerning NaCl , its deliquescence relative humidity is exceeded by the surface relative humidity from $L_s = 0^\circ$ until $L_s = 188^\circ$, from $L_s = 293^\circ$ until $L_s = 294^\circ$ and from $L_s = 299^\circ$ until $L_s = 360^\circ$. It is true for at most ten hours around the end of spring and between one or four hours during autumn and winter. Ultimately, $RH > DRH_{\text{MgSO}_4}$ for $L_s \in [0^\circ; 185^\circ]$, $L_s = 304^\circ$, 310° , 321° and $L_s \in [339^\circ; 360^\circ]$ for a maximum of nine hours (11 pm to 7 am) around $L_s = 80^\circ$. Thus the period satisfied by the requirement corresponds to spring, summer and end of winter.

5.2.6 Elysium Planitia

InSight, a lander constructed by Lockheed Martin and managed by NASA, has landed at Elysium Planitia on November 2018. The landing site is positioned at 4.5°N , 136°E [2]. The plain is close to the equator, generating a tropical climate with small seasonal variations [24] [21]. Moreover, its surface is relatively smooth and dotted with impact craters [21]. The temperature and relative humidity as a function of the solar longitude at Elysium Planitia are represented in Fig. 30(a) and 30(b) respectively.

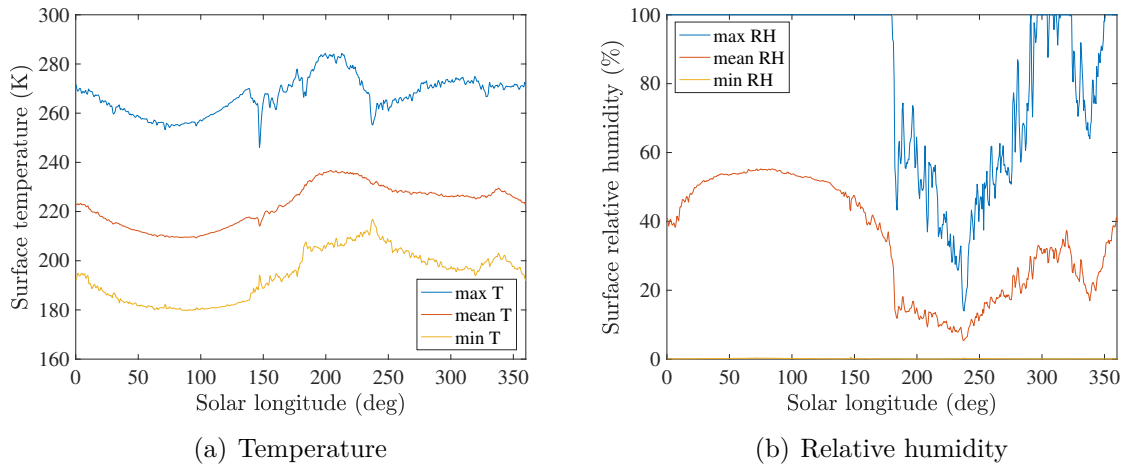


Figure 30: Temperature and relative humidity as a function of the solar longitude at Elysium Planitia. Mean, maximum and minimum values are represented.

During the first half of the year, data (temperature and relative humidity) is smooth but it begins to vary significantly just before $L_s = 150^\circ$. Moreover, the downward jump in the maximum temperature curve before $L_s = 250^\circ$ is visible. These jumps are linked

to the dust storms. Indeed, Fig. 31 shows the optical depth as a function of the solar longitude and one can clearly observe the rapid growth at $L_s = 150^\circ$ and $L_s = 250^\circ$.

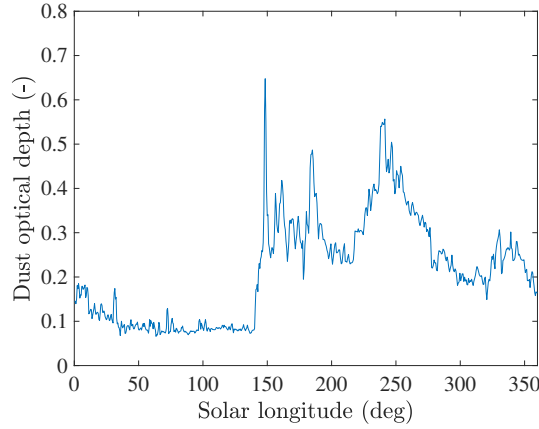


Figure 31: Dust optical depth as a function of the solar longitude at Elysium Planitia.

The highest temperature (284 K) occurs in $L_s = 199$. For that reason, the temperature permits the deliquescence of all the salts at least once a year except MgSO_4 . It is true often during twenty-four hours around the winter solstice for the $\text{Ca}(\text{ClO}_4)_2$ and the $\text{Mg}(\text{ClO}_4)_2$. For CaCl_2 , the minimum number of hours (from 11 am to 5 pm) is found around the summer solstice and the maximum again around the winter solstice (from 9 am to 11 pm). The temperature is favourable for the deliquescence of NaClO_4 and MgCl_2 for about the same number of hours (approximately ten hours) while for NaCl it is mostly in the afternoon (between 1 pm and 5 pm). The surface temperature is above the MgSO_4 eutectic temperature during only 284 sols: $L_s \in [0^\circ; 12^\circ]$, $[134^\circ; 139^\circ]$, $[163^\circ; 231^\circ]$ and $[273^\circ; 360^\circ]$.

Like the other relative humidity plots studied above, the average curve during the first half of the year forms an arc and this time it is quite pronounced. Although the first storm occurs around $L_s = 150^\circ$, the main downward step occurs around $L_s = 175^\circ$. After that, the maximum values drop completely and are very variable from day to day. Two main periods with relative humidity lower than 100% stand out ($[179^\circ; 295^\circ]$, $[322^\circ; 350^\circ]$). Therefore, the surface relative humidity is above the deliquescence relative humidity of NaClO_4 from $L_s = 0^\circ$ to $L_s = 215^\circ$, from $L_s = 258^\circ$ to $L_s = 360^\circ$ and in between punctually at $L_s = 248^\circ, 252^\circ, 254^\circ, 255^\circ$ for all hours of the day. It is almost the same conclusion for the $\text{Ca}(\text{ClO}_4)_2$ and the $\text{Mg}(\text{ClO}_4)_2$: $L_s \in [0^\circ; 214^\circ]$, $[258^\circ; 360^\circ]$ in the late evening and at night (around eleven hours) during spring and summer then for less hours (only in the early morning) during cold seasons. The condition is satisfied for the chlorides (CaCl_2 and MgCl_2) from $L_s = 0^\circ$ until $L_s = 181^\circ$ (mostly for the early hours and the evening) and from $L_s = 280^\circ$ to the end of the year. Concerning NaCl , the range narrows further and the surface relativity is above the deliquescence relative humidity for $L_s \in [0^\circ; 181^\circ]$ (early

hours and late evening) and $L_s \in [290^\circ; 360]$ (early in the morning). $RH > DRH_{MgSO_4}$ for $L_s \in [0^\circ; 179^\circ], [290^\circ; 360^\circ]$. Again, this is true for the first period between approximately 9 pm and 7 am. Regarding the second L_s range, it is valid between 4 am and 7 am. From what has been said, the requirement is met during autumn, winter, end of spring and summer.

5.2.7 Gale Crater

The Gale Crater (4.5°S , 137.4°E [1]) hosted the US MSL rover Curiosity. Located south of Elysium Planitia, its climate is also tropical [24]. The temperature and relative humidity as a function of the solar longitude at Gale Crater are represented in Fig. 32(a) and 32(b) respectively.

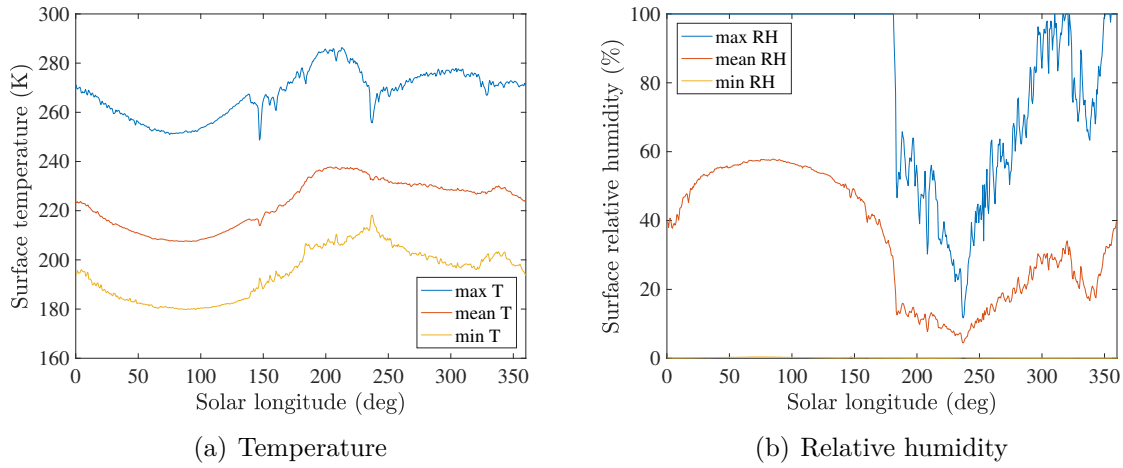


Figure 32: Temperature and relative humidity as a function of the solar longitude at Gale Crater. Mean, maximum and minimum values are represented.

Gale Crater is located in the Southern Hemisphere, resulting in lower temperatures during northern spring/summer and higher in northern autumn/winter. Since it is located south of Elysium Planitia, the trends are the same. The crater is impacted equally by the first and second dust storms although the second event seems to appear in a much more pronounced way (see Fig. 33). Comparably to Elysium Planitia, the surface temperature never falls below 250 K ($T_{max} = 286$ K in $L_s = 212^\circ$, mid-spring) being favourable to the deliquescence of $\text{Ca}(\text{ClO}_4)_2$, $\text{Mg}(\text{ClO}_4)_2$, CaCl_2 , NaClO_4 and MgCl_2 throughout the year. The discussion about the number of hours allowing the deliquescence is the same as in Sec. 5.2.6. Here, the surface temperature is above the MgSO_4 eutectic temperature for 315 sols: $L_s \in [0^\circ; 3^\circ]$, $L_s = 7^\circ$ and 10° and $L_s \in [163^\circ; 360^\circ]$ for at most five hours.

Albeit the Gale Crater is located in the Southern Hemisphere, Fig. 32(b) shows the same curves evolution as for the relative humidity at the nearby Elysium Planitia. Nevertheless, one can see that the relative humidity is worth 100% for a shorter period of

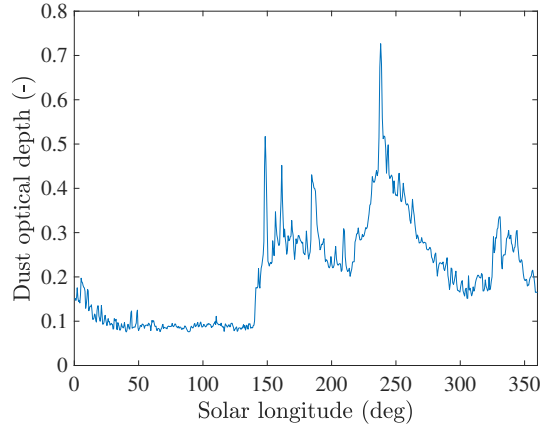


Figure 33: Dust optical depth as a function of the solar longitude at Gale Crater.

time with a different value from $L_s = 181$ to $L_s = 318$ and from $L_s = 321^\circ$ to $L_s = 350^\circ$ with one point value afterwards ($L_s = 354^\circ$). It corresponds to spring and part of the summer. The consequences for salts will therefore be slightly different. Regarding NaClO_4 , its deliquescence relative humidity is below the surface relative humidity for $L_s \in [0^\circ; 200^\circ]$, $[205^\circ; 206^\circ]$, $[210^\circ; 214^\circ]$, $[258^\circ; 360^\circ]$, 252° , 254° , 255° and all day long. $RH > DRH_{\text{Ca}(\text{ClO}_4)_2}$ for $L_s \in [0^\circ; 200^\circ]$, $[210^\circ; 214^\circ]$, $[258^\circ; 360^\circ]$ and at $L_s = 206^\circ$, 255° . The largest number of hours is from mid-autumn to mid-winter (approximately fourteen hours), then just one hour around spring equinox followed by an increase again. The surface relative humidity is above the $\text{Mg}(\text{ClO}_4)_2$ deliquescence relative humidity during $L_s \in [0^\circ; 200^\circ]$, 206° , $[210^\circ; 213^\circ]$, 255° , $[258^\circ; 360^\circ]$. The hours meeting the condition are the same than for $\text{Ca}(\text{ClO}_4)_2$. For CaCl_2 , the ranges are $[0^\circ; 182^\circ]$, $[187^\circ; 189^\circ]$, $[196^\circ; 197^\circ]$, 259° , $[265^\circ; 266^\circ]$, 268° , $[276^\circ; 360^\circ]$ and the condition is fulfilled for the longest time (between 8 pm and 8 am) around the winter solstice whereas it is met for the least number of hours (one hour at 5 am) around the summer solstice. Now, for the MgCl_2 , there are two distinct periods ($L_s \in [0^\circ; 182^\circ]$, $[289^\circ; 360^\circ]$), first between 2 am and 8 am then it increases up to twelve hours (8 pm to 8 am) and finally reduces during the second period. Same is true for the NaCl ($L_s \in [0^\circ; 182^\circ]$, $[290^\circ; 360^\circ]$) while for MgSO_4 , the condition is encountered during even shorter periods ($L_s \in [0^\circ; 181^\circ]$, $[303^\circ; 360^\circ]$) but with two punctual values ($L_s = 296^\circ$, 301°) with always the same hours scheme.

5.3 Discussion

This section will outline the times of year when temperature and relative humidity are simultaneously favourable to the deliquescence of the different salts, for all studied sites. First, a discussion about the overall temperature and relative humidity plots shape is made. The maximum temperature curves all follow the same seasonal trends (more pronounced for high latitudes locations and conversely for low latitudes locations) – except at Elysium Planitia and Gale Crater – : temperatures are higher during the first half of the year (maximum around the summer solstice) and decrease to reach a minimum at the winter solstice. The minimum curve, in turn, often reach a maximum at this period. At Gale Crater, the opposite is visible, which is not surprising since it is located in the Southern Hemisphere. The situation at Elysium Planitia appears to be more complex. This plain is located in the Northern Hemisphere, near the equator and has a temperature pattern similar to that of Gale Crater. This could be caused by the topography and/or soil properties. Moreover, only Vastitas Borealis and Utopia Planitia do not have temperature maximum high enough to satisfy the MgSO_4 condition (further north, their temperatures are lower). Last thing to note is that Chryse Planitia, Jezero Crater, Oxia Planum, Elysium Planitia and Gale Crater have a maximum temperature exceeding the melting temperature of pure water (273 K). Therefore, the surface temperature is theoretically not an obstacle to the melting of pure water at these locations.

The maximum relative humidity curves are similar for all places – except at Vastitas Borealis and Utopia Planitia – : the relative humidity is saturated during the first half of the year until $L_s = 150^\circ$, followed by a significant drop and lower maximums values reached around $L_s = 250^\circ$. Throughout this decrease, values strongly vary from day to day and the curve becomes chaotic. The minimum curves always stay close to 0%, sometimes reaching a maxima around $L_s = 250^\circ$. These two curves result in average values which follow broadly the same pattern characterised by a semi-circle in the first half of the year (with a maxima around $L_s = 100^\circ$) and then variations in the second half. The further south the latitude is, the more curved the semi-circle. Therefore, for these locations, the windows during which the surface relative humidity is above the deliquescence relative humidity are roughly the same whether they are in the northern or Southern Hemisphere and for all the salts. At Vastitas Borealis and Utopia Planitia, the situation is different but not equal. Concerning the northernmost one, the minimum relative humidity reaches a plateau of maximum values when the maximum temperature reaches a plateau of minimum values. Moreover, the minimum and maximum curves almost merge in the second half of the year. For Utopia Planitia, the maximum values stay at 100% throughout the year while the minimum values begin to increase after $L_s = 200^\circ$. Lastly, the relative humidities satisfy the condition at least several times a year for every salts.

The dust storms effects are always more pronounced in the temperatures plots than in the relative humidity plots. But they all have scars from the two storms to a greater or lesser extent. From the dust optical depth plots, the first regional dust storm was more intense at Jezero Crater, Elysium Planitia whereas the second event was more pronounced at Chryse Planitia and Gale Crater. The further away one is from these places, the lower the dust optical depth and therefore the less the effects of the storms are felt, if at all as in Vastitas Borealis and Utopia Planitia. As explained in Sec. 2.4, it is clear from the temperature plots that when a storm occurs, the maximum temperatures decrease and vice versa for the minimum temperatures.

Now, the focus is made on when the conditions are simultaneously met. The first thing to mention is that only the $\text{Ca}(\text{ClO}_4)_2$ and the $\text{Mg}(\text{ClO}_4)_2$ have a eutectic temperature and a deliquescence relative humidity simultaneously above the surface temperature and the surface relative humidity during a certain amount of time. Indeed, the more the salt's eutectic temperature is high, the smaller the period meeting the condition ($T > T_e$ or $RH > DRH$). It is thus consistent that the two salts having the lowest eutectic temperatures and deliquescence relative humidities are those that remain when both criteria are taken into account. All results for these two salts are detailed in Tab. 2 and Tab. 3 in the Annexes (see Sec. 7.2). The analysis of the simultaneous conditions will be done at each location. First, the surface temperature as a function of surface relative humidity will be investigated and specified for each of the two salts. Those plots will show the proportion of hours when the conditions are met compared to all hours in the year. To do so, black lines (representing the eutectic temperature and the deliquescence relative humidity of the salt considered) are drawn on the plots to delimit the correct hours from the others. All sites are concerned, except Utopia Planitia where the surface conditions are never above the $\text{Mg}(\text{ClO}_4)_2$ eutectic temperature and deliquescence relative humidity. Then, a description of the number of consecutive hours will be done. Note that when a small amount of hours is satisfying the conditions, the process of deliquescence will not take place. When several hours meet the conditions, it is not guaranteed that the brine will be stable. It depends on the surface temperature and surface pressure which modify the evaporation rate.

The surface temperature and the surface relative humidity at Vastitas Borealis simultaneously above the eutectic temperature and the deliquescence relative humidity of the $\text{Ca}(\text{ClO}_4)_2$ and the $\text{Mg}(\text{ClO}_4)_2$ are shown in orange in Fig. 34. The conditions are more favourable to the deliquescence of $\text{Ca}(\text{ClO}_4)_2$. Indeed, a lot of orange punctual points are visible in Fig. 34(a) while only a few in Fig. 34(b).

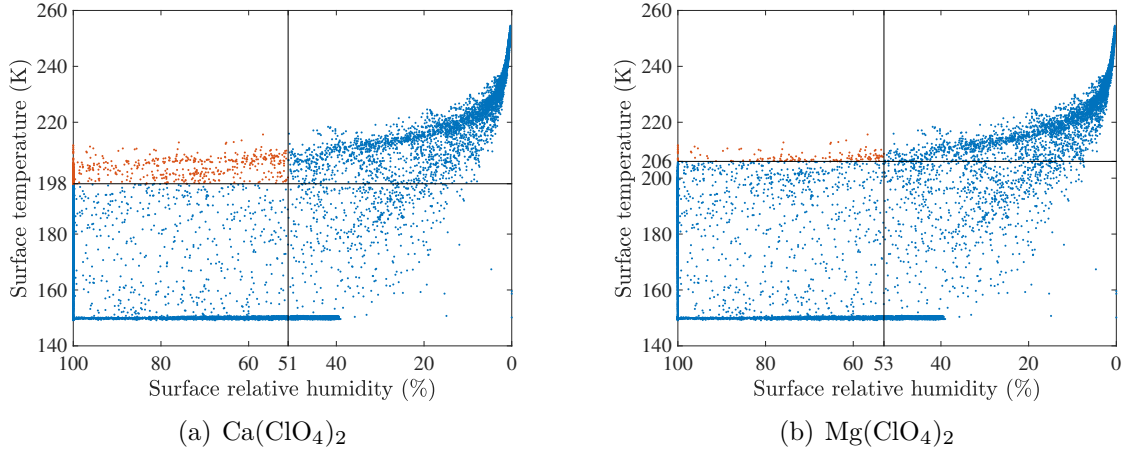


Figure 34: Surface temperature as a function of the surface relative humidity at Vastitas Borealis. Surface temperatures and relative humidities simultaneously meeting the salts conditions are shown in orange. The black lines represent the eutectic temperature and the deliquescence relative humidity of the salt considered.

In Fig. 35, $\text{Ca}(\text{ClO}_4)_2$ and $\text{Mg}(\text{ClO}_4)_2$ have eutectic temperatures and deliquescence relative humidities higher than surface conditions from the third of spring until the end of summer. The maximum number of hours meeting the conditions for $\text{Ca}(\text{ClO}_4)_2$ is nine hours at the summer solstice while it is only two hours for $\text{Mg}(\text{ClO}_4)_2$, around $L_s = 50^\circ$.

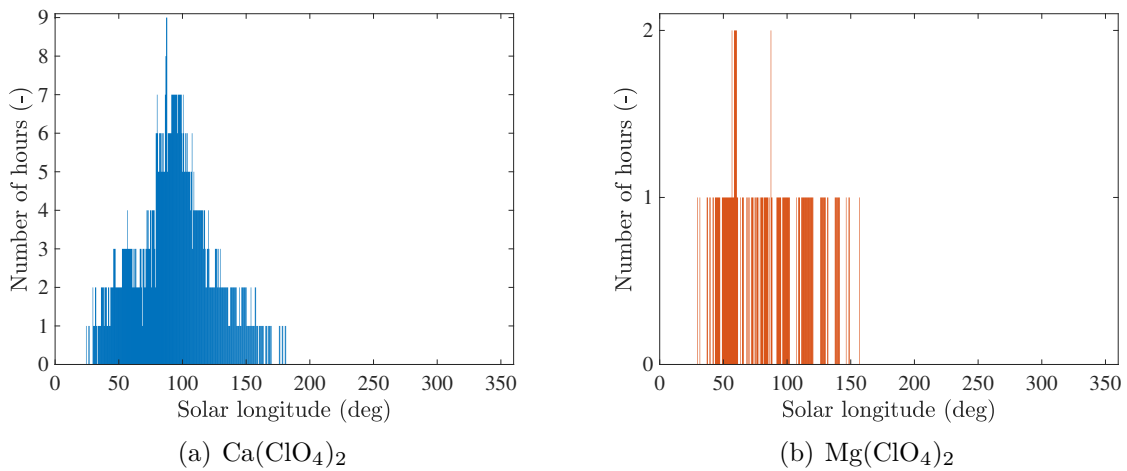


Figure 35: Number of hours for which the temperature and the relative humidity conditions are simultaneously met for consistent salts as a function of the solar longitude at Vastitas Borealis.

The surface temperature and the surface relative humidity at Utopia Planitia simultaneously above the eutectic temperature and the deliquescence relative humidity of the $\text{Ca}(\text{ClO}_4)_2$ are shown in orange in Fig. 60. Unlike the occasional points in Vastitas Borealis, here the points follow two distinct curves which confine the few point values.

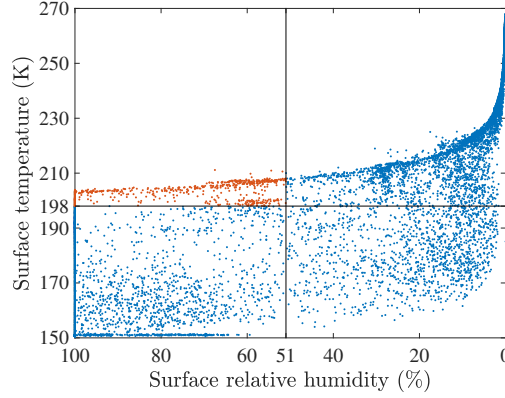


Figure 36: Surface temperature as a function of the surface relative humidity at Utopia Planitia. Surface temperatures and relative humidities simultaneously meeting the $\text{Ca}(\text{ClO}_4)_2$ conditions are shown in orange. The black lines represent the eutectic temperature and the deliquescence relative humidity of the salt considered.

The surface conditions are less favourable for the deliquescence of the salts, with only the eutectic temperature and relative humidity of $\text{Ca}(\text{ClO}_4)_2$ satisfying the conditions (see Fig. 37). Moreover, this is the case from late winter to late summer, at most for six hours around the summer solstice.

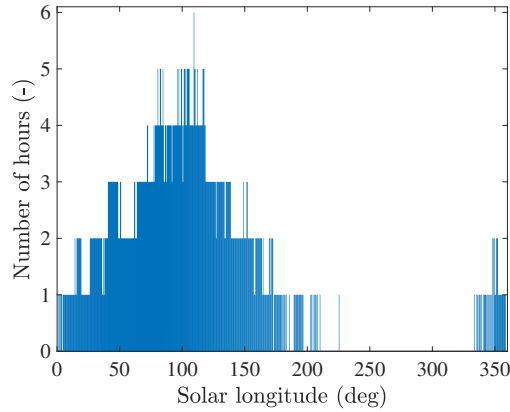


Figure 37: Number of hours for which the temperature and relative humidity conditions are simultaneously met for consistent salts as a function of the solar longitude at Utopia Planitia.

The surface temperature and the surface relative humidity at Chryse Planitia simultaneously above the eutectic temperature and the deliquescence relative humidity of the $\text{Ca}(\text{ClO}_4)_2$ and the $\text{Mg}(\text{ClO}_4)_2$ are shown in orange in Fig. 38. Here, the atmospheric conditions are such that the hours satisfying the conditions follow a curve and are less scattered. Moreover, there are much more hours favourable to the deliquescence of $\text{Ca}(\text{ClO}_4)_2$.

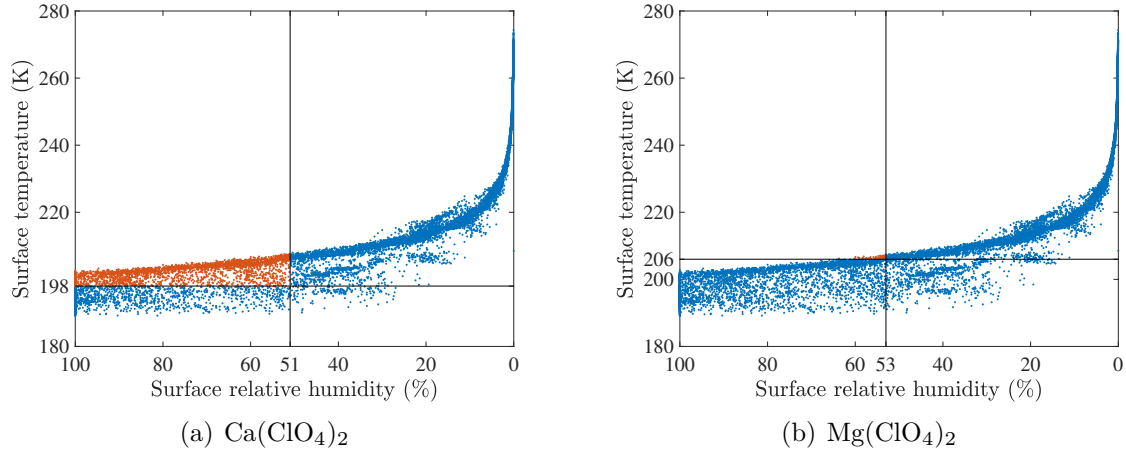


Figure 38: Surface temperature as a function of the surface relative humidity at Chryse Planitia. Surface temperatures and relative humidities simultaneously meeting the salts conditions are shown in orange. The black lines represent the eutectic temperature and the deliquescence relative humidity of the salt considered.

Surface conditions are more accommodating for $\text{Ca}(\text{ClO}_4)_2$ as seen in Fig. 39. Indeed, the conditions are satisfied all year round for a minimum of three hours (maximum twelve hours) apart from a few sols. In contrast, the situation concerning $\text{Mg}(\text{ClO}_4)_2$ is much less advantageous with only conditions encountered during the autumn (at most for three hours) and occasionally in winter and early spring for one hour.

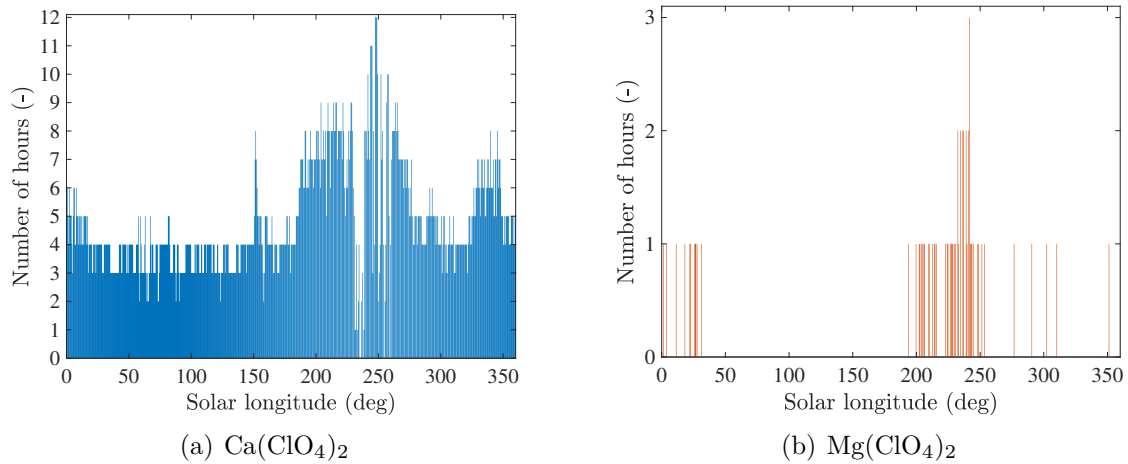


Figure 39: Number of hours for which the temperature and the relative humidity conditions are simultaneously met for consistent salts as a function of the solar longitude at Chryse Planitia.

The surface temperature and the surface relative humidity at Jezero Crater simultaneously above the eutectic temperature and the deliquescence relative humidity of the $\text{Ca}(\text{ClO}_4)_2$ and the $\text{Mg}(\text{ClO}_4)_2$ are shown in orange in Fig. 40. The $RH - T$ curves for the two salts are similar to that at Chryse Planitia although there are fewer favourable values on the Jezero plot, and therefore fewer favourable hours at this location.

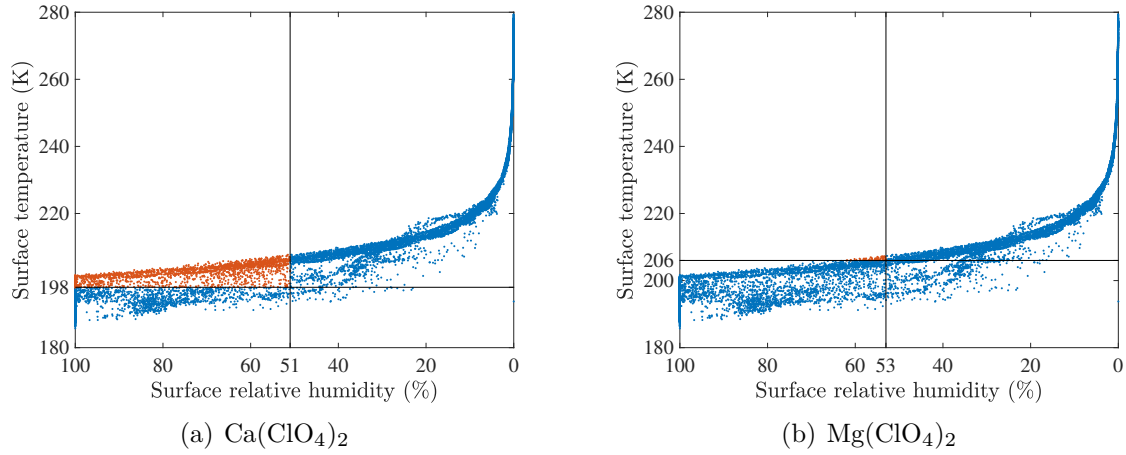


Figure 40: Surface temperature as a function of the surface relative humidity at Jezero Crater. Surface temperatures and relative humidities simultaneously meeting the salts conditions are shown in orange. The black lines represent the eutectic temperature and the deliquescence relative humidity of the salt considered.

In the Jezero crater (Fig. 41), the pattern is more or less the same than at Chryse Planitia with conditions met all year round for $\text{Ca}(\text{ClO}_4)_2$ (minimum for two hours and maximum just before the winter solstice for ten hours) except in mid-autumn. Conditions are even less favourable for $\text{Mg}(\text{ClO}_4)_2$ deliquescence since this is only possible in the second half of the year, for a maximum of two hours.

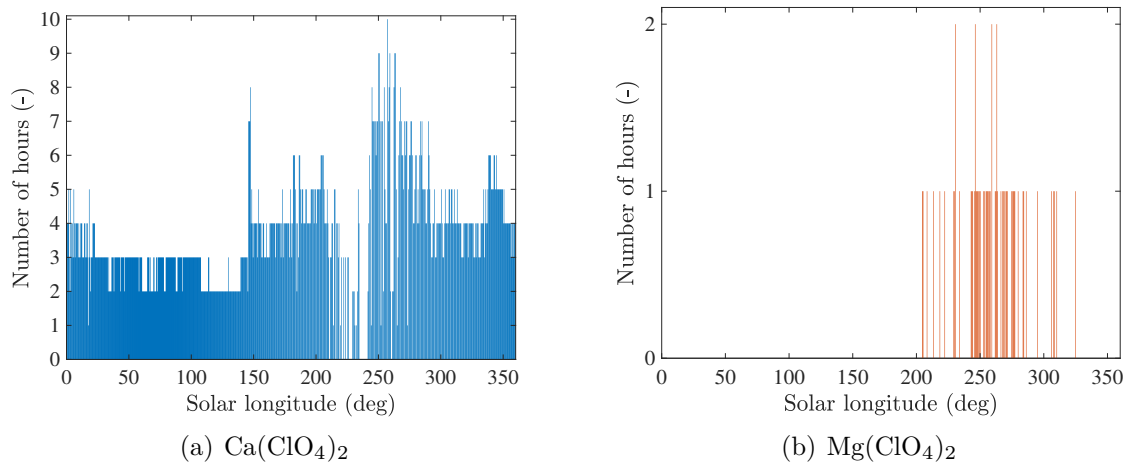


Figure 41: Number of hours for which the temperature and the relative humidity conditions are simultaneously met for consistent salts as a function of the solar longitude at Jezero Crater.

The surface temperature and the surface relative humidity at Oxia Planum simultaneously above the eutectic temperature and the deliquescence relative humidity of the $\text{Ca}(\text{ClO}_4)_2$ and the $\text{Mg}(\text{ClO}_4)_2$ are shown in orange in Fig. 42. The same pattern as in Chryse Planitia and Jezero Crater is visible. It is not surprising since Oxia Planum is located near Chryse Planitia and has the similar surface T and RH plots.

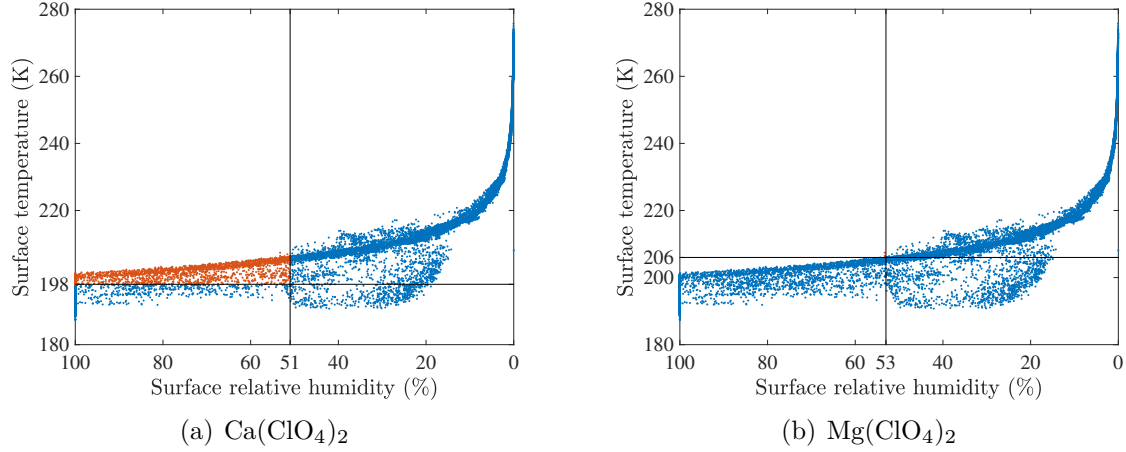


Figure 42: Surface temperature as a function of the surface relative humidity at Oxia Planum. Surface temperatures and relative humidities simultaneously meeting the salts conditions are shown in orange. The black lines represent the eutectic temperature and the deliquescence relative humidity of the salt considered.

At Oxia Planum (Fig. 43), the surface conditions are higher than the eutectic temperature and deliquescence relative humidity of $\text{Ca}(\text{ClO}_4)_2$ all year round except for a fairly long period in autumn. Eleven hours meet the conditions at the winter solstice while only two around the summer solstice. For $\text{Mg}(\text{ClO}_4)_2$, conditions are favourable only during three solar longitudes in late autumn and early winter for a maximum of one hour.

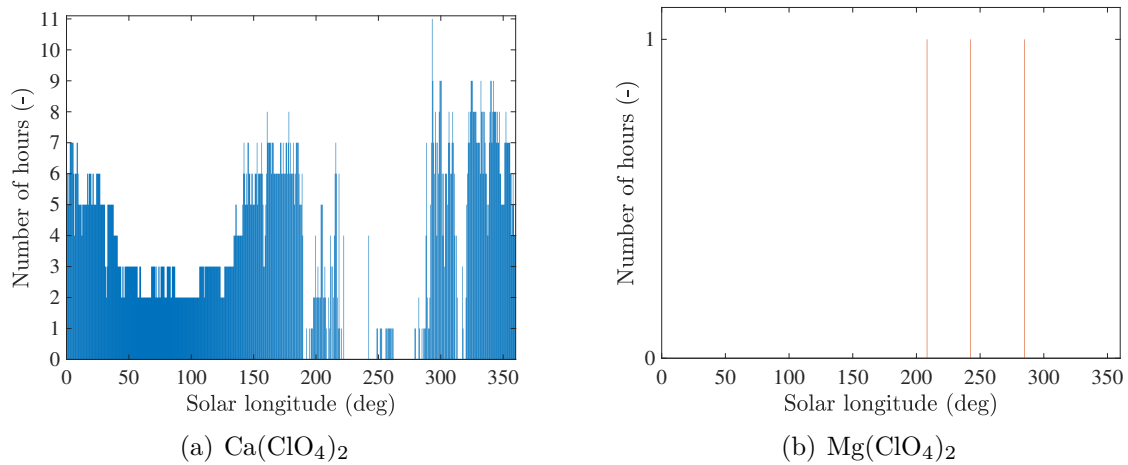


Figure 43: Number of hours for which the temperature and the relative humidity conditions are simultaneously met for consistent salts as a function of the solar longitude at Oxia Planum.

The surface temperature and the surface relative humidity at Elysium Planitia simultaneously above the eutectic temperature and the deliquescence relative humidity of the $\text{Ca}(\text{ClO}_4)_2$ and the $\text{Mg}(\text{ClO}_4)_2$ are shown in orange in Fig. 44. The proportion of favourable to unfavourable hours is reasonable for $\text{Ca}(\text{ClO}_4)_2$ while for $\text{Mg}(\text{ClO}_4)_2$ the surface conditions are very unfavourable resulting in few points above T and RH limits.

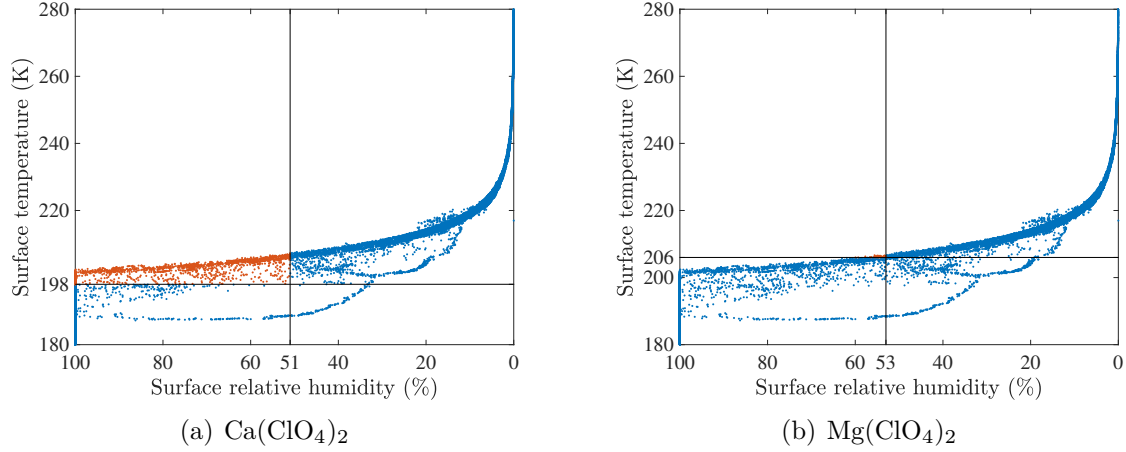


Figure 44: Surface temperature as a function of the surface relative humidity at Elysium Planitia. Surface temperatures and relative humidities simultaneously meeting the salts conditions are shown in orange. The black lines represent the eutectic temperature and the deliquescence relative humidity of the salt considered.

At Elysium Planitia (Fig. 45), maximum five hours satisfy the $\text{Ca}(\text{ClO}_4)_2$ conditions in early spring. This number decreases and reaches a minimum (1h) at the summer solstice, then increases again and keeps the same value (≈ 5 h and max. 7h) until the end of the year. In addition, a low period is visible from $L_s = 200^\circ$ to $L_s = 250^\circ$. For $\text{Mg}(\text{ClO}_4)_2$, some sols have simultaneously the right conditions but only for a maximum of one hour.

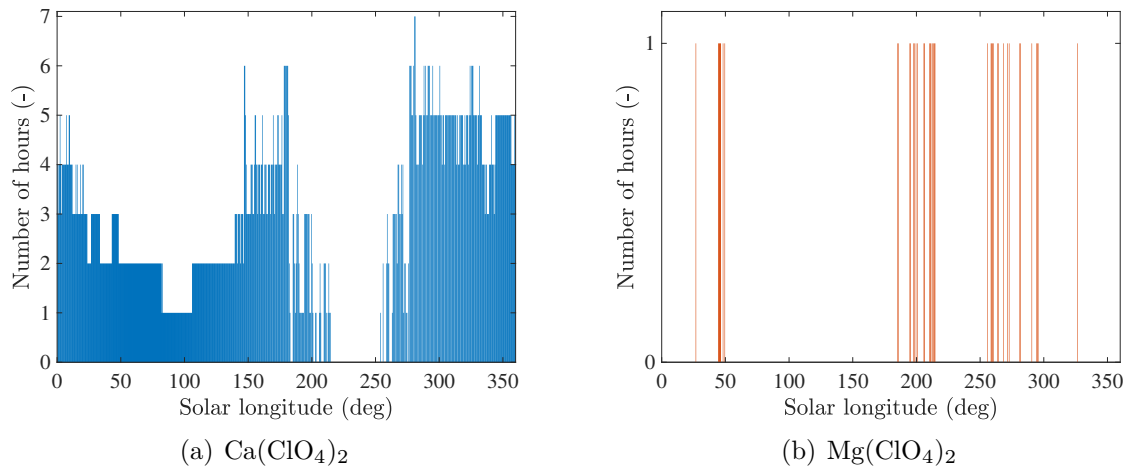


Figure 45: Number of hours for which the temperature and the relative humidity conditions are simultaneously met for consistent salts as a function of the solar longitude at Elysium Planitia.

The surface temperature and the surface relative humidity at Gale Crater simultaneously above the eutectic temperature and the deliquescence relative humidity of the $\text{Ca}(\text{ClO}_4)_2$ and the $\text{Mg}(\text{ClO}_4)_2$ are shown in orange in Fig. 46. Again, the pattern is similar to that of the nearby Elysium Planitia.

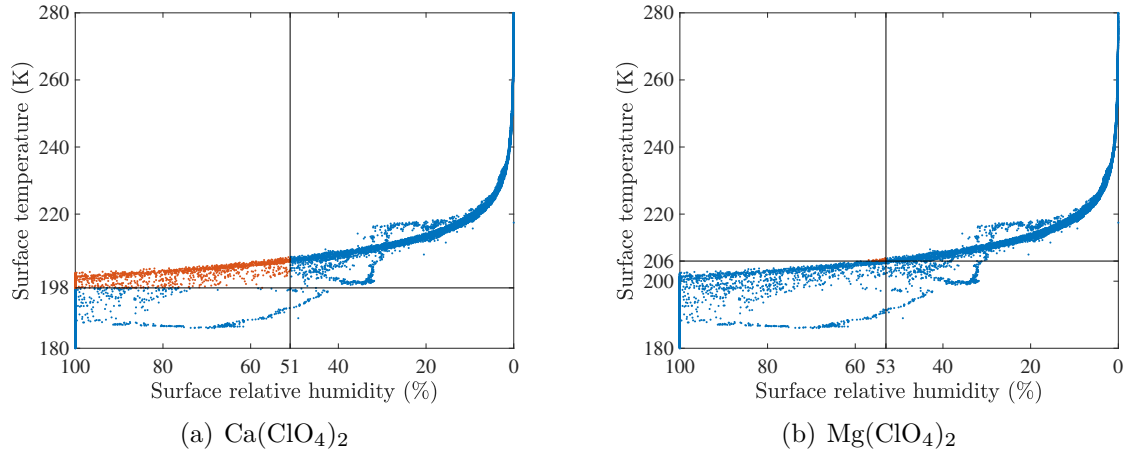


Figure 46: Surface temperature as a function of the surface relative humidity at Gale Crater. Surface temperatures and relative humidities simultaneously meeting the salts conditions are shown in orange. The black lines represent the eutectic temperature and the deliquescence relative humidity of the salt considered.

The hours situation in Gale Crater (Fig. 47) is very similar to that in Elysium Planitia with a decrease in the number of hours (1h) towards the summer solstice and a hollow period towards the winter solstice. The maximum number of hours encountering favourable conditions is eight hours.

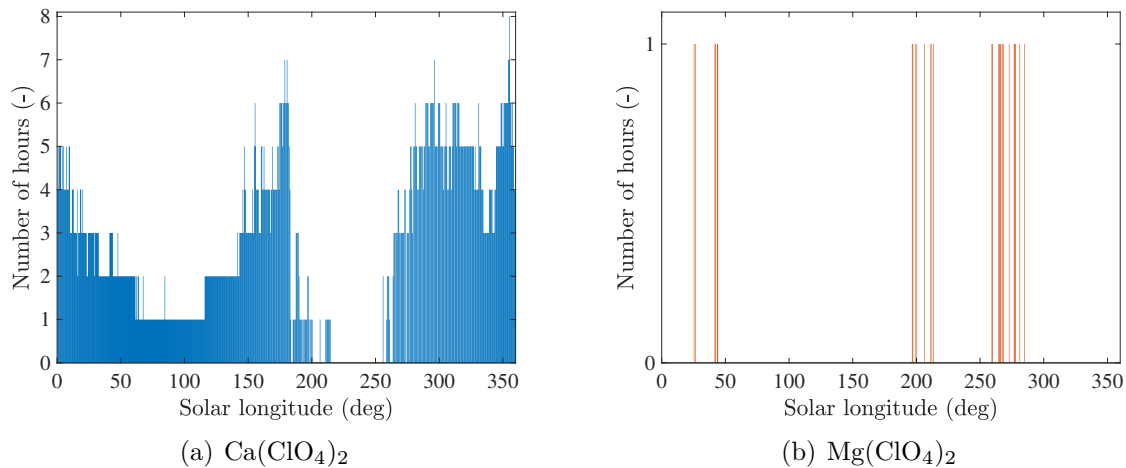


Figure 47: Number of hours for which the temperature and the relative humidity conditions are simultaneously met for consistent salts as a function of the solar longitude at Gale Crater.

6 RSL sites

Since landing sites have already been evaluated, this part will focus on locations where RSL have been detected and salts suspected. This chapter's structure is the same as in Sec. 5 with a methodology description, the outcomes analysis and a discussion to set up when brines would be available at those locations.

6.1 Methodology

Temperature and relative humidity from the GCM will be analysed and compared to the eutectic temperature and deliquescence relative humidity of the salt(s) present at the place of interest. It will be established when these places could welcome brines. To avoid redundancy, locations explored in Sec. 5, even though they may contain RSL, won't be investigated a second time. Thereupon, all places are located in the Southern Hemisphere where the seasons are reversed compared to the Northern Hemisphere.

6.2 Results

Results from the MarsWRF model (temperature and relative humidity) are presented for the six RSL sites.

6.2.1 Terra Meridiani

Terra Meridiani is a region of Meridiani Planum and is located at 2°S, 8°W [25]. In addition to magnesium sulphate, its soil may include a high concentration of hematite, a trace of either volcanic ash or a deposit from an ancient aqueous medium [25]. Almost located at the equator, the climate is tropical [24].

The temperature as a function of the solar longitude at Terra Meridiani is represented in Fig. 48(a). Temperatures remain very high throughout the year, with lows around 180 K and highs up to 290 K. In Fig. 49, one can observe the two peaks ($\tau \approx 0.5$) due to the dust storms already mentioned and in addition, a new peak around $L_s = 75^\circ$ appears. These jumps in optical depth are also observed in the temperature and humidity plots. The surface temperature exceeds the eutectic temperature of MgSO_4 from $L_s = 0^\circ$ until $L_s = 26^\circ$ and from $L_s = 128^\circ$ until $L_s = 360$. Therefore the condition is met in spring and summer for three or four hours and last till the first third of autumn first for four hours (1 pm until 4 pm) then less and less until it reaches only one hour a day (2 pm). As anticipated, temperatures are lower during winter with a minimum during the night of 179.8 K at $L_s = 67^\circ$, before the winter solstice.

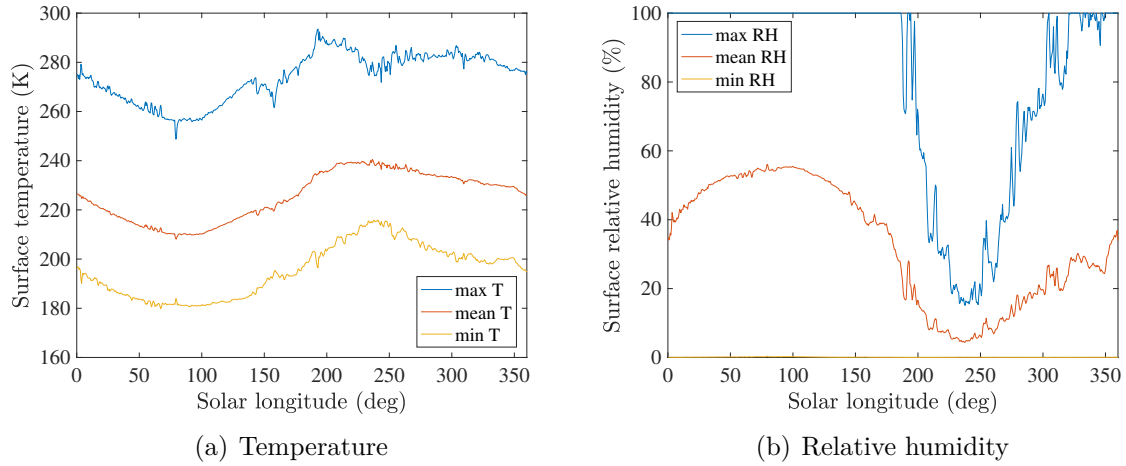


Figure 48: Temperature and relative humidity as a function of the solar longitude at Terra Meridiani. Mean, maximum and minimum values are represented.

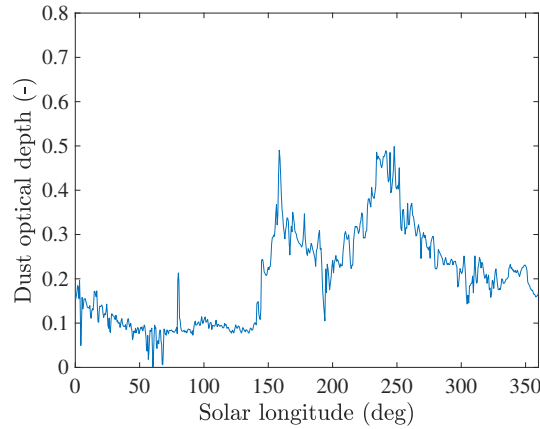


Figure 49: Dust optical depth as a function of the solar longitude at Terra Meridiani.

The relative humidity as a function of the solar longitude is depicted in 48(b). The relative humidity being at saturation once a day with an average value more or less contained between 40% and 60% until $L_s = 150^\circ$. Afterwards, the maximum relative humidity drops significantly (during summer solstice) and reaches as low values as 15%. Having the highest deliquescence relative humidity, the range when the surface relative humidity is above the MgSO_4 value is the shortest. It runs from $L_s = 0^\circ$ to $L_s = 194^\circ$ and from $L_s = 320^\circ$ to $L_s = 360^\circ$ with in between point values at $L_s = 197^\circ, 303^\circ, 304^\circ, 308^\circ, 310^\circ$ and 311° . In early autumn, the number of hours meeting the condition is four (from 4 am to 7 am). Then this number increases until it reaches twelve hours (from 8 pm to 7 am) around the winter solstice and then it decreases again. In the second period, the condition is first met only at 6 am and then the interval increases slightly until the end of the year.

6.2.2 Margaritifer Terra

Margaritifer Terra (4.9°S, 25°W [3]) is located at the mouth of Valles Marineris inducing nearly the same soil composition with among others MgSO_4 . The region is caught between two climatic zones: Tropical and Lowland Tropical [24]. The temperature and relative humidity as a function of the solar longitude at Margaritifer Terra are represented in Fig. 50(a) and 50(b) respectively.

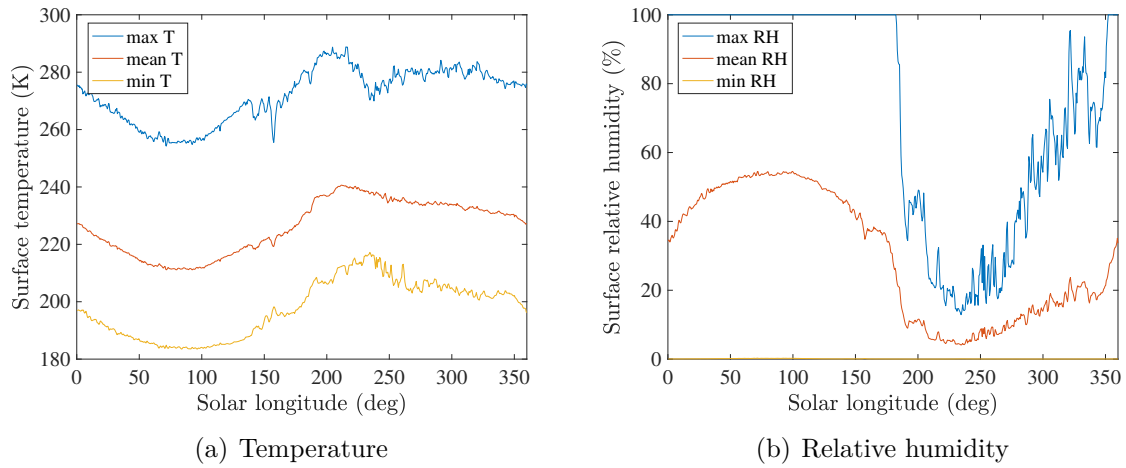


Figure 50: Temperature and relative humidity as a function of the solar longitude at Margaritifer Terra. Mean, maximum and minimum values are represented.

One can observe in Fig. 50(a) and Fig. 50(b) that after the first dust storm, values start to vary from one day to the next. In addition, the second jump in values due to the second dust storm is also visible, although less pronounced. Fig. 51 shows the same two 0.5 peaks than in Terra Meridiani but the first peak around $L_s = 75^\circ$ is missing.

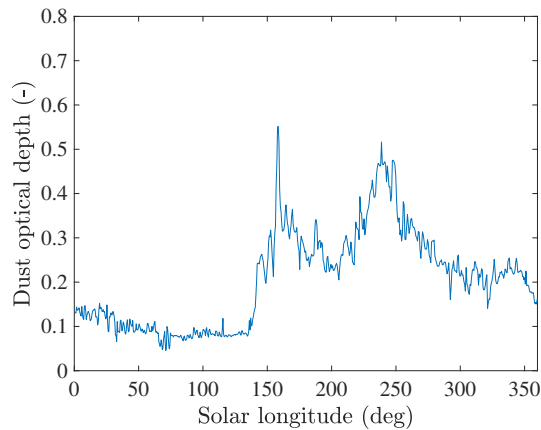


Figure 51: Dust optical depth as a function of the solar longitude at Margaritifer Terra.

The maximum temperature is 288.8 K and happens at $L_s = 215^\circ$ in mid-spring. Therefore, $T > T_{MgSO_4}$ for $L_s \in [0^\circ; 25^\circ]$ and $L_s \in [133^\circ; 360^\circ]$. During spring, several hours are affected by the condition with a maximum of six hours (11 am until 4 pm) for $L_s \in [208^\circ; 217^\circ]$. Summer has the correct temperatures only in the afternoon between 1 pm and 4 pm. Concerning autumn and end of winter, T is right one or two hours a day (1 pm, 2 pm).

Since Margaritifer Terra is also near Terra Meridiani, the discussion about the relative humidity overall shape is similar as what have been said above but with lower average temperatures. Here, $RH > DRH_{MgSO_4}$ for a less amount of sols: $L_s \in [0^\circ; 182^\circ]$, $[351^\circ; 360^\circ]$ and during one punctual time ($L_s = 321^\circ$). The number of hours during which the condition is satisfied is equivalent to that of Terra Meridiani with a maximum of hours around $L_s = 70^\circ$.

6.2.3 Valles Marineris

Valles Marineris is a vast system of canyons along the equator of Mars. It is 3770 km long, up to 600 km wide and centred in 13.7°S , 59.2°W [7]. This place is also distinguished by its Lowland Tropical climate which is characteristic of this type of structure [24]. As a salt, magnesium sulphate ($MgSO_4$) was also observed here. The temperature and relative humidity as a function of the solar longitude at Valles Marineris are represented in Fig. 52(a) and 52(b) respectively.

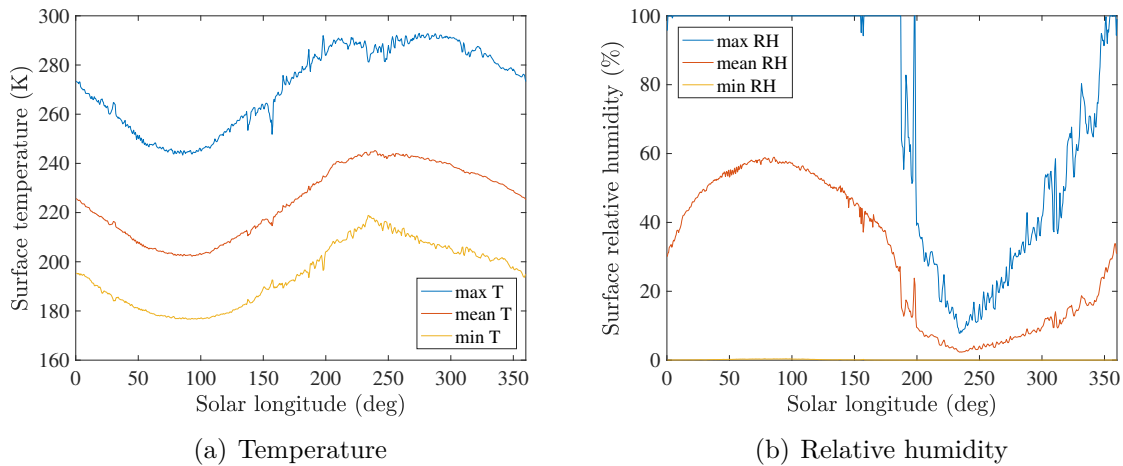


Figure 52: Temperature and relative humidity as a function of the solar longitude at Valles Marineris. Mean, maximum and minimum values are represented.

Not far from Terra Meridiani and Margaritifer Terra, the temperature and relative humidity trends (in Fig. 52(a) and Fig. 52(b)) are similar. Concerning temperatures, they are slightly more pronounced between winter and summer due to the higher latitude of

Valles Marineris and less fluctuations from day to day in the second part of the year are visible. For the relative humidity, the arc is more curved in the first half of the year and the maximums fall lower (7.8%) in around $L_s = 234^\circ$. The downward jumps in the maximum temperature curve are barely visible but the value of the dust optical depth at these times is high ($\tau = 0.5$) like in Margaritifer Terra (see Fig. 53).

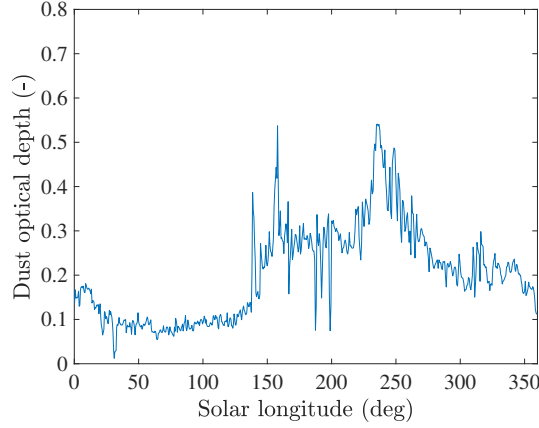


Figure 53: Dust optical depth as a function of the solar longitude at Valles Marineris.

The MgSO_4 eutectic temperature is below the surface temperature during the early autumn ($L_s \in [0^\circ; 7^\circ]$), end of winter and all spring and summer ($L_s \in [161^\circ; 360^\circ]$). The hours during which the condition is met are not numerous. Only three hours in autumn and winter and up to six hours in early summer ($L_s = 286^\circ$ to $L_s = 302^\circ$).

One can see in Fig. 52(b) that the relative humidity is 100% except in $L_s \in [187; 197]$, $[199; 353]$, $[359; 360]$ and at point values 0° , 4° , 154° and 157° . The surface relative humidity is thus above the MgSO_4 deliquescence relative humidity from $L_s = 0^\circ$ to $L_s = 187^\circ$ and from $L_s = 350^\circ$ to $L_s = 360^\circ$ with occasional values for $L_s \in [197^\circ; 198^\circ]$. Here the maximum number of hours meeting the condition is thirteen hours and ranges from $L_s = 72^\circ$ to $L_s = 86^\circ$.

6.2.4 Horowitz Crater

Horowitz Crater is a 65 km diameter crater found at 32.1°S , 140.75°E . Its climate is extreme Transitional [24]. According to the absorption spectrum of this area, sodium perchlorate is present. The temperature and relative humidity as a function of the solar longitude at Horowitz Crater are represented in Fig. 54(a) and 54(b) respectively.

The first downward jump in the maximum temperature curve is almost non-existent which is explained by a small increase in the dust optical depth ($\tau = 0.25$ in Fig. 55). In contrast, the second peak is higher ($\tau = 0.65$). This pattern suggests that the first storm

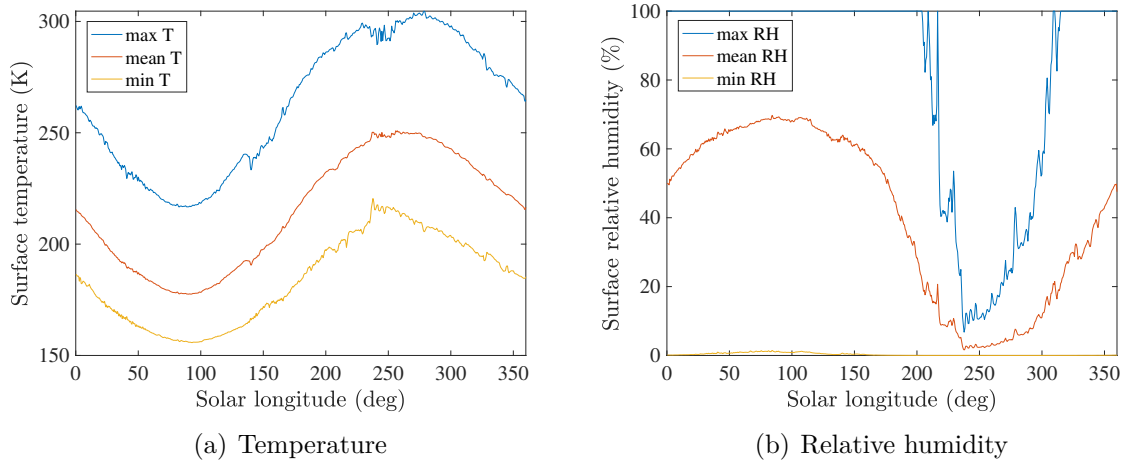


Figure 54: Temperature and relative humidity as a function of the solar longitude at Horowitz Crater. Mean, maximum and minimum values are represented.

did not impact the crater as much as the second one which was more intense. Fig. 54(a) has more pronounced disparities between winter and summer. The maximum temperature (299 K) occurs around $L_s = 229^\circ$, i.e. in mid spring, while $L_s \in [90^\circ; 97^\circ]$ (winter solstice) is the coldest period of the year (around an average of 156 K). The temperature range is very wide so that the surface temperature is higher than the eutectic temperature of NaClO_4 (236 K) from $L_s = 0^\circ$ to $L_s = 34^\circ$, from $L_s = 129^\circ$ to $L_s = 360^\circ$ (all year except during part of autumn and winter, during nine to fifteen hours a day in summer).

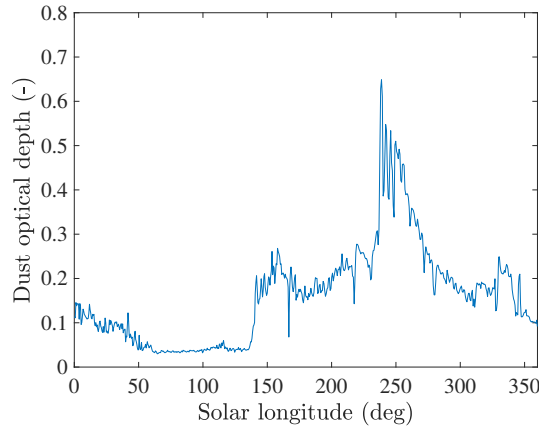


Figure 55: Dust optical depth as a function of the solar longitude at Horowitz Crater.

The relative humidities in Fig. 54(b) oscillate around the same values from day to day until about $L_s = 150^\circ$ followed by a significant drop. The window during which the relative humidity does not reach saturation is smaller (from $L_s = 204^\circ$ to $L_s = 314^\circ$ corresponding to a period from mid-spring to mid-summer). The lowest maximum value is 6.8% in $L_s = 237^\circ$. The deliquescence relative humidity used to do the comparison is the lowest on (48%) and belongs to NaClO_4 . Hence it is lower than the one used in the three locations above and the period for which $RH > DRH_{e, \text{NaClO}_4}$ runs from $L_s = 0^\circ$ to

$L_s = 217^\circ$ and from $L_s = 294^\circ$ to $L_s = 360^\circ$ with two occasional values in $L_s = 226^\circ$, and 229° . The condition is satisfied for twenty-four hours in the consistent intervals.

6.2.5 Hale Crater

Hale Crater positioned at 35.7°S , 36.6°W is localized north of the Argyre basin. Consequently, the climate there is extreme Transitional, at the limit of Subpolar Lowland [24]. This place follows the same trends as in the Horowitz Crater because they are positioned at close latitudes and have similar thermal inertias [39]. According to Ohja et al. (2015), the soil would be composed rather of $\text{Mg}(\text{ClO}_4)_2$. The temperature and relative humidity as a function of the solar longitude at Hale Crater are represented in Fig. 56(a) and 56(b) respectively.

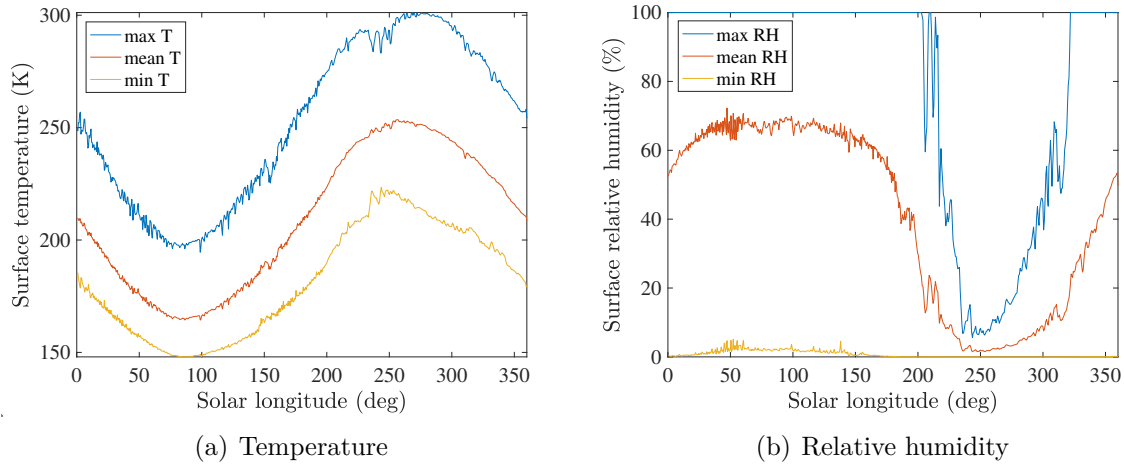


Figure 56: Temperature and relative humidity as a function of the solar longitude at Hale Crater. Mean, maximum and minimum values are represented.

Having almost the same longitude as the Horowitz Crater, the curves seen in Fig. 56 look like those in Fig. 54. However, the maximum temperature falls lower at the winter solstice and the relative humidity curve is more irregular. The minimum temperature experienced at Hale Crater is equal to 148 K (around $L_s = 90^\circ$) while interval where $RH \neq 100\%$ extends from $L_s = 203^\circ$ to $L_s = 321^\circ$. Here too the second storm was more severe, but less so than at Horowitz Crater due to the lower dust optical depth value ($\tau = 0.55$ at $L_s = 250^\circ$ in Fig. 57).

The surface temperature exceeds the $\text{Mg}(\text{ClO}_4)_2$ eutectic temperature from $L_s = 0^\circ$ until $L_s = 61^\circ$ and then for $L_s \in [111^\circ; 360^\circ]$. During autumn, the range of hours having $T > T_{\text{Mg}(\text{ClO}_4)_2}$ shrinks over time. At the beginning, eleven hours meet the condition while when $L_s = 61^\circ$, only one hour has a valid temperature (3 pm). Regarding the end of winter, spring and summer, the condition is fulfilled for the most hours (24h) between

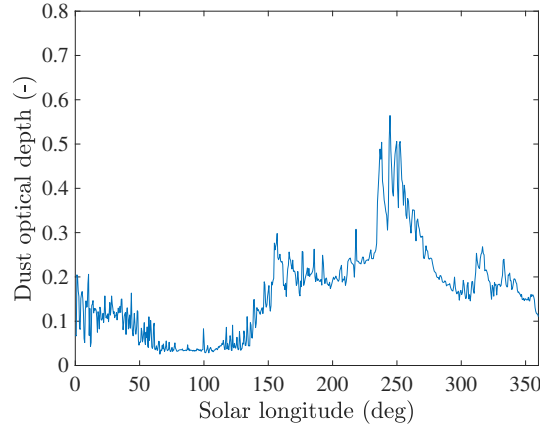


Figure 57: Dust optical depth as a function of the solar longitude at Hale Crater.

$L_s = 217^\circ$ and $L_s = 301^\circ$.

At Hale Crater, average relative humidities are also high but not as much as in Horowitz Crater. Moreover, the lowest maximum values are smaller (5.6% at $L_s = 243^\circ$). The window where $RH \neq 100\%$ results in a value higher than the $\text{Mg}(\text{ClO}_4)_2$ deliquescence relative humidity for $L_s \in [0^\circ; 219^\circ]$, $[304^\circ; 311^\circ]$, $[316^\circ; 360^\circ]$ and during $L_s = 302^\circ, 313^\circ$. As previously, the condition is met for the longest time around the winter solstice (from 6 pm to 10 am) and the least amount of time (7 am) around $L_s = 300^\circ$.

6.2.6 Palikir Crater

Located the furthest south of all the sites analysed, the Palikir Crater (41.6°S , 157.8°W) is 16 km wide and is part of the larger Newton Crater (around 300 km). There, at least two magnesium salts have been discovered: $\text{Mg}(\text{ClO}_4)_2$ and MgCl_2 .

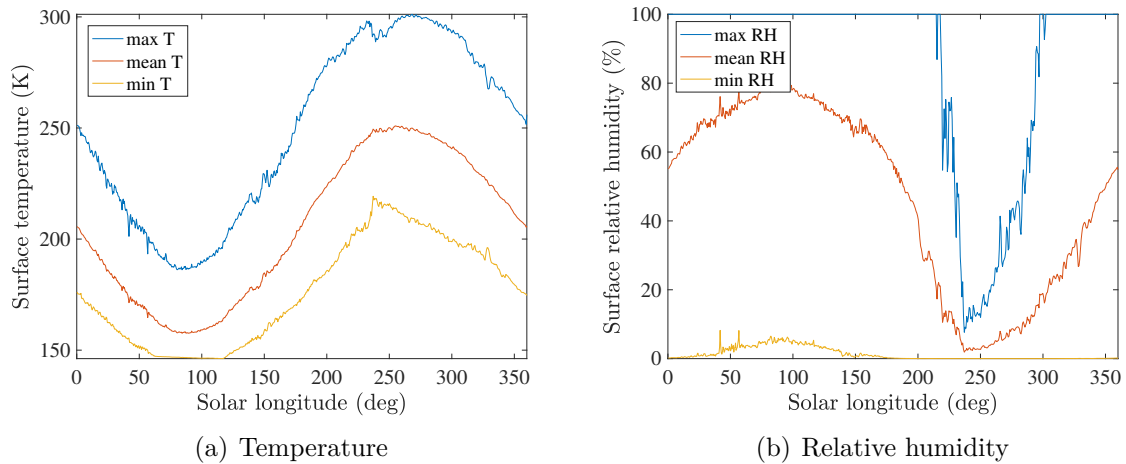


Figure 58: Temperature and relative humidity as a function of the solar longitude at Palikir Crater. Mean, maximum and minimum values are represented.

The temperature as a function of the solar longitude at Palikir Crater is represented in Fig. 58(a). Although the dust optical depth peak in $L_s = 250^\circ$ is high ($\tau = 0.7$ in Fig. 59), this is not reflected in the temperature plot where only a very slight decrease is observed at this time. The increase in $L_s = 150^\circ$ is not to be considered as it is too low. This place is the southernmost, leading to even higher discrepancies between seasons and lower maximum temperature. The minimum temperature (146 K) at the winter solstice forms a plateau from $L_s = 72^\circ$ to $L_s = 118^\circ$ due to the obliquity of Mars. The maximum is, in turn, 300 K around $L_s = 268^\circ$. The surface temperature exceeds the $\text{Mg}(\text{ClO}_4)_2$ eutectic temperature ($T = 212$ K) from $L_s = 0^\circ$ until $L_s = 49^\circ$ and from $L_s = 125^\circ$ until the end of the year. From mid-spring ($L_s = 229^\circ$) to early summer ($L_s = 278^\circ$), the condition is satisfied all day long. Again, this is the consequence of Mars' obliquity and the longer surface insulation during spring and summer. Considering MgCl_2 , its eutectic temperature ($T = 240$ K) is quite larger than that of $\text{Mg}(\text{ClO}_4)_2$ hence $T > T_{e,\text{MgCl}_2}$ during early autumn ($L_s \in [0^\circ; 14^\circ]$) and from $L_s = 168^\circ$ until $L_s = 360^\circ$ starting with one hour per day at the correct temperature, up to fourteen hours per day.

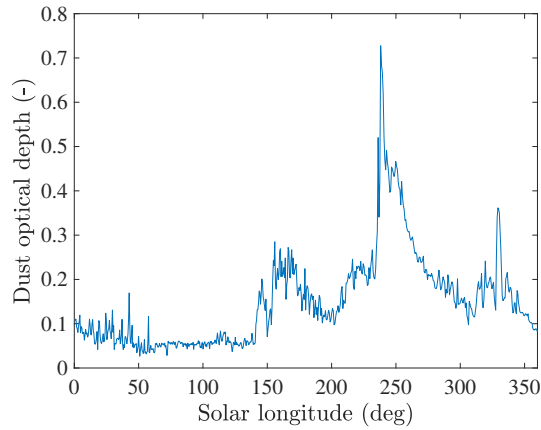


Figure 59: Dust optical depth as a function of the solar longitude at Palikir Crater.

The relative humidity as a function of the solar longitude is represented in Fig. 58(b). It is different from 100% for $L_s \in [218^\circ; 296^\circ]$ and reaches a low maximum value of 7.6% at $L_s = 237^\circ$. The minimum values differ from 0% from $L_s = 41^\circ$ to $L_s = 138^\circ$ leading to an increase of the average values. For the $\text{Mg}(\text{ClO}_4)_2$, the surface relative humidity exceeds its eutectic value for $L_s \in [0^\circ; 228^\circ]$, $[286^\circ; 360^\circ]$ and $L_s = 284^\circ$. Concerning the second salt present at Palikir Crater (MgCl_2), the range having a good relative humidity is smaller since its eutectic value is higher. Indeed, the two intervals go from $L_s = 0^\circ$ to $L_s = 219^\circ$ and from $L_s = 294^\circ$ to the end of the year. For the two salts, the two periods are found during all seasons except for a few days during spring and early summer.

6.3 Discussion

As previously, a discussion on where and when the conditions on the temperature and the relative humidity are encountered simultaneously is presented. For the RSL sites, Hale Crater is the only location having favourable surface conditions to the deliquescence of the salt present there ($\text{Mg}(\text{ClO}_4)_2$). As in the previous discussion (Sec.), Fig. 60 shows the proportion of hours with surface temperature and relative humidity simultaneously higher than the surface conditions. As seen in this figure, only four hours meet the conditions for the deliquescence of $\text{Mg}(\text{ClO}_4)_2$ meaning the proportion of valid hours versus not valid hours is extremely low.

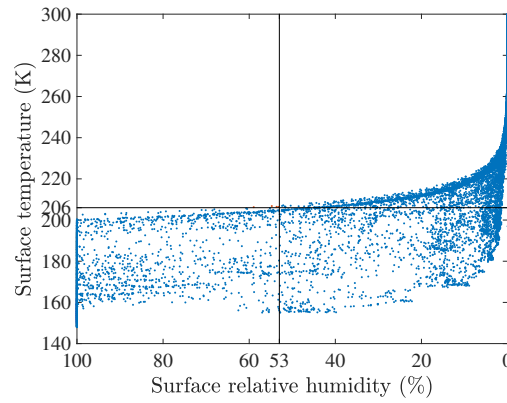


Figure 60: Surface temperature as a function of the surface relative humidity at Hale Crater. Surface temperatures and relative humidities simultaneously meeting the $\text{Ca}(\text{ClO}_4)_2$ conditions are shown in orange. The black lines represent the eutectic temperature and the deliquescence relative humidity of the salt considered.

Then Fig. 61 depicts exactly how many hours satisfy the conditions and when they occur. The two periods having the right conditions are in mid-autumn (see Tab. 2 for detailed results) for only one hour. This is not sufficient to observe the $\text{Mg}(\text{ClO}_4)_2$ deliquescence process.

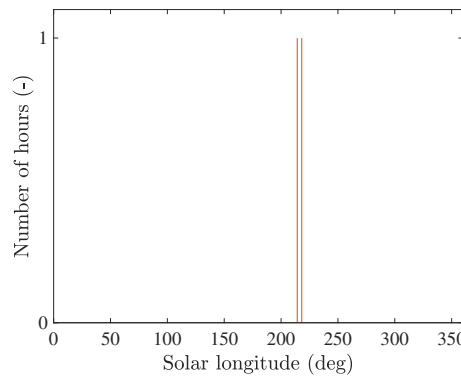


Figure 61: Number of hours for which the temperature and the relative humidity conditions are simultaneously met for the $\text{Mg}(\text{ClO}_4)_2$ as a function of the solar longitude at Hale Crater.

Concerning the overall shapes, the temperature ranges for the places analysed in this section are wider than those of Sec. 5. This is consistent with Hargitai (2010) who says that the climate in the Southern Hemisphere is more extreme with higher temperatures during summer and lower temperatures during winter. Moreover, the overall shape follows the same trend than for the northern places: seasonal variations are more pronounced the further the site is from the equator. As above, the temperature could allow the melting of pure water at every location.

The average relative humidities curves still show the same pattern as for the landing sites: a slight increase until $L_s = 100^\circ$ then a decrease (where the maximum temperatures reach their lowest value) followed by an increase again but not as much as in the first part of the year. The half-circle arc is again more pronounced for more southerly latitudes. The second half of the year curves are also more chaotic compared to the smoother first half curves. Finally, the window where the relative humidity satisfies the condition is narrower the further south the site is.

Regarding the dust storms effects, they are again less pronounced in the relative humidity plot than in the temperature plot. At Terra Meridiani, both storms are visible in the dust optical depth plot but a new peak is present before the other two events. These 3 storms are therefore marked in the temperature curves. At Margaritifer Terra and Valles Marineris, both storms are visible but less strong at the latter. In Horowitz crater, the second increase in optical depth is much larger, while in Hale crater, the two peaks are equal. In the temperature plot, both storms are visible for both craters. Finally, the dust optical depth of the second storm explodes in Palikir crater, although the consequence on the temperature curves is not significant.

7 Conclusion and future work

This last chapter presents first the final conclusion and then the perspectives that could improve the study.

7.1 Conclusion

The objective of this work was to study the temperature and relative humidity conditions on the surface of Mars in order to establish the deliquescence potential of particular locations on the Red Planet as well as globally. To achieve this, a general description of Mars was made, followed by a state of the art establishing some of the concepts necessary to understand the rest of the work. During the latter, a list of salts known to be present on Mars was determined (in Recurring Slope Linea locations), as well as some of their properties (eutectic temperature and relative humidity). For the deliquescence process to take place, two surface conditions must be met simultaneously: the temperature must be above the eutectic temperature of the salt and the relative humidity must be above the deliquescence relative humidity of the salt.

A global simulation with the MarsWRF model was performed and validated with an uncertainty of 40%. The outcomes allowed to model the global climate of Mars in terms of diurnal and seasonal variations. In addition, the global places on the planet with the most favourable conditions for salt deliquescence were established.

Then, the investigation was divided into two main parts. The first part focused on the study of the missions landing sites that have taken place on Mars. The surface temperature and relative humidity were compared with the eutectic temperature and relative humidity of the various salts. In this case it was necessary to test for all salts since the salts present at the landing sites have not been widely studied. What emerges from this analysis is that $\text{Ca}(\text{ClO}_4)_2$ is the most likely salt to deliquesce, for all landing sites. At high latitude locations, the hours when the surface temperature and surface relative humidity are higher than the eutectic temperature and deliquescence relative humidity respectively, are in the first half of the year. For mid-latitude locations, surface conditions are favourable throughout the year, although according to the number of hours satisfying the requirements, the only favourable period is the winter solstice (maximum twelve consecutive hours). Finally, for locations at the equator, no hours are favourable during the autumn although the greatest number of consecutive hours meeting the conditions are around the northern autumn equinox and the northern winter solstice (maximum seven hours). Concerning the $\text{Mg}(\text{ClO}_4)_2$, favourable conditions are rarely met.

The second part used the same methodology as in the first part, but at sites with Recurring Slope Linea where the absorption spectrum revealed the presence of one or more specific salts. Thus, surface temperature and relative humidity were compared to the eutectic temperature and relative humidity of the salt(s) present in situ. The conclusion is that the only RSL location allowing salt deliquescence is Hale Crater. However, the surface conditions there are favourable just after the autumn equinox and for a maximum of one hour, which does not allow the process to take place.

7.2 Future work

A number of improvement perspectives arise from this work. The first two are related to the simulation itself with the MarsWRF model. Indeed, it would be optimal to simulate the atmospheric conditions on Mars with the finest possible numerical resolution. This would change the outputs and therefore the conclusions of this work. Secondly, to solve the problem of the overestimation of the water vapour mixing ratio. As a result, the calculation of the relative humidity would be more accurate.

There are also perspectives to perform further studies. A first idea would be to simulate the atmospheric conditions at a mesoscale in the locations favourable for the deliquescence of salts, determined via the global scale simulation (in Sec. 4). A second study could take on the task of obtaining the favourable locations and times for ice melting on Mars (following the same procedure as established in this work). This would require simulating the pressure and saturation vapour pressure with the model and determining where $p > p_{sat}$ knowing that salts also decrease the pressure at which the condition is satisfied. The final study idea is to consider brines composed of several salts (named multi-component brines) rather than brines obtained from a single salt. Indeed, thanks to the different salts, the eutectic temperature and the deliquescence relative humidity of the brine are lower than those of the single component brines, resulting in a brine availability over a larger surface of Mars and for a longer period of time.

References

- [1] National Aeronautics and Space Administration. *Curiosity's Landing Site: Gale Crater*. URL: <https://mars.nasa.gov/msl/timeline/prelaunch/gale-crater/>.
- [2] National Aeronautics and Space Administration. *Landing Site for InSight*. URL: <https://mars.nasa.gov/resources/6981/landing-site-for-insight/?site=insight>.
- [3] National Aeronautics and Space Administration. *Margaritifer Terra*. URL: <https://mars.nasa.gov/resources/25971/margaritifer-terra-false-color/>.
- [4] National Aeronautics and Space Administration. *Mars Panorama of Phoenix Landing Site and Lander Deck*. URL: <https://mars.nasa.gov/resources/3475/mars-panorama-of-phoenix-landing-site-and-lander-deck/>.
- [5] National Aeronautics and Space Administration. *Mars24 Sunclock — Time on Mars*. URL: <https://www.giss.nasa.gov/tools/mars24/help/guide.html>.
- [6] National Aeronautics and Space Administration. *Perseverance Rover's Landing Site: Jezero Crater*. URL: <https://mars.nasa.gov/mars2020/mission/science/landing-site/>.
- [7] National Aeronautics and Space Administration. *Valles Marineris*. URL: <https://mars.nasa.gov/resources/3874/valles-marineris/>.
- [8] National Aeronautics and Space Administration. *Warm-Season Flows on Slope in Newton Crater*. Retrived March 21, 2021 from the website: https://www.nasa.gov/mission_pages/MRO/multimedia/pia14472.html.
- [9] European Space Agency. *Oxia Planum*. URL: <https://exploration.esa.int/web/mars/-/54724-oxia-planum>.
- [10] Travis Altheide et al. "Experimental investigation of the stability and evaporation of sulfate and chloride brines on Mars". In: *Earth and Planetary Science Letters* 282.1-4 (2009). DOI: 10.1016/j.epsl.2009.03.002.
- [11] Don Banfield et al. "The atmosphere of Mars as observed by InSight". In: *Nature Geoscience* 13.3 (2020). DOI: 10.1038/ngeo2014.
- [12] Michael H. Carr and J. W. Head III. "Geologic history of Mars". In: *Earth and Planetary Science Letters* 294.3-4 (2010). DOI: 10.1016/j.epsl.2009.06.042.
- [13] Vincent F. Chevrier, J. Hanley, and T. S. Altheide. "Stability of perchlorate hydrates and their liquid solutions at the Phoenix landing site, Mars". In: *Geophysical Research Letters* 36.10 (2009). DOI: 10.1029/2009GL037497.

- [14] Vincent F. Chevrier and E. G. Rivera-Valentín. “Formation of recurring slope lineae by liquid brines on present-day Mars”. In: *Geophysical Research Letters* 39.21 (2012). DOI: 10.1029/2012GL054119.
- [15] Vincent F. Chevrier et al. “Global Temporal and Geographic Stability of Brines on Present-day Mars”. In: *The Planetary Science Journal* 1.3 (2020). DOI: 10.3847/PSJ/abbc14.
- [16] Mars Climate Database. *Mars Climate Database v5.3: The Web Interface*. URL: http://www-mars.lmd.jussieu.fr/mars/time/solar_longitude.html.
- [17] Colin M. Dundas et al. “Seasonal Flows on Warm Martian Slopes”. In: *American Association for the Advancement of Science* 333.6043 (2011). DOI: 10.1126/science.1204816.
- [18] E. Fisher et al. “Relative Humidity on Mars: New Results From the Phoenix TECP Sensor”. In: *Journal of Geophysical Research: Planets* 124.11 (2019). DOI: 10.1029/2019JE006080.
- [19] Aline Gendrin et al. “Sulfates in Martian Layered Terrains: The OMEGA/Mars Express View”. In: *Science* 307.5715 (2005). DOI: 10.1126/science.1109087.
- [20] Daniel P. Glavin et al. “Evidence for perchlorates and the origin of chlorinated hydrocarbons detected by SAM at the Rocknest aeolian deposit in Gale Crater”. In: *Journal of Geophysical Research: Planets* 118.10 (2013). DOI: 10.1002/jgre.20144.
- [21] M. Golombek et al. “Geology of the InSight landing site on Mars”. In: *Nature Communications* 11.1 (2020). DOI: 10.1038/s41467-020-14679-1.
- [22] R. V. Gough et al. “Solid-solid hydration and dehydration of Mars-relevant chlorine salts: Implications for Gale Crater and RSL locations”. In: *Icarus* 321 (2019). DOI: 10.1016/j.icarus.2018.10.034.
- [23] Robert M. Haberle et al. “On the possibility of liquid water on present-day Mars”. In: *Journal of Geophysical Research: Planets* 106.E10 (2001). DOI: 10.1029/2000JE001360.
- [24] H. Hargitai. *Mars climate zone map based on TES data*. 41st Lunar and Planetary Science Conference. 2010.
- [25] Brian M. Hynek, Raymond E. Arvidson, and Roger J. Phillips. “Geologic setting and origin of Terra Meridiani hematite deposit on Mars”. In: *Journal of Geophysical Research* 107.E10 (2002). DOI: 10.1029/2002JE001891.
- [26] Andrew P. Ingersoll. “Mars: Occurrence of Liquid Water”. In: *Science* 168.3934 (1970). DOI: 10.1126/science.168.3934.972.
- [27] Bradley L. Jolliff et al. *Chapter 10 - Mars Exploration Rover Opportunity: Water and Other Volatiles on Ancient Mars*. Elsevier, 2019. ISBN: 978-0-12-804191-8.

- [28] Conway Leovy. “Weather and climate on Mars”. In: *Nature* 412.6843 (2001). DOI: 10.1038/35084192.
- [29] F. Javier Martín-Torres et al. “Transient liquid water and water activity at Gale crater on Mars”. In: *Nature Geoscience* 8.5 (2015). DOI: 10.1038/ngeo2412.
- [30] Alfred S. McEwen et al. “Granular flows at recurring slope lineae on Mars indicate a limited role for liquid water”. In: *Nature Geoscience* 10.12 (2017). DOI: 10.1038/s41561-017-0012-5.
- [31] Alfred S. McEwen et al. “Recurring slope lineae in equatorial regions of Mars”. In: *Nature Geoscience* 7.1 (2014). DOI: 10.1038/ngeo2014.
- [32] Kathryn Mersmann. *The Fact and Fiction of Martian Dust Storms*. URL: <https://www.nasa.gov/feature/goddard/the-fact-and-fiction-of-martian-dust-storms>.
- [33] Claire E. Newman, J. Gómez-Elvira, M. Marin, et al. “Winds measured by the Rover Environmental Monitoring Station (REMS) during the Mars Science Laboratory (MSL) rover’s Bagnold Dunes Campaign and comparison with numerical modeling using MarsWRF”. In: *Icarus* 291 (2017). DOI: 10.1016/j.icarus.2016.12.016.
- [34] Lujendra Ojha et al. “Spectral evidence for hydrated salts in recurring slope lineae on Mars”. In: *Nature Geoscience* 8.11 (2015). DOI: 10.1038/ngeo2546.
- [35] David A. Paige. “Ancient Mars: Wet in Many Places”. In: *Science* 307.5715 (2005). DOI: 10.1126/science.1110530.
- [36] B. Pál and Kereszturi Á. “Possibility of microscopic liquid water formation at landing sites on Mars and their observational potential”. In: *Icarus* 282 (2016). DOI: 10.1016/j.icarus.2016.09.006.
- [37] O. N. Pestova et al. “Polythermal Study of the Systems $M(\text{ClO}_4)_2\text{-H}_2\text{O}$ ($M^{2+} = \text{Mg}^{2+}, \text{Ca}^{2+}, \text{Sr}^{2+}, \text{Ba}^{2+}$)”. In: *Russian Journal of Applied Chemistry* 78.3 (2005). DOI: 10.1007/s11167-005-0306-z.
- [38] Jorge Pla-García et al. “Meteorological Predictions for Mars 2020 Perseverance Rover Landing Site at Jezero Crater”. In: *Space Science Reviews* 216.8 (2020). DOI: 10.1007/s11214-020-00763-x.
- [39] Nathaniel E. Putzig et al. “Global thermal inertia and surface properties of Mars from the MGS mapping mission”. In: *Icarus* 173.2 (2005). DOI: 10.1016/j.icarus.2004.08.017.
- [40] Mark I. Richardson, Anthony D. Toigo, and Claire E. Newman. “PlanetWRF: A general purpose, local to global numerical model for planetary atmospheric and climate dynamics”. In: *Journal of Geophysical Research* 112.E09001 (2007). DOI: 10.1029/2006JE002825.

- [41] E. G. Rivera-Valentín et al. “Distribution and habitability of (meta)stable brines on present-day Mars”. In: *Nature Astronomy* 4.8 (2020). DOI: 10.1038/s41550-020-1080-9.
- [42] Edgard G. Rivera-Valentín et al. “Constraining the Potential Liquid Water Environment at Gale Crater, Mars”. In: *Journal of Geophysical Research: Planets* 123.5 (2018). DOI: 10.1002/2018JE005558.
- [43] John D. Rummel et al. “A New Analysis of Mars "Special Regions": Findings of the Second MEPAG Special Regions Science Analysis Group (SR-SAG2)”. In: *Astrobiology* 14.11 (2014). DOI: 10.1089/ast.2014.1227.
- [44] William Sheehan. *Chapter 13*. University of Arizona Press, 1996. ISBN: 978-0-8165-1640-7.
- [45] A. G. Siddle et al. “Global characteristics of gravity waves in the upper atmosphere of Mars as measured by MAVEN/NGIMS”. In: *Icarus* 333 (2019). DOI: 10.1016/j.icarus.2019.05.021.
- [46] Planetary Society. *Mars’ Calendar*. URL: <https://www.planetary.org/articles/mars-calendar>.
- [47] Orkun Temel et al. “Strong seasonal and regional variations in the evaporation rate of liquid water on Mars”. In: *Journal of Geophysical Research: Planets* (2021).
- [48] Orkun Temel et al. “When and where to search for liquid water on Mars: Evaporation rate estimations”. In: (2021).
- [49] Jonathan D. Toner and D.C. Catling. “Water activities of NaClO_4 , $\text{Ca}(\text{ClO}_4)_2$, and $\text{Mg}(\text{ClO}_4)_2$ brines from experimental heat capacities: Water activity > 0.6 below 200 K”. In: *Geochimica et Cosmochimica Acta* 181 (2016). DOI: 10.1016/j.gca.2016.03.005.
- [50] Nicholas J. Tosca, Andrew H. Knoll, and Scott M. McLennan. “Water Activity and the Challenge for Life on Early Mars”. In: *Science* 320.5880 (2008). DOI: 10.1126/science.1155432.
- [51] David R. Williams. *Viking mission to Mars*. URL: <https://nssdc.gsfc.nasa.gov/planetary/viking.html>.

Annexes

| | Ca(ClO ₄) ₂ | | Mg(ClO ₄) ₂ | |
|------------------|---|---------------------------------------|--|----------------|
| | <i>L_s</i> | Hours | <i>L_s</i> | Hours |
| Chryse Planitia | [0°;360°] except 235° | Max 12h [247°;248°] | 1°, 3°, 11°, 18°, 22°, [25°;27°], 31°, 193°, 199° [202°;206°], [209°;210°], [212°;215°], 222°, 224°, [226°;230°], [232°;234°], [236°;237°], [239°;244°], 248°, 251°, 253°, 276°, 290°, 302°, 310°, 351°, 360° | Max 3h 241° |
| Elysium Planitia | [0°;200°], [202°;203°], [205°;207°] [209°;214°], [254°;255°], [258°;260°] [263°;274°], [276°;360°] | Max 7h [280°;281°] | 26°, [44°;46°], [48°;49°], 185° [194°;195°], [197°;200°], [205°;206°], [210°;214°] 255°, [258°;260°], [263°;264°], 268°, [271°;272°], 281°, 290°, [294°;298°], 326° | Max 1h |
| Gale Crater | [0°;197°], [199°;200°], 206°, [210°;214°] 255°, [258°;261°], [263°;360°] | Max 8h 355° | [25°;26°], [41°;44°], [196°;197°], [199°;200°], 206°, 210°, [212°;213°], 259°, [264°;268°], 272°, [276°;277°] 281°, 284° | Max 1h |
| Hale Crater | [0°;9°], [11°;17°], 26°, 146° [154°;155°], [163°;170°], [173°;182°], 185°, [191°;197°], 200°, [207°;219°] 302°, [304°;313°], [316°;360°] | Max 6h [324°;325°], [331°;333°] | [213°;214°], [217°;218°] | Max 1h |

Table 2: Summary of solar longitude (*L_s* column) having surface conditions (*T*, *RH*) above the eutectic temperature and the deliquescence relative humidity of Ca(ClO₄)₂ and MgClO₄)₂. The Hours column specifies for which *L_s* the number of hours meeting the conditions is maximum.

| | Ca(ClO ₄) ₂ | | Mg(ClO ₄) ₂ | |
|-------------------|--|-----------------|---|-------------------------------------|
| | L_s | Hours | L_s | Hours |
| Jezero Crater | [0°;220°], [222°;223°], [225°;226°], [229°;234°], [250°;259°] | Max 10h 257° | [204°;205°], 208°, 213°, 218°, 222°, [229°;230°], 253°, [242°;250°], [252°;257°], 259°, [261°;263°], [266°;268°], [270°;271°], [274°;277°], 279°, [283°;284°], 286°, 294°, 305°, [307°;308°], 310°, 324° | Max 2h 230°, 246°, 259°, 265° |
| Oxia Planum | [0°;190°], 192°, 194°, [196°;208°] [210°;220°], 222°, 242°, [248°;249°] [251°;252°], [255°;261°], 279°, [282°;284°], [286°;313°], 317°, [320°;360°] | Max 11h 193° | 208°, 242°, 284° | Max 1h |
| Utopia Planitia | [1°;179°], [181°;183°], 185°, [189°;196°] [202°;208°], 210°, [225°;333°] [335°;339°], [341°;358°] | Max 6h 109° | none | none |
| Vastitas Borealis | 24°, 26°, [29°;169°], [175°;176°] 178°, [180°;181°] | Max 9h 87° | 29°, 31°, [37°;39°], [41°;47°], [49°;61°], [63°;65°], [68°;70°], [72°;77°], [79°;88°], [91°;101°], [107°;109°], [111°;120°], [126°;132°], [137°;141°], 146°, [148°;149°], 157° | Max 2h 56°, [58°;60°], 87° |

Table 3: Summary of solar longitude (L_s column) having surface conditions (T, RH) above the eutectic temperature and the deliquescence relative humidity of Ca(ClO₄)₂ and Mg(ClO₄)₂. The Hours column specifies for which L_s the number of hours meeting the conditions is maximum.